National Institute for Public Health
and the Environment
Ministry of Health, Welfare and Sport

Leaching of plant protection products to field ditches in the Netherlands

Development of a drainpipe scenario for arable land

RIVM report 607407003/2012

A. Tiktak | J.J.T.I. Boesten | R.F.A. Hendriks |
A.M.A. van der Linden

National Institute for Public Health
and the Environment
Ministry of Health, Welfare and Sport

Leaching of plant protection products to field ditches in the Netherlands

Development of a drainpipe scenario for arable land

RIVM Report 607407003/2012

Colofon

A. Tiktak, PBL Netherlands Environmental Assessment Agency
J.J.T.I. Boesten, Wageningen UR, Alterra
R.F.A. Hendriks, Wageningen UR, Alterra
A.M.A. van der Linden, RIVM

Contact:
Aaldrik Tiktak
PBL Netherlands Environmental Assessment Agency
Aaldrik.Tiktak@pbl.nl

This investigation has been performed by order and for the account of the Ministry of Infrastructure and the Environment (research programme M/607407) and the Ministry of Economic Affairs (research programme BO12-007-004), within the framework of Development of risk assessment methodology.

Abstract

Leaching of plant protection products to field ditches in the Netherlands.
Development of a drainpipe scenario for arable land

In the current Dutch authorisation procedure for calculating exposure of surface water organisms to plant protection products, deposition of drift is considered to be the only source. Drainage from agricultural fields is being ignored. Because drainage may be an important source for exposure of water organisms, RIVM, Wageningen UR and the Board for the authorisation of plant protection products and biocides derived a new procedure in which drainage is included. The update of the current procedure was initiated by the Dutch government to bring the Dutch procedure more in line with the EU procedure, which already takes account of drainage.

Cracking clay soils
A large part of the drainage may occur via cracks in the soil resulting from clay shrinking upon drought. The PEARL model was extended with a module to account for this preferential flow route and tested against field data. PEARL appeared to be able to simulate the preferential flow processes reasonably well.

Substance properties still important
Calculations for a number of hypothetical substances showed that sorption and degradation still play an important role in the leaching of these substances. Substances with a longer half-life and a lower sorption coefficient show the highest leaching potential. The effect of the substance properties is, however, less pronounced than in a situation without cracks, because most of the active layer of the soil is bypassed.

Keywords:
authorisation, drainage, exposure scenario, GeoPEARL, preferential flow, surface water

Rapport in het kort

Uitspoeling van gewasbeschermingsmiddelen naar kavelsloten.
Ontwikkeling van een drainpijpscenario voor akkerbouw

In de Nederlandse toelatingsbeoordeling voor gewasbeschermingsmiddelen wordt de blootstelling van waterorganismen te eenzijdig berekend. In de huidige beoordeling wordt namelijk geen rekening gehouden met belasting van het oppervlaktewater via drainagesystemen in de bodem van landbouwpercelen. Het RIVM heeft daarom in samenwerking met Wageningen UR een scenario ontwikkeld waarin wel rekening wordt gehouden met deze drainage. Dat is nodig om de toelatingsbeoordeling beter overeen te laten komen met Europese toelatingsprocedures voor dergelijke stoffen, waarin drainage al langer wordt meegenomen.

Drainage via scheuren in kleigronden
Drainage vindt vooral plaats via scheuren in kleigronden. Dergelijke scheuren ontstaan als de bodem uitdroogt en vervolgens krimpt. Het Nederlandse model PEARL, dat in de Nederlandse toelating van gewasbeschermingsmiddelen wordt gebruikt, hield nog geen rekening met drainage via scheuren. Het model is daarom uitgebreid met een module om stroming via kleischeuren te berekenen. Het nieuwe model is getoetst aan metingen. Hierbij bleek het model de stroming via kleischeuren goed te berekenen.

Stofeigenschappen blijven belangrijk
Net als in de oude versie van het model is de drainage van gewasbeschermingsmiddelen afhankelijk van de eigenschappen van het middel. Stoffen die langzaam afbreken en stoffen die slecht binden aan de bodem spoelen het meest uit. Omdat bij stroming via kleischeuren de bodem gepasseerd wordt, is de afhankelijkheid van stofeigenschappen in het nieuwe model echter minder groot.

Trefwoorden:
drainage, GeoPEARL, gewasbeschermingsmiddelen, oppervlaktewater, preferent transport, toelating

Preface

A few years ago the Dutch government decided to initiate an improvement of the methodology for the assessment of effects on aquatic organisms. In order to establish a comprehensive methodology, the Dutch government initiated six working groups to cover various aspects of the new methodology:

- a working group on legal aspects, dealing amongst others with the relation between the WFD and EU directive 91/414/EC (replaced by Regulation 1107/2009);
- a working group on exposure of aquatic organisms;
- a working group on effects on aquatic organisms;
- a working group on multiple stress;
- a working group on emissions from glasshouses (currently split into two working groups);
- a working group on the feedback of monitoring results to the authorisation procedure.

As part of the revision, the Dutch government charged the working group on exposure with the development of a drainpipe exposure scenario. In contrast to the current evaluation of active substances at the EU-level, the current Dutch authorisation procedure does not consider input from drainpipes. Given the abundant occurrence of drained soils in the Netherlands, the Dutch government considered this no longer defensible. This report describes the development and parameterisation of this scenario. This scenario will be included in the user friendly software tool DRAINBOW, which will be described elsewhere.

This report is produced within the framework of the working group on exposure of aquatic organisms. The following persons have been or are currently members of this working group: Paulien Adriaanse (Alterra), Jos Boesten (Alterra), Joost Delsman (Deltares), Aleid Dik (Adviesbureau Aleid Dik), Corine van Griethuysen (Ctgb), Mechteld ter Horst (Alterra), Janneke Klein (Deltares), Ton van der Linden (RIVM), Jan Linders (RIVM), Aaldrik Tiktak (PBL) and Jan van de Zande (PRI). The authors of this report acknowledge the work done by the members of this working group, their participation in discussions, and suggestions for improvement.

Contents

Summary

As part of the Dutch authorisation procedure for Plant Protection Products (PPPs), an assessment of exposure of aquatic organisms in surface water adjacent to agricultural fields is required. In contrast to the current evaluation of substances at the EU-level, the current Dutch authorisation procedure does not consider input from drainpipes. In view of EU-harmonisation, the Dutch government requested the development of a methodology to assess the input of plant protection products through drainage. This report describes the development of a drainpipe exposure scenario that corresponds to the 90th overall percentile of the exposure concentration in Dutch ditches that potentially receive input from drainpipes taking all arable land (excluding grassland) into consideration. This scenario is based on data from an experimental field site on a cracking clay soil.

The peak concentration in the ditch is considered to be the most important exposure endpoint for assessing the effects on aquatic organisms. The peak concentration in drain water is primarily affected by preferential flow through macropores, so we extended the Dutch pesticide leaching model PEARL with a preferential flow module. Central to this new model is a description of the geometry of the macropores and the presence of a so-called internal catchment domain. This internal catchment domain consists of macropores that end above drain depth.

The model concepts were tested at the Andelst field site. We showed that most parameters could be obtained from direct measurements or from commonly available data sources using pedotransfer functions; only three macropore parameters needed calibration, i.e. the volume of macropores at soil surface, the fraction of the internal catchment domain at soil surface and the runoff-extraction ratio. The concentration in drain water appeared to be rather insensitive to the volume of macropores at soil surface, so only two important calibration parameters remained. The fraction of the internal catchment domain had to be increased to 90 per cent, indicating that a significant part of the substances still had to move through the soil matrix. After calibration, the leaching and drainage of two substances was fairly well described by the model.

The Andelst dataset covered a period of approximately one year. To minimise the effect of application time on the predicted exposure concentration, we decided that the exposure assessment should be carried out for a long-term period. The Andelst dataset was therefore extended to a 15-year dataset, using data from a weather station at a distance of 10 km and from a neighbouring groundwater bore hole. Thus a time series of 15 years could be simulated resulting in 15 annual maximum concentrations. We found that the peak concentration in surface water of a weakly sorbing and quickly degrading substance showed much more variability between the years than the peak concentration of a moderately sorbing persistent substance. As a consequence, the frequency distribution function of the annual maximum concentration is steeper for weakly sorbing and quickly degrading compounds. This behaviour was judged plausible and is related to the short residence time of the substance in the mixing layer.

The assessment at the Andelst site resulted in a temporal frequency distribution function consisting of 15 annual peak concentrations. The temporal percentile that predicts the same concentration as the overall 90th percentile of the

exposure concentration was called the target temporal percentile. The overall 90th percentile was obtained with the spatially distributed leaching model GeoPEARL. This model was combined with a metamodel of TOXSWA, so that it was possible to simulate the initial concentration in all Dutch ditches. Nearly all preferential flow parameters could be obtained from generally available data sources using pedotransfer functions. Three macropore related parameters had to be taken directly from the Andelst field site. (These are the same parameters that also needed calibration at the Andelst site.) Two of these parameters (the fraction of the internal catchment domain and the runoff extraction ratio) are extremely important for the peak concentration in drain water. We consider this an important limitation of the current parameterisation, because it is uncertain whether this single field site is sufficiently representative for the entire area of drained arable soils.

The simulated spatial pattern was judged plausible with high predicted peak concentrations in clayey soils and low peak concentrations in sandy soils. The simulations showed that not only the rapid drainage fluxes were enhanced by preferential flow, the predicted mass fluxes in matrix drainage were also enhanced. This was caused by transport through the internal catchment domain, which causes substances to bypass the most reactive part of the soil profile.

The predicted spatial pattern of the peak concentration was substance dependent. For weakly sorbing substances, drainage conditions appeared to be optimal when the boundary hydraulic conductivity was low, whereas for moderately sorbing substances a low organic matter content was also necessary.

The target temporal percentile was substance dependent. Its value ranged from 78 per cent for weakly sorbing and quickly degrading compounds to 0 per cent for strongly sorbing and persistent compounds. Contour diagrams showed that the spatial percentile for the Andelst scenario ranged from approximately 85 per cent to 100 per cent. For strongly sorbing and persistent substances, the high temporal percentile cannot be compensated by a low temporal percentile (because it is already 0 per cent), which means that for those substances the Andelst scenario is more worst-case than the overall 90th percentile. In view of uncertainties in the estimation of the temporal percentiles, the working group proposes using one single temporal percentile for all substances. The 63rd temporal percentile appeared to be the best compromise.

The target maximum concentration (i.e. the concentration in ditch water for the year corresponding to the target percentile) increased by increasing *DegT50* and decreased by increasing K_{om}. The predicted differences of the target maximum concentration were small compared to the difference of the leaching concentration predicted by the convection-dispersion equation. This was judged plausible, because the maximum concentration is primarily caused by preferential flow where the substance bypasses most of the reactive part of the soil profile.

1 Introduction

1.1 Aim and background of the study

As part of the Dutch authorisation procedure for plant protection products (PPPs), an assessment of exposure of aquatic organisms in surface waters adjacent to agricultural fields is required. Spray drift, drainage and runoff are the most important processes involved in loading of edge-of-field surface waters with PPPs (Figure 1). In the evaluation of active substances at the EU level, the importance of all these entry routes is acknowledged (FOCUS 2001). In the current Dutch authorisation procedure, however, spray drift is the only pathway for substances entering the surface water (Beltman and Adriaanse1999, Ctgb 2010). In view of EU-harmonisation, the responsible Dutch Ministries therefore requested the development of a state-of-the-art methodology to also assess the input of PPPs through drainage. This new methodology will become part of a new exposure scenario, which is currently being developed (Tiktak et al. 2012b).

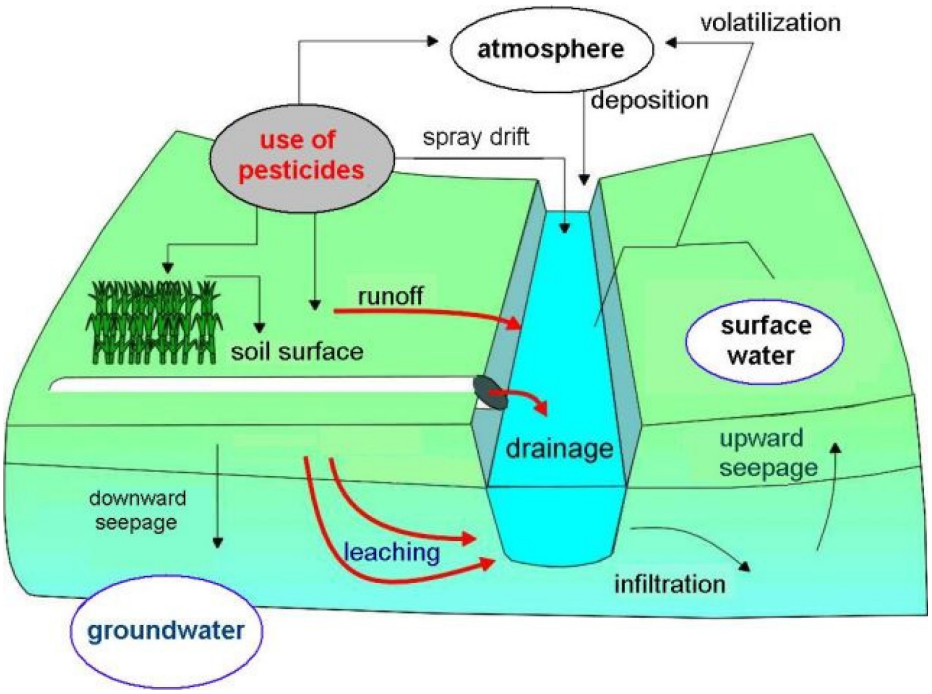

Figure 1 Main processes involved in loading of edge-of-field surface waters with plant protection products.

The aims of the study reported here are (i) to adapt the current exposure model PEARL in such a way that it is capable of describing the relevant leaching concentration sufficiently well, and (ii) to parameterise this exposure model for realistic worst-case conditions. Realistic worst-case conditions are generally defined as a combination of soil and climate properties within a certain region for which the predicted environmental concentration (PEC) is equal to a certain percentile of the distribution of concentrations for all climate and soil properties within a region (EFSA 2010). The exact definition of the term 'realistic worst case conditions' in the context of the drainpipe exposure scenario is given in Section 1.2.

1.2 Endpoint of the drainpipe exposure assessment

1.2.1 Risk management decisions

The derivation of the exposure scenario starts with the definition of the endpoint of the exposure assessment. The responsible Dutch ministries decided that the endpoint of the exposure assessment of aquatic organisms should be the 90th percentile of the concentration in Dutch ditches. The ministries additionally decided that the population should be limited to those ditches that will potentially receive both a spray drift load and a drainpipe load of a substance. Figure 2a gives a schematic representation of this population of ditches. The representation shows that this population may be a small subpopulation of the total population of ditches in the Netherlands. See Tiktak et al. (2012b) for further details.

In the Netherlands, ditches are classified into four groups, i.e. small or temporarily dry ditches ('tertiary ditches'), ditches smaller than 3 m ('secondary ditches'), ditches with a width of 3-6 m at water level ('primary ditches'), and ditches with a width greater than 6 m. All these ditch types may be edge-of-field ditches. The ministries decided that all these ditch types – also the temporarily dry ditches – should be included in the population of ditches. The work group additionally decided to exclude the ditches with a width greater than 6 m because only 8 per cent of the ditches are in this width class.

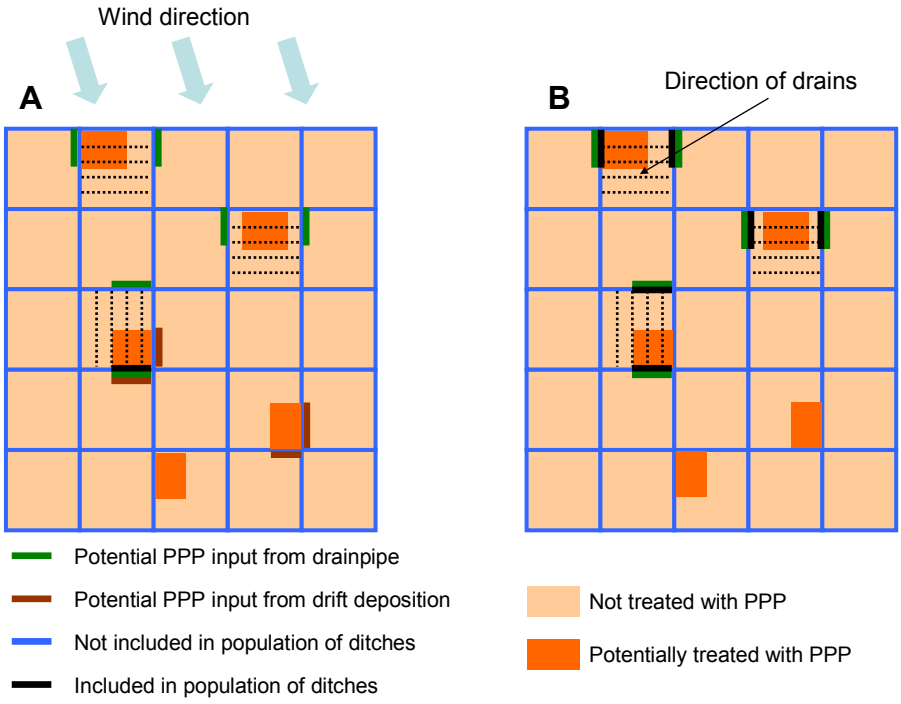

Figure 2 Schematic representation of the population of Dutch ditches to be considered in the estimation of the percentile of the concentration of PPP in the surface water. The left-hand panel (A) shows the population to be considered if the selection is based on both drift and drain input. The right-hand panel (B) shows the population to be considered if only drain input is considered. The dashed lines indicate drains.

1.2.2 *Interpretation of the endpoint of the exposure assessment by the working group*

The working group decided that the drainpipe exposure scenario should apply to the 90th percentile of all ditches that potentially receive PPPs from drainpipes (Figure 2b). In the drainpipe scenario, wind direction is not part of the selection criterion. The implicit assumption is that there is no relationship between wind direction and orientation of ditches, so that it is not possible to exclude ditches based on dominant wind direction. Figure 3 shows that a large proportion of Dutch arable land (40 per cent) has a pipe drainage system.

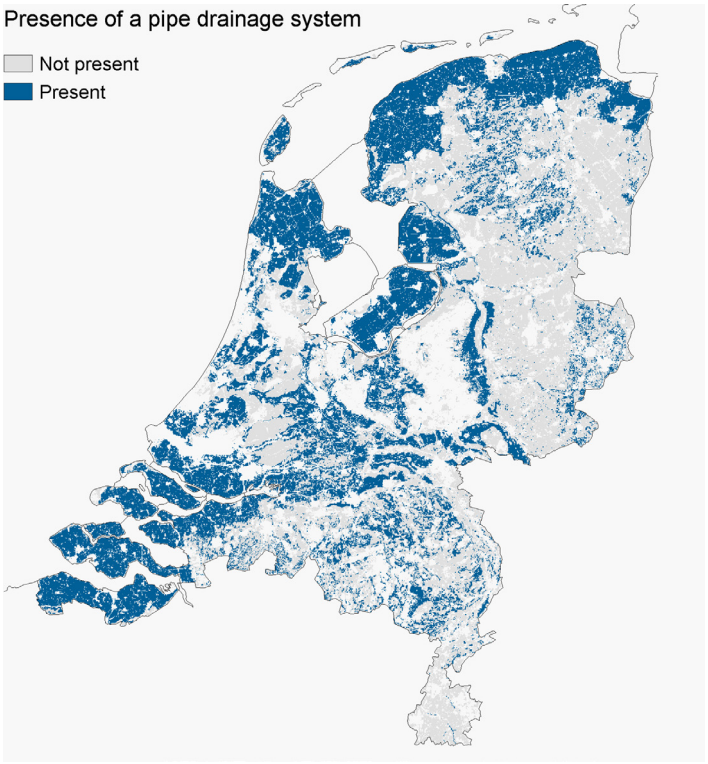

Figure 3 Presence of a pipe drainage system in the Netherlands (Kroon et al. 2001). The 90th percentile of the exposure concentration applies to ditches in the blue area.

The working group further decided that in view of the available time only one drainpipe scenario will be developed. This single scenario should apply to the entire area of arable land. Grassland was excluded from the population of ditches, because PPP-use in grassland is small compared to PPP-use in arable land. In earlier authorisation procedures (Van der Linden et al. 2004), percentiles were based on the area that is potentially treated with the actual PPP for which a notifier requests an authorisation. Application of this procedure would, however, imply that multiple scenarios need to be developed.

Due to the non-linearity of the relation between soil parameters, PPP parameters and predicted environmental concentrations, the ranking of scenarios may be different for different ecotoxicologically relevant concentrations. A scenario that is conservative for the peak concentration in water may therefore not be conservative for a time weighted average concentration in water. Moreover, such a scenario is probably not conservative for the PPP-concentration in sediment as well. Nevertheless, the working group decided that the 90th percentile should be based on the annual peak concentration in water. The choice for the peak concentration was based on guidance provided by the ELINK

workshop (Brock et al. 2009). The ELINK report states that an effect assessment based on acute toxicity data should always be compared with the peak concentration, whilst in chronic risk assessments in the first instance the peak concentration and under certain conditions a time weighted average concentration may be used. The choice for the peak concentration in water implies that the selected scenarios cannot be used for assessment of concentrations in sediment.

In view of the effect of application time on drainpipe concentration, the workgroup decided that the exposure assessment should be carried out for a long-term period, so multiple annual peak concentrations were obtained for each scenario. The workgroup decided that all annual peak concentrations should be used independently, which implies that there is no distinction between space and time. For example 100 ditches and 15 years give 1500 annual maximum concentrations and the target is the 90^{th} percentile of all 1500 values.

1.3 Structure of report

Chapter 2 gives an overview of the procedures applied in this report. Chapter 3 gives a description of the preferential flow concepts in PEARL and GeoPEARL. This new conceptual model is applied to the Andelst experimental field site. A description of this application is given in Chapter 4. Chapter 5 describes how additional weather data and groundwater observation data were used to build the exposure scenario. In Chapter 6, we describe the parameterisation and the application of the GeoPEARL model. Chapter 7 describes the derivation of the target temporal percentile to be used in the exposure assessment. Finally, Chapter 8 provides conclusions and recommendations for further developments.

2 Overview of procedures

The endpoint of the drainpipe exposure assessment is the 90th percentile of the annual maximum concentration in all ditches that potentially receive PPPs from drainpipes. This definition implies that the peak concentration must be known for the entire population of ditches and for multiple years. Spatially distributed PPP-fate models can be used to generate maps of the exposure concentration for the entire area of interest. If an appropriate exposure model exists, the scenario where the 90th percentile peak concentration occurs can be selected directly from the overall distribution function of the so-obtained maps (EFSA 2010). So the first step is to derive an appropriate exposure model.

In the Netherlands, the GeoPEARL model (Tiktak et al. 2002, 2003) is the default model for evaluating the leaching of PPPs at the national scale. The model simulates leaching towards drainpipes as well. The current version of GeoPEARL cannot describe the peak concentration in the drainpipe sufficiently well, because this peak concentration is primarily affected by rapid drainage mechanisms due to preferential flow through macropores. For this reason, we developed a new version of (Geo)PEARL, which includes a description of preferential flow. Figure 4 shows the main flow pathways included in this new version. Theoretical backgrounds of the new model are given in Chapter 3.

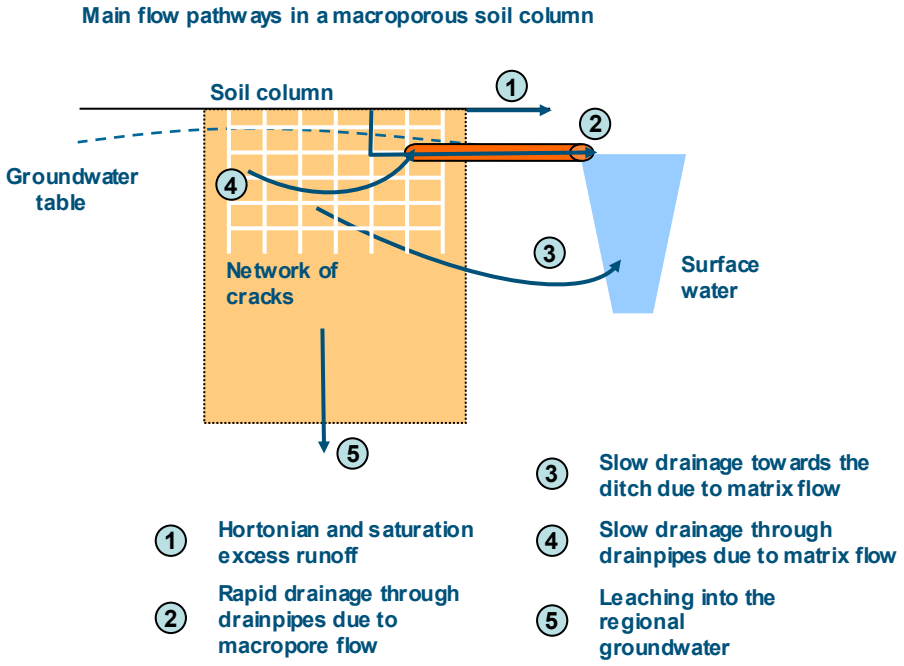

Figure 4 Main flow pathways in a typical Dutch macro-porous soil. The version of GeoPEARL described in Tiktak et al. (2002, 2003) did not include pathway 2.

GeoPEARL describes the concentration of PPPs in the drainpipe, but we need the concentration in the ditch. In the exposure scenario, the concentration in ditch water is simulated with the TOXSWA model (Adriaanse 1996). A regional-scale version of TOXSWA is not (yet) available, so we developed a metamodel of TOXSWA, which describes the dilution of the drainpipe concentration in the ditch

using a single dilution factor. This factor is a function of the volume of the ditch at the start of the day, the daily volume of drain flow from the upstream catchment and the daily volume of drain flow from the adjacent field. Details of this metamodel are described in Section 3.5.

The most straightforward way to obtain the exposure scenario would be by selecting one of the GeoPEARL map-units (also called plots) and base the exposure assessment directly on simulations for this single map unit. We considered this approach as not appropriate, because the lower boundary condition of the GeoPEARL model is extremely simplified: it consists of a long-term average soil water flux on which a sine-function with a fixed amplitude is imposed (Kroon et al. 2001). Because the substance concentration in drain water cannot be simulated sufficiently well with this simplified boundary condition, we decided to use the GeoPEARL simulations only to calculate the relative vulnerability and to base the new drainpipe exposure scenario on a real site instead of on one of the GeoPEARL map-units. The site chosen was the Andelst experimental field site described in Scorza Júnior et al. (2004). At this site sufficient data is available to parameterise and test the PEARL model. The advantage of taking a real site is that full benefit could be taken from the experimental data, so that a consistent and credible exposure scenario could be built. Details on the experimental site are given in Chapter 4.

The Andelst dataset covers a period of approximately one year, but the exposure assessment must be carried out for a multi-year period. The dataset was therefore extended to a 15-year period using data from a weather station at a distance of 40 km and a nearby groundwater observation point (the length of the dataset was 15 years and not 20 years as in GeoPEARL because the groundwater observation dataset had a length of 15 years). Consequently, the exposure assessment results in 15 annual peak concentrations. GeoPEARL was used to determine which of these annual peak concentrations corresponds to the 90^{th} percentile of the exposure concentration in all ditches. This was done as follows:

1. GeoPEARL was run for a 20-year period, so 20 annual peak concentrations were obtained for each map unit;
2. A cumulative distribution function (cdf) of all annual peak concentrations was constructed in which each peak concentration was given a weight proportional to the total ditch length associated with the corresponding GeoPEARL plot, and the 90^{th} percentile was calculated from this overall cdf (red line in Figure 5);
3. For the Andelst scenario, a cumulative distribution function of the 15 annual maximum concentrations was created (green line in Figure 5);
4. The target temporal percentile is the temporal percentile that predicts the same concentration as the 90^{th} percentile of the overall cdf. This percentile can be looked up by following the arrows A, B and C in Figure 5. In our example, the target temporal percentile to be used in the exposure assessment is 20 per cent.

Further details on the derivation of the target percentiles are given in Chapter 7.

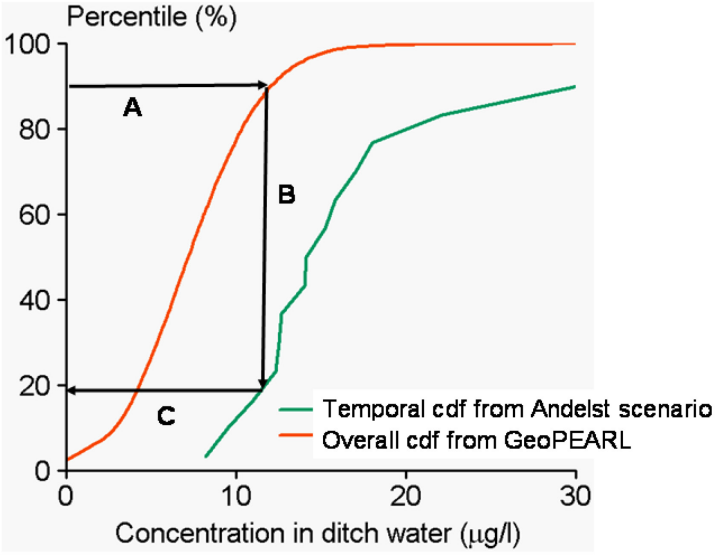

Figure 5 Procedure to derive the target temporal percentile to be used in the exposure assessment. For the Andelst scenario, the target temporal percentile predicts the same concentration as the 90th percentile of the overall cumulative distribution function (red line).

The selected temporal percentile should be sufficiently conservative for all relevant substances. However, due to the non-linearity of the relation between soil parameters, PPP-fate parameters and predicted environmental concentrations, the ranking of climate and soil property combinations is different for different substance properties. As a consequence, a temporal percentile derived for one substance may not be sufficiently conservative when applied to another substance. To overcome this problem, the target temporal percentile was calculated for multiple substances with different degradation half-lives and sorption coefficients. Based on these two properties, the software tool DRAINBOW will automatically select the target temporal percentile to be used in the exposure assessment.

The above procedure differs in two fundamental ways from the scenario selection procedure that was recently published by EFSA (2010). EFSA (2010) proposes selecting an exposure scenario using a (simplified) spatially distributed model and then parameterising this scenario. In our procedure, we have reversed this order: we parameterise an exposure scenario using data from an existing field site and then put the simulations into context using results from a spatially distributed model. This was done because we wanted to benefit from the monitoring data available at the field site.

The second difference is that we did not consider uncertainty during the scenario development. Van den Berg et al. (2008), Heuvelink et al. (2010) and Vanderborght et al. (2011) showed that the 90th percentile of the leaching concentration of PPPs generally shifts towards higher values if uncertainty of PPP-properties and scenario properties is considered. Because ignoring uncertainty may lead to scenarios that are not sufficiently conservative, EFSA (2010) recommends already taking uncertainty into account when developing new scenarios. An uncertainty analysis with the newly developed GeoPEARL model is, however, not yet available.

3 Macropore concepts in (Geo)PEARL

3.1 Introduction

PEARL and GeoPEARL are now commonly used in PPP authorisation procedures and policy evaluations. For example, in the Netherlands the GeoPEARL model (Tiktak et al. 2002, 2003) is used to evaluate the leaching to the groundwater (Van der Linden et al. 2004). In surface waters, the peak concentration is considered an important exposure endpoint. This endpoint is mainly determined by the peak concentrations in the drainpipe. So far, PEARL has been less suitable to describe this peak concentration, because it is primarily affected by rapid drainage mechanisms and surface overland flow. For this reason, macropore versions of PEARL and GeoPEARL have been developed. The macropore versions of the two models play a crucial role in the new exposure scenario.

The macropore version of PEARL is based on FOCUS PEARL_3_3_3, which is described in Leistra et al. (2000), Tiktak et al. (2000) and Van den Berg et al. (2006). PEARL is a one-dimensional, multi-layer model, which describes the fate of a PPP and its transformation products in the soil-plant system. The model is linked with the Soil Water Atmosphere Plant (SWAP version 3.2) model (Kroes et al. 2008). The macropore version of PEARL describes the transport of PPPs through the soil matrix and through two preferential flow domains, i.e. a bypass domain and an internal catchment domain (Kroes et al. 2008). Macropores can be either permanent or temporary (due to shrinking of soils). The feature of describing swell and shrink characteristics of soils was considered important, because Dutch clayey soils generally have a high content of vermiculites and smectites (Breeuwsma 1985, Breeuwsma et al. 1986, Van der Salm 2001). Soils with these clay minerals have a large shrink and swell potential (Scheffer et al. 1979, Bronswijk and Evers-Vermeer 1990).

3.1.1 Dominant flow paths

The Netherlands is situated in a relatively flat delta area, characterised by shallow groundwater tables and a high density of the drainage network. Description of the interaction between soil water, regional groundwater and surface water is indispensable in lowland areas (Figure 4). Surface overland flow (in PPP modelling often called 'runoff') can occur if the infiltration capacity is exceeded in (fine-textured) soils (Horton 1940). When macropores are present, overland flow may be routed into macropores at the soil surface. Parts of these macropores penetrate deeply into the soil and are horizontally connected. Water routed into these macropores bypasses the reactive unsaturated soil, leading to rapid drainage towards drainpipes and short circuiting between the soil surface and the groundwater. A part of the macropores ends at various depths in the unsaturated zone, forcing macropore water to infiltrate in the soil matrix at a larger depth (Van Stiphout et al. 1987). Under wet conditions, however, soils may be swollen so that macropores are closed. In this case, overland flow may be routed directly into surface waters. The importance of surface overland flow in lowland areas was confirmed in recent studies in the Netherlands (Rozemeijer and Van der Velde 2008, Rozemeijer et al. 2010, van der Velde et al. 2010) and Illinois (Algoazany 2007). In regions with shallow groundwater tables, overland flow may also occur when the soil profile is completely saturated. This process – called saturation excess overland flow – may occur after light rainfall of long duration. In coarsely textured soils, matrix flow is the dominant process.

3.1.2 Chapter overview

This chapter describes the theory behind the macropore version of PEARL. In this report, only those processes are described which are relevant for understanding the parameterisation of the new drainpipe exposure scenario. Section 3.2 describes the mathematical description of macropore geometry in SWAP. Section 3.3 gives a short overview of the hydrological concepts conceived in SWAP. A more comprehensive description of macropore concepts in SWAP can be found in Kroes et al. (2008). Section 3.4 gives a description of the PPP transport routines. PEARL calculates the concentration in drain water, but we need the concentration in ditch water. In the exposure scenario, this concentration is simulated with the TOXSWA model (Adriaanse 1996). In the scenario selection phase, we used a simple metamodel of TOXSWA, which is described in Section 3.5.

3.2 Macropore geometry

3.2.1 Conceptual model

In SWAP, macropore geometry is described on the basis of three properties, i.e. continuity, persistency and macropore shape.

Continuity
Macropores are divided into two domains (Figure 6):

- The main bypass flow domain, which is a network of continuous, horizontally interconnected macropores. These macropores penetrate deep into the soil profile and are assumed to be horizontally interconnected. In the main bypass domain, water is transported fast and deep into the soil profile, bypassing the soil matrix. This may lead to rapid drainage towards drainpipes and short-circuiting between the soil surface and the groundwater.
- The internal catchment domain, which consists of discontinuous, non-interconnected macropores ending at different depths in the profile. In this domain, water is captured at the bottom of individual macropores, resulting in forced infiltration of macropore water into the soil matrix.

Persistency
The macropore volume of the two domains is further subdivided into a static macropore volume and a dynamic macropore volume. The static macropore volume consists of structural shrinkage cracks, bio-pores and macropores that originate from tillage operations. Dynamic macropores originate from the shrinking of the soil matrix due to soil moisture loss. Shrinking is generally restricted to soils that contain a substantial amount of interlayered clay minerals (particularly smectites and vermiculites) and/or organic matter (peats).

Macropore shape
Macropore shape is described by an effective soil matrix polygon diameter (d_{pol}). Macropore shape affects the exchange of water between the soil matrix and the macropores: in soils with a large effective matrix polygon diameter, exchange will be relatively slow because of the relatively small vertical area of macropore walls per unit of horizontal area. The effective matrix polygon diameter is also related to crack width, which affects rapid drainage to drainpipes. It is assumed that the effective soil matrix polygon diameter is a function of depth with its minimum value at the soil surface where macropore density is maximal, and consequently distances between macropores are relatively small.

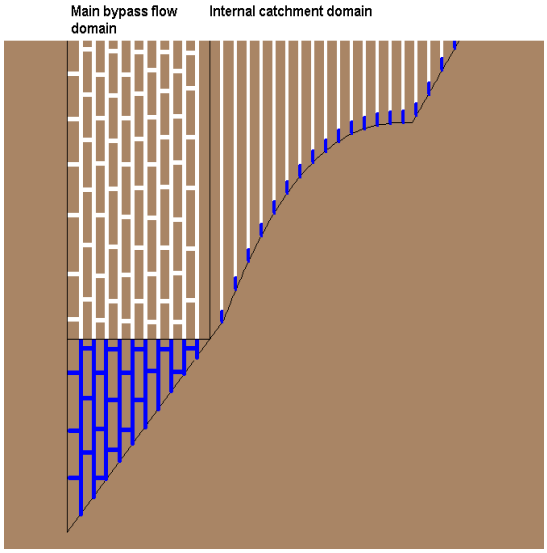

Figure 6 Schematic representation of the two macropore domains, i.e. the main bypass domain transports water deep into the soil profile possibly leading to rapid drainage and the internal catchment domain in which infiltrated water is trapped into the unsaturated soil matrix at different depths. The black lines represent the schematic representation of the macropore volume as depicted in Figure 7.

3.2.2 *Mathematical model*

SWAP offers a large number of options to describe macropore geometry (Kroes et al., 2008). In PEARL, only those options are implemented for which parameters can be found through pedotransfer functions (see Chapter 6).

Depth distribution of macropores

In PEARL, the volume fraction of static macropores in the two domains as a function of depth ($V_{sta,z}$ (m^3 m^{-3})) is described by a stepwise linear function (denoted by the solid line in Figure 7):

$$\begin{aligned} V_{sta,z} &= V_{sta,byp,0} + V_{sta,ica,0} && \text{for} \quad 0 \geq z > z_{Ah} \\ V_{sta,z} &= V_{sta,byp,0} - V_{sta,ica,0}\left(\frac{z_{Ah} - z}{z_{Ah} - z_{ica}}\right) && \text{for} \quad z_{Ah} \geq z > z_{ica} \\ V_{sta,z} &= V_{sta,byp,0} - V_{sta,byp,0}\left(\frac{z_{ica} - z}{z_{ica} - z_{sta}}\right) && \text{for} \quad z_{ica} \geq z > z_{sta} \end{aligned} \qquad (1)$$

where $V_{sta,byp,0}$ (m^3 m^{-3}) is the volume fraction of the static macropores in the bypass domain at soil surface, $V_{sta,ica,0}$ (m^3 m^{-3}) is the volume fraction of static macropores in the internal catchment domain at soil surface, z_{Ah} (m) is the depth of the plough layer, z_{ica} (m) is the bottom depth of the internal catchment domain, and z_{sta} (m) is the bottom depth of the static macropore domain. In PEARL, the user has to input the total volume fraction of static macropores at soil surface and the volumetric proportion of the internal catchment domain with respect to the static macropores at the soil surface, $P_{ica,\,0}$ (-):

$$P_{ica,0} = \frac{V_{sta,0,ica}}{V_{sta,0}} = \frac{V_{sta,0,ica}}{V_{sta,0,ica} + V_{sta,0,byp}} \qquad (2)$$

$P_{ica,0}$ determines the distribution over the two main domains of the precipitation water routed into the macropores at soil surface.

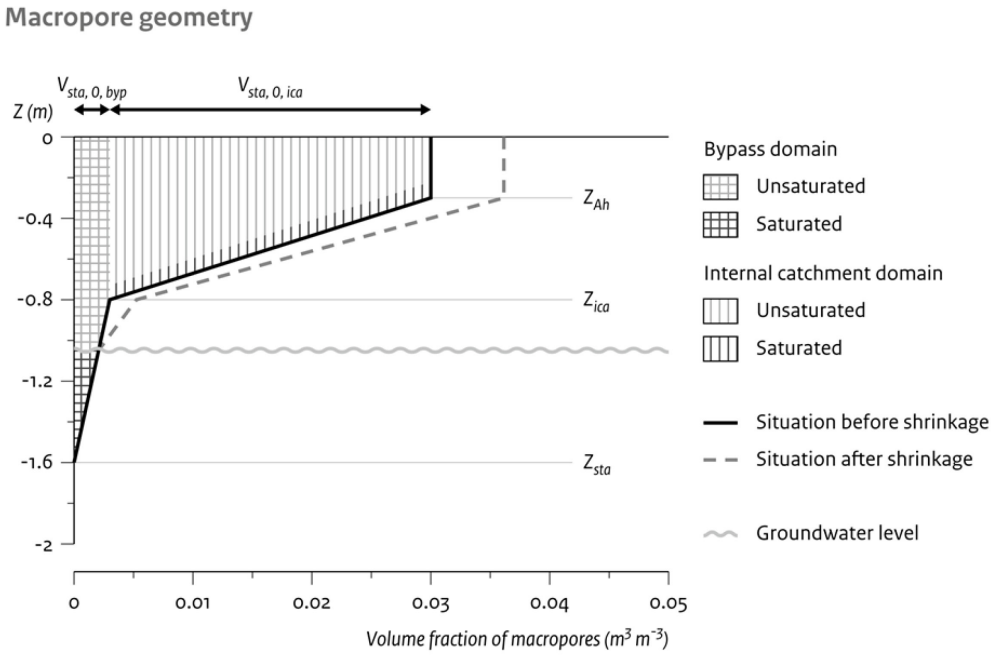

Figure 7 Mathematical representation of the static macropore volume as a function of depth. z_{ah} (m) is the depth of the plough layer, z_{Ica} (m) is the bottom depth of the internal catchment domain, z_{sta} (m) is the bottom depth of the permanent macropores, $V_{Sta,byp,0}$ (m^3 m^{-3}) is the volume fraction of macropores in the bypass domain, and $V_{Sta,Ica,0}$ (m^3 m^{-3}) is the volume fraction of macropores in the internal catchment domain.

Dynamic macropores due to soil shrinkage

Besides static macropores, also dynamic macropores (due to soil shrinkage) may be present. The volume fraction of dynamic macropores is added to the volume fraction of the static macropores (Figure 7). The constant $P_{ica,0}$ (Equation 2) is used to distribute the total macropore volume over the two macropore domains, so for static and dynamic alike. See Kroes et al. (2008) for details. Notice that due to shrinkage, macropores can be temporarily present at greater depths than z_{sta} in Figure *7.* The increase of the volume of dynamic macropores is equal to the volume of horizontal shrinkage of the soil matrix. For the relation between horizontal and total shrinkage of the soil matrix isotropic shrinkage is assumed. Total shrinkage is measured by drying soil aggregates (Bronswijk and Evers-Vermeer 1990). For each soil, there is a fixed relationship between moisture content and the volume of the soil matrix (the shrinkage characteristic). Figure 8 shows a typical example of a shrinkage relationship of a clay soil. Three stages of shrinkage can be distinguished (Scheffer et al. 1979; Bronswijk and Evers-Vermeer 1990), i.e. normal shrinkage (volume loss of aggregates is equal to moisture loss), residual shrinkage (volume loss of aggregates is less than moisture loss) and zero shrinkage (soil particles have reached their densest configuration). Description of the shrinkage characteristic requires two user-specified parameters, i.e. the void ratio at moisture ratio zero (oven dry water content) and the moisture ratio at transition of residual to normal shrinkage. The void ratio and the moisture ratio are defined as:

$$e = \frac{V_p}{V_{soil}} \tag{3}$$

$$\phi = \frac{\theta}{1 - \theta_s} \tag{4}$$

where e (-) is the void ratio, V_p ($m^3\ m^{-3}$) is the volume fraction of pores in the soil matrix, and V_{sol} ($m^3\ m^{-3}$) is the volume fraction of the solid soil, φ (-) is the moisture ratio, θ ($m^3\ m^{-3}$) is the volume fraction of soil water, and θ_s ($m^3\ m^{-3}$) is the volume fraction of soil water at saturation. The relation between void ratio as function of moisture ratio and shrinkage volume is:

$$V_{\text{shr}} = (e - e_{\text{s}})V_{\text{sol}} \tag{5}$$

where e_s is void ratio at saturation.

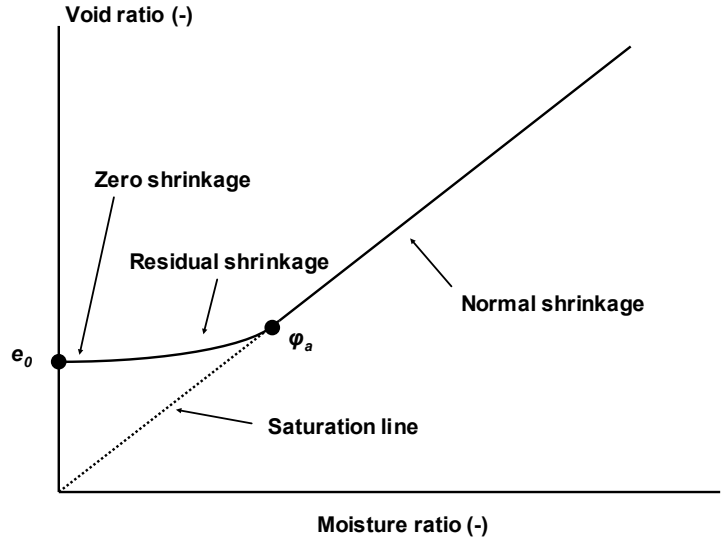

Figure 8 Typical shrinkage characteristic of a clay soil showing the three shrinkage stages. The black dots represent the typical points that have to be specified by the user, i.e. the void ratio at zero moisture content e_0 (-) and the moisture ratio at transition from normal to residual shrinkage φ_a (-).

Effective diameter of soil polygons
The effective diameter of the soil polygons is assumed to be a function of depth with its minimum value at soil surface where macropore density is highest and consequently distances between macropores are small, and its maximum value deeper in the soil profile:

$$d_{pol,z} = d_{pol,\min} + (d_{pol,\max} - d_{pol,\min})\left(1 - \frac{V_{sta,z}}{V_{sta,0}}\right) \tag{6}$$

Where $d_{pol,min}$ (m) is the minimum polygon diameter, $d_{pol,max}$ (m) is the maximum polygon diameter, V_{sta} ($m^3\ m^{-3}$) is the volume fraction of static macropores ($m^3\ m^{-3}$), and $V_{sta,0}$ ($m^3\ m^{-3}$) is the volume fraction of static macropores at soil surface.

3.3 Water flow

SWAP simulates the water balance of the bypass domain and the internal catchment domain separately:

$$\frac{\mathrm{d}W_{byp}}{\mathrm{d}t} = I_{p,byp} + I_{r,byp} - \int_{zgwl}^{z=0} R_{lu,byp}\mathrm{d}z - \int_{zsta}^{z=zgwl} R_{ls,byp}\mathrm{d}z - \int_{zsta}^{z=zgwl,byp} R_{d,byp}\mathrm{d}z \quad (7)$$

With

$$\frac{\mathrm{d}W_{ica}}{\mathrm{d}t} = I_{p,ica} + I_{r,ica} - \int_{zgwl}^{z=0} R_{lu,ica}\mathrm{d}z - \int_{zica}^{z=zgwl} R_{ls,ica}\mathrm{d}z \quad (8)$$

where suffix *byp* refers to the bypass domain, suffix *ica* is the internal catchment domain, W ($m^3\ m^{-2}$) is the areic volume of water in the macropores, t (d) is time, I_p ($m^3\ m^{-2}\ d^{-1}$) is the areic volume rate of infiltration of water at soil surface by direct precipitation, I_r ($m^3\ m^{-2}\ d^{-1}$) is the areic volume rate of infiltration through runoff, R_{lu} ($m^3\ m^{-2}\ d^{-1}$) is the volumic volume rate of lateral infiltration into the unsaturated matrix, R_{ls} ($m^3\ m^{-2}\ d^{-1}$) is the volumic volume rate of lateral flow into and out of the saturated soil matrix, R_d ($m^3\ m^{-2}\ d^{-1}$) is volumic volume rate of drainage, z is the depth, z_{gwl} is the depth of the groundwater table, and $z_{gwl,byp}$ (m) is the depth of the water table in the bypass domain. All balance terms are positive, except R_{ls} which is positive in case of flow into the matrix and negative in the case of flow out of the matrix, and R_d which is positive in the case of flow towards the drainage system and negative in the case of flow from the drainage system. Note that the water balance of the internal catchment domain does not contain a drainage term because it is assumed that macropores in this domain end above the drains. Vertical flow in the macropores is calculated from the water balance of the individual soil layers, see Kroes et al. (2008) for details. SWAP can also simulate water flow into macropores by interflow, which may occur if a perched groundwater table is present. This term is not further described here, because it is not used within PEARL.

Inflow at soil surface
The rate of precipitation and irrigation water routed directly into the macropores at soil surface is calculated as:

$$I_{p,ica} = P_{ica,0} A_{mac} P \quad (9)$$

$$I_{p,byp} = (1 - P_{ica,0}) A_{mac} P \quad (10)$$

where P ($m^3\ m^{-3}\ d^{-1}$) is the sum of precipitation, irrigation rate and snowmelt, $P_{ica,0}$ (-) is the proportion of the internal catchment domain at soil surface (Eqn. 2), and A_{mac} ($m^2\ m^{-2}$) is the horizontal macropore volume fraction at soil surface, which is assumed to be equal to the total macropore volume at soil surface, $V_{mac,0}$.

Runoff into macropores occurs when the total rate of precipitation, irrigation and snowmelt exceeds the infiltration capacity of the soil matrix (Hortonian overland flow). In this case, ponding occurs, and the infiltration rate is calculated as:

$$I_r = \frac{h_0}{\gamma_r} \quad (11)$$

where h_0 (m) is the ponding depth and γ_r (d) is the resistance for macropore inflow at soil surface. In surface runoff calculations, usually a threshold ponding depth is used before runoff starts. This is not the case in the calculation of runoff into macropores, because it is assumed that micro depressions are connected to macropores. It can further be shown (Bouma and Anderson 1973) that infiltration resistances are low (0.01-0.001 d). The effect of both assumptions is that ponding water is routed preferentially into the macropores. Distribution of I_r over the bypass domain ($I_{r,byp}$) and the internal catchment domain ($I_{r,ica}$) is according to their volumetric proportions at soil surface, $P_{byp,0}$ and $P_{ica,0}$. Runoff from the field directly into the adjacent ditch occurs only if the macropores are fully saturated.

Lateral infiltration into the unsaturated matrix
Lateral infiltration of macropore water into the unsaturated soil matrix occurs over the depth where macropore water is in contact with the unsaturated matrix. In PEARL, it is assumed that absorption is the dominate process. Absorption is described with Philip's sorptivity (Philip 1957):

$$R_{lu} = \frac{4S(\theta)_p\sqrt{t - t_0}}{d_{pol}\sqrt{1 - V_{mac}}} \tag{12}$$

Where R_{lu} ($m^3\ m^{-3}\ d^{-1}$) is the volumic volume rate of absorption over time interval $t_0 \rightarrow t$ (d), and $S(\theta)_p$ ($m^3\ m^{-2}\ d^{0.5}$) is Philip's sorptivity. Philip's sorptivity depends on the initial water content.

Lateral infiltration into and exfiltration out of the saturated matrix
Lateral infiltration of macropore water into the saturated soil matrix occurs over the depth where macropore water is in contact with the saturated matrix. Lateral infiltration and exfiltration is calculated with a Darcy equation (Eqn. 13):

$$R_{ls} = \frac{f_{shp}8K_s(h_{mac} - h_{mic})}{d_{pol}^2} \tag{13}$$

where R_{ls} ($m^3\ m^{-3}\ d^{-1}$) is the volumic volume rate of infiltration, and K ($m\ d^{-1}$) is the saturated hydraulic conductivity of the soil matrix, h_{mac} (m) is the hydraulic head in the macropore, and h_{mic} (m) is the hydraulic head in the micropore domain. Parameter f_{shp} (-) is a shape factor, which accounts for uncertainties in the theoretical description of lateral infiltration by Darcy flow originating from uncertainties in the exact shape of soil matrix polygons. In PEARL, a default value of 1 is used (Kroes et al. 2008). Note that infiltration occurs if $h_{mac} > h_{mic}$ and exfiltration occurs if $h_{mac} < h_{mic}$.

Rapid drainage
Rapid drainage to drainage systems may occur via a network of horizontally interconnected macropores. In SWAP, rapid drainage is calculated using a drainage resistance:

$$q_{rd} = \frac{z_{gwl,byp} - z_{dra}}{\gamma_{rd,act}} \tag{14}$$

where q_{rd} ($m^3\ m^{-2}\ d^{-1}$) is the rapid drainage flux, $z_{gwl,byp}$ (m) is the water level in the bypass domain, z_{dra} (m) is the depth of the pipe drainage system, and $\gamma_{rd,act}$ (d) is the actual rapid drainage resistance. The drainage resistance decreases with increasing groundwater level, and is calculated from the reference drainage

resistance and the ratio between the actual and reference transmissivity [*KD*] of the macropores:

$$\gamma_{act} = \frac{[KD]_{act}}{[KD]_{ref}} \gamma_{ref} \tag{15}$$

where

$$[KD] = \int_{zsta}^{zgwlbyp} K_{lat} \mathrm{d}z = C \int_{zsta}^{zgwlbyp} \frac{w_{mp}}{d_{pol}} \mathrm{d}z \tag{16}$$

in which K_{lat} (m d^{-1}) is the lateral hydraulic conductivity of the macropores, z_{sta} (m) is the bottom depth of the bypass domain when reaching into the saturated soil, z_{gwlbyp} (m) is the depth of the water level in this domain, and w_{mp} (m) is the macropore width. The value of C is a hypothetical constant, which is not relevant because it is eliminated in Eqn. 15. The volumic volume rate of rapid drainage in Eqn 7 is calculated by distributing the rapid drainage flux over the water filled soil layer (i.e. the layer from zsta to $z_{gwl,byp}$) according to the relative transmissivity of the macropores in the bypass domain:

$$R_{d,byp} = \frac{[KD]}{\int_{zsta}^{z=zgwl,byp} [KD] \mathrm{d}z} q_{rd} \tag{17}$$

3.4 Substance behaviour

Substance balance

Substances in the macropore domain are assumed to reside in a water layer at the bottom of the two macropore domains (Figure 6). The major pathway for substances entering the macropores is surface runoff. Substances can also enter the macropores by exfiltration out of the saturated soil matrix. Notice, however, that this process can only occur in static macropores, because the volume fraction of dynamic macropores is zero in saturated soils due to swelling. In the internal catchment domain, infiltration from the macropores into the saturated or unsaturated soil is the only loss process. In the bypass domain, rapid drainage is an additional loss term, possibly leading to direct surface water contamination. It is further assumed that degradation in the macropore domain is zero. This is justified, because of the short residence times in the macropores.

The substance balances of the two macropore domains read:

$$\frac{\mathrm{d}A_{ica}}{\mathrm{d}t} = \int_{zmix}^{z=0} J_{r,ica} \mathrm{d}z + \int_{zsta}^{z=0} J_{e,ica} \mathrm{d}z \tag{18}$$

$$\frac{\mathrm{d}A_{byp}}{\mathrm{d}t} = \int_{zmix}^{z=0} J_{r,byp} \mathrm{d}z + \int_{zsta}^{z=0} J_{e,byp} \mathrm{d}z + \int_{zsta}^{z=0} J_{d,byp} \mathrm{d}z \tag{19}$$

where A_{ica} (kg m^{-2}) is the areic mass of substance in the macropore system, J_r (kg m^{-3} d^{-1}) is the volumic mass rate of substance runoff into the macropores, J_e (kg m^{-3} d^{-1}) is the volumic mass rate of exchange between the soil matrix and the macropore system, and J_d (kg m^{-3} d^{-1}) is the lateral volumic discharge rate of substance due to rapid drainage. All balance terms are positive, except for R_e, which is negative when substance flow is from the macropores into the matrix.

The suffixes *ica* and *byp* refer to internal catchment domain and bypass domain, respectively. The variable z_{mix} (m), the mixing layer depth, is explained in the following paragraph. The areic mass of substance is calculated as:

$$A_{ica} = W_{ica} c_{L,ica} \tag{20}$$

$$A_{byp} = W_{byp} c_{L,byp} + f_{s,byp} \xi_{byp} X_{byp} \tag{21}$$

where W ($m^3\ m^{-2}$) is the areic volume of water in the macropore (i.e. the water layer), c_L (kg m^{-3}) is the substance concentration in the macropore, $f_{s,byp}$ (-) is the fraction of solid phase in contact with the bypass domain, ξ_{byp} (kg m^{-2}) is the areic mass of solid phase in soil over the water-filled depth of the bypass domain, and X_{byp} (kg kg^{-1}) is the mass of substance sorbed per mass of dry soil in the bypass domain. So ξ_{byp} is defined as

$$\zeta_{byp} = \int_{z_{wet,byp,start}}^{z_{wet,byp,end}} \rho \, dz \tag{22}$$

where $z_{wet,byp,start}$ (m) is the depth where the wet part of the bypass domain starts and $z_{wet,byp,end}$ (m) is the depth where the wet part of the bypass domain ends.

For the bypass domain only Freundlich equilibrium sorption is assumed. The Freundlich coefficient, $K_{F,byp}$ is described by

$$K_{F,byp} = OM_{byp} K_{OM} \tag{23}$$

where OM_{byp} (kg kg^{-1}) is average organic matter over the depth of the water-filled bypass domain. From Eqn 21, the expression of the substance concentration in the bypass domain, c^*_{byp}, can be derived by dividing all terms by $Z_{wet,byp}$, i.e. the thickness of the wet part of the bypass domain. This gives:

$$c^*_{byp} = \theta_{byp} c_{L,byp} + f_{s,byp} \rho_{byp} X_{byp} \tag{24}$$

where θ_{byp} is the volume fraction of water of the bypass domain and ρ_{byp} is the average dry bulk density over the depth of the water-filled bypass domain. Please note that Eqn. 24 is only needed for calculating the distribution over solid and liquid phase within the bypass domain. Mass conservation is ensured by Eqn. 21.

The substance balance of the soil matrix is extended as follows:

$$\frac{\partial c^*_{eq}}{\partial t} = -J_s - \frac{\partial J_{p,L}}{\partial z} - \frac{\partial J_{g,L}}{\partial z} - J_t + J_f - J_u - J_d - J_e \tag{25}$$

Here, c^*_{eq} (kg m^{-3}) is the substance concentration in the equilibrium domain of the soil system, J_s (kg m^{-3} d^{-1}) is the volumic mass rate of substance sorption in the non-equilibrium domain, $J_{p,L}$ (kg m^{-2} d^{-1}) is the mass flux of substance in the liquid phase, $J_{p,g}$ (kg m^{-2} d^{-1}) is the mass flux of substance in the gas phase, J_t (kg m^{-3} d^{-1}) is the transformation rate, J_f (kg m^{-3} d^{-1}) is the formation rate, J_u (kg m^{-3} d^{-1}) is the rate of substance uptake by plant roots, J_d (kg m^{-3} d^{-1}) is the lateral discharge rate of substances, and J_e (kg m^{-3} d^{-1}) is the lateral exchange rate between the matrix and the macropore domain (negative if

substance flow is from the macropore domain into the matrix). The substance balance of the non-equilibrium domain is not affected.

Input of substance by surface runoff
Surface overland flow is the main pathway for substances entering the macropores. PEARL uses a mixing layer concept to describe the interaction between surface runoff and the top soil layer. In this concept, it is assumed that chemicals are released from a thin layer of topsoil that interacts with rainfall and runoff (Ahuja et al. 1982, Sharpley 1985). Sharpley (1985) reviewed several runoff studies and found mixing layer depths between 0.13 and 3.7 cm. They also found that the 'effective depth of interaction' increased with rainfall intensity and slope (i.e. with runoff energy) and decreased with increasing soil aggregation. Because data are lacking to parameterise these relationships, PEARL uses a constant mixing layer depth, z_{mix}.

In PEARL, the first numerical soil compartment acts as the mixing layer. The mass balance for the first compartment is extended with a runoff term:

$$\frac{\partial c^{*}_{eq}}{\partial t} = -J_s - \frac{\partial J_{p,L}}{\partial z} - \frac{\partial J_{g,L}}{\partial z} - J_t + J_f - J_u - J_d - J_e - J_r \qquad (26)$$

where J_r (kg m^{-3} d^{-1}) volumic mass rate of substance discharge in runoff.
J_r consists of three terms, i.e. runoff into the bypass domain ($J_{r,byp}$), runoff into the internal catchment domain ($J_{r,ica}$) and runoff from the field ($J_{r,fld}$). These terms are calculated as follows:

$$J_{r,byp} = (f_{mix} I_{r,byp} c_{L,mix}) / z_{mix} \qquad (27)$$

$$J_{r,ica} = (f_{mix} I_{r,ica} c_{L,mix}) / z_{mix} \qquad (28)$$

$$J_{r,fld} = (f_{mix} I_{r,fld} c_{L,mix}) / z_{mix} \qquad (29)$$

Parameter f_{mix} (-) is the runoff extraction ratio. This parameter is a lumped parameter that accounts for physical non-equilibrium between the soil and runoff (Gouy et al. 1999). Physical non-equilibrium results, among others, from water flow on the soil surface, which is not homogeneous.

Exchange between the soil matrix and the macropores
Convection is the only process considered in the exchange between macropores and the soil matrix:

$$\begin{aligned} J_{e,byp} &= R_{e,byp} c_{L,byp} \quad \text{if} \quad R_{e,byp} \le 0 \\ J_{e,byp} &= R_{e,byp} c_{L,mic} \quad \text{if} \quad R_{e,byp} > 0 \end{aligned} \qquad (30)$$

$$\begin{aligned} J_{e,ica} &= R_{e,ica} c_{L,ica} \quad \text{if} \quad R_{e,ica} \le 0 \\ J_{e,ica} &= R_{e,ica} c_{L,mic} \quad \text{if} \quad R_{e,ica} > 0 \end{aligned} \qquad (31)$$

where $c_{L,mic}$ (kg m^{-3}) is the substance concentration in the liquid phase of the micropore domain, $c_{L,byp}$ (kg m^{-3}) is the substance concentration in the bypass domain and $c_{L,ica}$ (kg m^{-3}) is the substance concentration in the internal catchment domain. The volumic volume rate of exchange between the macropore and the soil matrix, $R_{e,byp}$ or $R_{e,ica}$, is equal to the lateral infiltration into or exfiltration out of the saturated matrix (R_{ls}) in the saturated zone, and equal to volumic volume rate of infiltration R_{lu} in the unsaturated zone.

Substance discharge by drainage
PEARL calculates rapid drainage from the bypass domain as well as lateral discharge through the soil matrix (Section 3.1). Lateral discharge of substances by drainage is taken proportional to the volumic volume rates of water:

$$\begin{aligned} J_{d,byp} &= R_{d,byp} c_{L,byp} \quad \text{if} \quad R_{d,byp} > 0 \\ J_{d,byp} &= 0 \quad \text{if} \quad R_{d,byp} \le 0 \end{aligned} \tag{32}$$

$$\begin{aligned} J_{d,mic} &= R_{d,mic} c_{L,mic} \quad \text{if} \quad R_{d,mic} > 0 \\ J_{d,mic} &= 0 \quad \text{if} \quad R_{d,mic} \le 0 \end{aligned} \tag{33}$$

where $J_{d,byp}$ (kg m^{-3} d^{-1}) is the volumic mass rate of substance discharge in rapid drainage, $J_{d,mic}$ (kg m^{-3} d^{-1}) is the volumic mass rate of substance discharge from the soil matrix, $R_{d,byp}$ (m^3 m^{-3} d^{-1}) is the volumic volume rate of rapid drainage, and $R_{d,mic}$ (m^3 m^{-3} d^{-1}) is the volumic volume rate of drainage from the soil matrix. Eqn. 32 and 33 imply that it is assumed that concentration gradients in the lateral direction are negligible (i.e. no diffusion and dispersion). The concentration in drainage water, $c_{L,d}$, is calculated using flux-weighted averaging procedure:

$$c_{L,d} = \frac{\int_0^\infty J_{d,mic} \mathrm{d}z + \int_0^\infty J_{d,byp} \mathrm{d}z}{\int_0^\infty R_{d,mic} \mathrm{d}z + \int_0^\infty R_{d,byp} \mathrm{d}z} \tag{34}$$

3.5 The peak concentration in ditch water

PEARL describes the concentration of substances in drain water, but we need the concentration in the ditch. In the final exposure scenario, substance fate in ditch water is simulated with the TOXSWA model (Adriaanse, 1996). In the scenario selection phase, we need a regional-scale substance fate model, because we need the peak concentrations for the entire population of Dutch ditches (Section 1.2). A regional-scale version of TOXSWA is, however, not (yet) available. For this reason, Adriaanse (personal communication, 2009) created a metamodel of TOXSWA, which calculates the dilution of the drainpipe concentration based on the volume of the ditch at the start of the day, the daily volume of drain flow from the upstream catchment and the daily volume of drain flow from the adjacent field:

$$c_{ditch} = e^{-\alpha B} \frac{V_{adj}}{V_{ditch}} c_{L,d} + (1 - e^{-\alpha B}) \frac{V_{adj} + f_{upstr.treated} V_{upstr,total}}{V_{adj} + V_{upstr,total}} c_{L,d} \tag{35}$$

where c_{ditch} (µg/l) is the concentration in ditch water, V_{adj} (m^3 m^{-1}) is the lineic volume[1] of daily drain flow from the adjacent field, V_{ditch} (m^3 m^{-1}) is the lineic volume of the ditch at the start of the day, $V_{upstr,total}$ (m^3 m^{-1}) is the lineic volume of daily drain flow from the upstream catchment, $f_{upstr,treated}$ (-) is the fraction of the upstream catchment that is treated, $c_{L,d}$ (µg/l) is the concentration in drain water calculated with Eqn. 34, α (-) is a calibration factor, and B (-) is equal to:

[1] The volume of water per length

$$B = \frac{V_{adj}}{V_{ditch}} \frac{V_{adj} + V_{upstr,total}}{V_{adj} + f_{upstr,treated} V_{upstr,total}} \quad (36)$$

The initial lineic volume of the ditch is calculated with the equation:

$$V_{ditch} = bh + s_1 h^2 \quad (37)$$

where b (m) is the width at ditch bottom, h (m) is the water depth, and s_1 (-) is the slope of the watercourse sides, expressed as the ratio of the horizontal distance and the vertical distance.

The daily volume of drain water is calculated with the equations:

$$V_{adj} = \int_{t}^{t+\Delta t} q_d A_{adj} \mathrm{d}t \quad (38)$$

$$V_{upstr,total} = \int_{t}^{t+\Delta t} q_d A_{upstr} \mathrm{d}t \quad (39)$$

in which A_{adj} (m^2 m^{-1}) is the area of the adjacent field per unit ditch length, A_{upstr} (m^2 m^{-1}) is the area of the upstream catchment per unit ditch length, t (d) is time and q_d (m^3 m^{-2} d^{-1}) areic volume flux of drainage from the adjacent field. The implicit assumption is that the drainage flux from the upstream catchment is equal to the drainage flux from the adjacent field. The drainage flux consists of rapid drainage due to flow through the main bypass domain and a slow drainage term due to flow through the soil matrix:

$$q_d = q_{d,mic} + q_{d,byp} \quad (40)$$

where $q_{d,mic}$ (m^3 m^{-2} d^{-1}) is the areic volume flux of drainage due to flow through the soil matrix, and $q_{d,byp}$ (m^3 m^{-2} d^{-1}) is the areic volume flux of drainage due to flow through the main bypass domain.

The metamodel was calibrated to the FOCUS D3 scenario (FOCUS 2001). The so-obtained value of α was equal to 2. Example results for a range of ditch volumes are shown in Figure 9.

It can be seen that the initial concentration in ditch water equals the concentration in drain water at high drainage fluxes. At small initial ditch volumes, a daily drainage flux of 2 mm d^{-1} is sufficient to completely refresh the water initially present in the ditch.

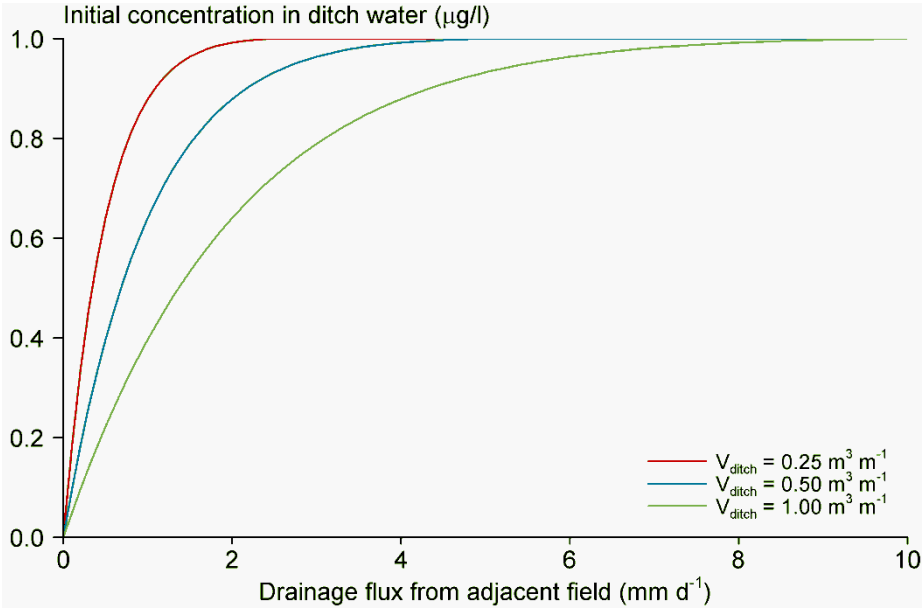

Figure 9 Initial concentration in ditch water as a function of the drainage flux from the adjacent field. The concentration in the drainpipe was set to 1 µg/L, a was set to 2, and both the area of the adjacent field and the area of the upstream catchment were set to 100 m^2 m^{-1}. As a conservative assumption, 100% of the area upstream was assumed to be treated.

4 Application of the macropore version of PEARL to the Andelst field study

4.1 Introduction

The Andelst field study plays a crucial role in the development of the drainpipe exposure scenario. It is currently the only Dutch dataset where sufficient data is available to parameterise and test all modules of the preferential flow version of PEARL. Other field studies are available for testing parts of the model as well, but they either lack measurements of pesticide fate (Hendriks et al. 1999; Van den Beek et al. 2008) or were carried out in a sandy soil (Boesten and Van der Pas 2002). For this reason, we decided to base the new drainpipe exposure scenario on data obtained from the Andelst experimental field site.

This chapter presents the application of PEARL to the Andelst experimental field site. The purpose of the study reported in this chapter was to test the conceptual model described in Chapter 3. Section 4.2 gives a brief introduction to the Andelst dataset. Section 4.3 describes the derivation of the input data. In Section 4.4, results are presented and discussed. Finally, Section 4.5 gives some general conclusions. Chapter 5 will describe the parameterisation of the PEARL drainpipe scenario, based on the experiences gained in this chapter.

4.2 Field study

The experiment was carried out from April 1998 until April 1999 in a field located near the municipality of Andelst (51^{o} 53'N; 5^{o} 43'E; altitude 8 m above sea level) and is described in detail by Smelt et al. (2001) and Scorza Júnior et al. (2004). The experimental field was 160 m long and 50 m wide. The experimental field was drained at a depth of 80 – 90 cm. Drain spacing is 10 m. The experimental field comprised the entire catchment area of six drainpipes. Three adjacent drain outlets were merged into one drain set, hence we have two drain sets. The water table resided at a depth of 60 – 180 cm below the soil surface. The soil is a young Holocene river bank deposit of the river Rhine and is classified as a Eutric Fluvisol (FAO 1988). Table 1 summarises some general soil properties. Notice that the organic matter content was obtained from the organic carbon content and not from ignition loss. Shrinkage cracks were observed at the soil surface. Permanent macropores (for example worm holes) were regularly found in the subsoil (26 – 100 cm soil layer). At a depth of about 3 m, a thick layer of coarse sand underlies the clay profile, which is in direct contact with the river Waal (at 1 km distance), and thus acts as a natural drain.

On 23 October 1997 winter wheat was sown, and harvested on 20 August 1998. On 8 December 1998, the field was ploughed (25–30 cm) and winter wheat was sown again. A very mobile chemical (bentazone [3-isopropyl-1 *H*-2,1,3,benzothiadizin-4-(3*H*)-one 2,2 dioxide]) was applied on 7 April 1998 at a rate of 1.33 kg active ingredient ha^{-1}. Within 12 hours after bentazone application, 6 mm of rain fell, which washed off most of the chemical from the wheat crop. A moderately sorbing, persistent chemical (imidacloprid [1-((6-chloro-3-pyridinyl)-methyl)-*N*-nitro-2-imidazolidinimine] was applied on 27 May 1998 at a rate of 0.7 kg active ingredient ha^{-1}.

Table 1 Soil properties at the experimental field in Andelst. Values are averages of four samples and percentages are given by mass. Standard deviation is generally less than 10%.

Layer	Properties					
(cm)	*p*H-KCl	OM[a] (%)	Clay (%)	Silt (%)	Sand (%)	Bulk density (kg m^{-3})
0–26	7.1	2.1	28	53	19	1466
26–50	7.1	1.1	30	51	19	1508
50–70	7.4	1.0	35	51	14	1520
70–90	7.4	1.0	37	49	14	1504
90–120	7.5	1.0	37	47	16	1620

a) calculated from the organic carbon content (%OM = %OC/0.58), where 0.58 is the average C-content of organic matter (Scheffer et al. 1979).

Rainfall was measured continuously with a tipping bucket device installed at the experimental site. Soil temperatures, phreatic groundwater levels and drain discharge were measured continuously as well. Other meteorological data were obtained from meteorological station 'De Haarweg' in Wageningen, situated at 10 km from the experimental site.

Soil samples were taken from 16 soil columns (diameter 10 cm) at 1, 22, 52, 69, 125, 167, 239 and 378 days after bentazone application. Sampling was to a depth of 1.2 m. After sampling, the columns were sliced into 10 cm layers, and the concentration of the chemicals in the soil was determined. Soil water content and the dry bulk density were measured as well. A total of 16 groundwater sampling tubes were installed with filters at 1.0 – 1.2 m, 1.3 – 1.5 m and 1.9 - 2.8 m depth. Soil and groundwater samples from corresponding depths were combined to four samples and analysed for bentazone and imidacloprid. Drain water was proportionally sampled in the two drain sets using a cooled ISCO model 3700 R sampler that was attached to an ISCO 3200 flow meter.

4.3 Model parameterisation

Where possible, the input parameters were based on direct measurements, expert judgement and pedotransfer functions. Only in those cases where parameters could not be obtained in this way, was calibration carried out. This section describes the first group of parameters, the calibration parameters are described in Section 4.4.

Boundary conditions and drainage characteristics
The bottom boundary flux was calculated using the hydraulic head difference between the phreatic groundwater and the groundwater in the underlying semi-confined aquifer (Cauchy condition):

$$q_{bot} = \frac{\Phi_{aqf} - \Phi_{gwl}}{\gamma_{aqt}} \qquad (41)$$

where Φ_{aqf} (m) is the hydraulic head of the semi-confined aquifer, Φ_{gwl} (m) is the phreatic head and γ_{aqt} (d) is the vertical resistance of the acquitard. Hydraulic heads were available from continuous measurements. The measurements showed that the head gradient was generally small, so the vertical resistance was set to a small value of 5 days.

The drainage base and the drainage resistance were obtained from linear regression between measured drain fluxes and groundwater levels (Ter Horst et al. 2006). They obtained a drainage base of 0.8 m and a drainage resistance of 14 days. The so-obtained drainage resistance was assigned to the rapid drainage system (i.e. the macropores). Because the drainage resistance of the soil system as a whole (i.e. macropores and soil matrix) should have approximately the same value, we assigned a high drainage resistance of 10 times the rapid drainage resistance to the matrix drainage resistance.

Macropore geometry
In PEARL, macropore geometry is described with six parameters (Figure 7), i.e. the depth of the plough layer (Z_{Ah}), the bottom depth of the internal catchment domain (Z_{Ica}), the bottom depth of the permanent macropores (Z_{Sta}), the volume fraction of permanent macropores in the bypass domain at soil surface ($V_{Sta,byp,0}$), the volume fraction of permanent macropores in the internal catchment domain at soil surface ($V_{Sta,ica,0}$), and the shape parameter m.

The depth of the plough layer, Z_{Ah}, was set to 0.26 m. The bottom depth of the permanent macropores, Z_{Sta}, was assumed to be equal to the depth of average deepest groundwater level (1.6 m). At this level, the formation of structural shrinkage cracks due to ripening of clay will be limited. Also, biological macropore initiating processes such as the formation of holes by roots, worms, insects and small mammals are likely to be negligible (Lindahl et al. 2009). Water that is captured into macropores that end above drain depth must re-infiltrate into the soil matrix before it can reach the drainpipe, so all macropores that end above drain depth are by definition part of the internal catchment domain. Consequently, the bottom depth of the internal catchment domain was set equal to the drain depth. Shape parameter m was set to 1.0, so a linear decrease of macropore volume with depth was assumed. Total macropore volume and the distribution of the total macropore volume over the two macropore domains were obtained by calibration.

PEARL needs the effective soil matrix polygon diameter at soil surface ($d_{pol,min}$) and the effective soil matrix polygon diameter for deeper soil layers ($d_{pol,max}$). The soil matrix polygon diameter at soil surface was calculated with a pedotransfer function by Jarvis et al. (2007):

$$d_{pol,\min} = 2 * 10^{(0.409 - 0.133 f_{om}/1.724 + 0.034 f_{clay})} \quad (42)$$

where $d_{pol,min}$ (mm) is the soil matrix polygon diameter at soil surface, f_{om} (%) is organic matter content of the top soil, and f_{clay} (%) is the clay content of the topsoil. We introduced a factor of 2 into Eqn. 42, because the original pedotransfer function by Jarvis gives an expression for the effective diffusion path length. We assumed that this path length equals half the effective matrix polygon diameter d_{pol}. Eqn. 42 predicts a value of 31 mm for the topsoil. Based on structural descriptions in Smelt et al. (2001), the maximum value was set to 5 times the value of the shallow layers.

Physical properties
Soil water retention characteristics and unsaturated hydraulic conductivity characteristics were measured simultaneously using the Wind evaporation method (Halbertsma and Veerman 1997). These characteristics are represented in PEARL by the Mualem Van Genuchten functions (Van Genuchten 1980):

$$\theta(h) = \theta_r + \frac{\theta_s - \theta_r}{\left[1 + \left(\alpha |h|\right)^n\right]^m} \tag{43}$$

and

$$K(h) = K_s S_e^{\lambda}\left[1 - \left(1 - S_e^{1/m}\right)^m\right]^2 \tag{44}$$

where θ_s ($m^3\ m^{-3}$) is the saturated volume fraction of water, θ_r ($m^3\ m^{-3}$) is the residual volume fraction of water, h (m) is the soil water pressure head, α (m^{-1}) reciprocal of the air entry value, K_s (m d^{-1}) saturated hydraulic conductivity, n (-) and λ (-) are parameters, m = 1-1/n, and S_e (-) is the relative saturation, which is given by:

$$S_e = \frac{\theta - \theta_r}{\theta_s - \theta_r} \tag{45}$$

Parameters of these functions were simultaneously fitted using the RETC package (van Genuchten et al. 1991). Results of this fit are presented in Table 2.

Table 2 Parameters of the Mualem van Genuchten functions to describe the soil physical properties.

Layer	θ_s ($m^3\ m^{-3}$)	θ_r ($m^3\ m^{-3}$)	α (cm^{-1})	n (-)	λ (-)	K_s (m d^{-1})
0–26	0.405	0.050	0.0278	1.11	-9.5	0.0287
26–34	0.393	0.100	0.0075	1.11	-14.45	0.0017
34–50	0.395	0.010	0.0172	1.09	-5.8	0.0163
50–70	0.444	0.000	0.0117	1.07	-0.25	0.0251
70–120	0.442	0.050	0.0078	1.09	-7.70	0.0125

The sorptivity function (Eqn. 12) was derived from the soil hydraulic characteristics according to Parlange (1975). The so-obtained theoretical sorption can be multiplied by a factor that accounts for the effect of water repellent coatings on the surface of clay aggregates, which may hamper infiltration into these aggregates (Dekker and Ritsema 1996). Because there was no evidence that this parameter was necessary, this factor was set to the default value of 1.0, which implies no hampering effect from these coatings. Following Vanderborght and Vereecken (2007), the dispersion length was set to 0.05 m. Shrinkage characteristics were obtained from on-site measurements.

The runoff module contains two adjustable preferential flow parameters, i.e. the thickness of the mixing layer and the runoff extraction ratio (Eqn. 27-29). The thickness of the mixing layer was set to 1 cm, which is the mean of the values proposed by Sharpley (1985). The runoff extraction ratio was obtained by calibration of PEARL to the drain water concentration.

Crop data and crop water use
Parameters for crop development and crop water uptake were either based on observations, literature or default values as supplied by the model (Table 3). Crop emergence and harvest time were based on field observations (Scorza Júnior et al. 2004). The leaf area index at different times was estimated based on light interception measurements made at the soil surface (Smelt et al. 2001). The following equation was used (van Keulen and Wolf 1986):

$$f_h = \left(1 - e^{-k_e * LAI}\right) \quad (46)$$

where f_h (-) is the fraction of light intercepted by the canopy, and k_e (-) is the extinction coefficient for visible light. The extinction coefficient for visible light was assumed to be 0.6 (van Laar et al. 1992). Crop factors were taken from Feddes (1987). The decrease of the LAI and the crop factor at the end of the crop cycle results from ripening of the crop. The maximum root depth was based on field observations and was set to 1 m. Relative root density was to 1 for the 0-0.3 m soil layer, 0.2 at a depth of 0.5 m and decreases linearly to zero at 1 m depth. So the majority of the roots were in the top 0.3 m, and only a few roots following cracks and worm holes were present in the 0.5-1.0 m soil layer.

Parameter values for the reduction function for root water uptake were taken from Van Dam et al. (1997). The reduction function for root water uptake (Feddes 1978) was set to a value of 1 between h = -1 cm and h = -500 cm. No root water uptake was assumed at values $h \geq 0$ cm and h ≤ -16 000 cm. A linear decrease/increase was assumed for -1 < h 0 and -16 000 < h -500 cm. Actual soil evaporation was calculated according to Boesten and Stroosnijder (1986). Parameter β in this equation was set to 0.79 $cm^{1/2}$, which is the average of four values for clay or clay loam soils reported by Boesten (1986 p.63/64). The 'crop factor' for evaporation of bare soil was set to 1.2 (Feddes 1987).

Table 3 Crop parameters as a function of time used as input to PEARL.

Time (days) (d)	Date	LAI (m^2 m^{-2})	Crop factor (-)	Root depth (-)
-64	27-10-1997	0.05	1.2	0.05
1	01-01-1998	0.13	1.2	0.30
61	01-03-1998	0.18	1.2	0.30
91	01-04-1998	0.94	1.2	0.56
122	01-05-1998	2.70	1.2	0.83
153	01-06-1998	4.09	1.2	1.00
183	01-07-1998	2.32	0.9	1.00
232	20-08-1998	1.16	0.6	1.00

Bentazone data
The dosage of bentazone used in the simulations was 1.4 kg ha^{-1} (the average amount recovered from soil one day after application). This dosage corresponds well with the initially calculated dosage of 1.33 kg ha^{-1}. Substance data were derived from laboratory studies as described by Scorza Júnior et al. (2004). Experiments with soil-water suspensions showed that no bentazone sorption could be measured and therefore the coefficient for sorption on organic matter, K_{om}, was set to zero. Based on incubation experiments, the bentazone half-life at reference conditions, $DegT_{50,ref}$, was estimated to be 30 days and the Arrhenius activation energy equal to 74 kJ mol^{-1} (Scorza Júnior et al. 2004). The factor for the depth dependence of transformation (f_z) was set to 1.0 for the 0-35 cm soil layer, 0.5 for 35–70 cm and 0.15 below 75 cm depth. All f_z values

were calculated by dividing the measured degradation rate coefficient (k) for each layer by the measured k-value of the topsoil at reference conditions. The plant uptake parameter, f_u, was assumed to be 0.78 (Ciucani et al. 2002) and the default value of 0.7 (Boesten and van der Linden 1991) was used for parameter B in the equation of the effect of soil water on transformation (Tiktak et al. 2000 Eqn. 57).

Imidacloprid data
The dosage of imidacloprid used in the simulations was 0.55 kg ha^{-1}, which is the average amount recovered from soil two days after application. This dosage corresponds to 79 per cent of the initially calculated dosage. Equilibrium sorption input parameters were obtained from soil water suspension experiments (Scorza Júnior et al., 2004). Non-equilibrium sorption parameters were derived from incubation studies, which were combined with desorption studies in soil-water suspensions. The resulting input parameters were K_{om} = 64.4 L kg^{-1}, N = 0.81, k_d = 0.075 d^{-1} and F = 0.18. The fraction of sorption sites in contact with the macropores was set to 0.02. This value is within the range reported by Dubus et al. (2000), and is also the default value for the MACRO model. Although this parameter is considered to be highly uncertain (Dubus et al. 2001), we decided not to calibrate this parameter, because Scorza Júnior et al. (2005) showed that the sensitivity of the drainage concentration simulated with MACRO to this parameter was very small. The half-life under reference conditions for imidacloprid was obtained in the laboratory and was 91 days. Calibration of this laboratory half-life was not necessary (Scorza Júnior et al. 2005). The Arrhenius activation energy was 68.1 kJ mol^{-1}. The values of f_z were set to 1.0 for the 0-35 cm soil layer, 0.71 for 35–70 cm and 0.24 below 75 cm depth. Default values for the plant uptake parameter (f_u = 0.5) and parameter B were used.

4.4 Model calibration

Calibration strategy
As described above, three macropore parameters needed calibration, i.e. the volume of macropores at soil surface ($V_{sta,0}$), the fraction of the internal catchment domain at soil surface ($P_{ica,0}$) and the runoff extraction ratio (f_{mix}). Vanclooster et al. (2000) proposed a stepwise approach for model calibration. In this approach, firstly, the submodel for water flow is calibrated using hydrological observations. Then the pesticide fate model is calibrated against field measurements of pesticides. This strategy has worked well for models based on the convection-dispersion equation (Boesten and Gottesbüren, 2000; Tiktak et al., 1998; Scorza Júnior and Boesten, 2005). Based on this experience, we started with a parameterisation of the SWAP model delivered by Walvoort et al. (personal communication, 2010). They optimised the water flow parameters of SWAP using a Bayesian calibration method and obtained values of 0.03 m^3 m^{-3} for $V_{sta,0}$, and 0.5 for $P_{icao,0}$. During the application of PEARL it became clear, however, that it was not possible to simulate the concentration in drainage water reasonably well without adaptation of these two parameters. For this reason, observations of the maximum concentration of bentazone in drainage water were additionally used to calibrate the three preferential flow parameters (i.e. the two parameters above and the runoff extraction ratio).

The concentration in drainage water cannot be described without an appropriate description of the persistence of the substance. Therefore, we decided to test the persistence of the substance in soil first. In this test, we used the SWAP parameters delivered by Walvoort et al. (personal communication) in

combination with a runoff extraction ratio of 0.1 (i.e. the mean of plausible values reported by Gouy et al. (1999)).

Calibration results
The areic mass of bentazone in the soil profile was overestimated when degradation half-lives obtained from soil incubation experiments were used (Figure 10), so calibration of the bentazone half-life was necessary. The calibrated value was 14 days, which is slightly higher than the value of 12 days obtained by Scorza Júnior and Boesten (2005). Calibration of the degradation half-life to field persistence data is only possible if degradation is the only loss process during the calibration period. Scorza Júnior and Boesten (2005) showed that this was indeed the case: during the first 150 days after application, there was no rainfall excess and photo degradation and volatilisation were likely to be negligible because 6 mm of rain fell within 12 hours after application of bentazone. They further showed that the parameterisation of the plant-uptake module of PEARL did not affect the calibration of the degradation half-life.

Figure 10 also shows that the areic mass of imidacloprid is described well with the degradation half-life time obtained in the laboratory, so calibration of the degradation half-life of imidacloprid was not necessary.

With the optimised value of the degradation half-life, the other three parameters were calibrated. Simulations were carried out for the entire range of plausible values of the three parameters, so $P_{ica,0}$ was varied between 0.5 and 0.9, f_{mix} was varied between 0.05 and 0.20, and $V_{sta,0}$ was varied between 0.01 and 0.05 $m^3\ m^{-3}$. The peak concentration of the two substances was almost insensitive to the volume of macropores at soil surface. This is caused by the low resistance to inflow of run-off water at the soil surface, as calculated from the theoretical slit model of Bouma and Anderson (1973). Even at the lower limit of macropore width (100 µm), resistance is so low (0.001-0.01 d) that flow of run-off water into the macropores is not limited by the inflow resistance. Because of the low sensitivity to the macropore volume, this parameter was kept at its original value of 0.03 $m^3\ m^{-3}$. The remaining 20 simulations were analysed visually (Figure 11). Parameter combinations that gave good results for both substances were $P_{ica,0}$ = 0.9 and f_{mix} = 0.10-0.20. The final parameter value for f_{mix} was 0.125, because with this value the peak concentration of the two substances was within the range of observed peak values (89-91 µg/l for bentazone and 4-6 µg/l for imidacloprid).

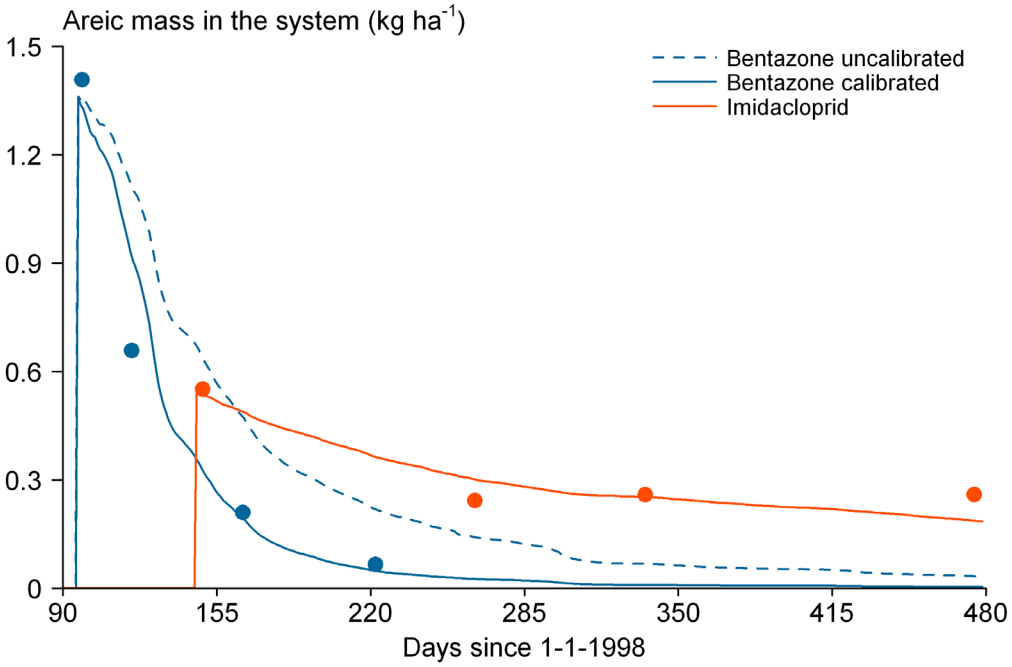

Figure 10 Measured and simulated amounts of bentazone and imidacloprid recovered from the top 120 cm of the soil profile as a function of time at the experimental field Andelst. The uncalibrated run refers to the run with DegT50 values obtained from the laboratory.

A high value for the fraction of the internal catchment domain at soil surface was necessary ($P_{ica,0}$ = 0.9). This implies that a large fraction of water entering the macropore system must re-infiltrate into the soil matrix (so is caught internally), thus reducing the fraction of rapid flow. Using results from a dye-tracer infiltration experiment in a Spanish soil, Van Schaik et al. (2010) found high values for the fraction of the internal catchment domain as well (0.9-0.99).

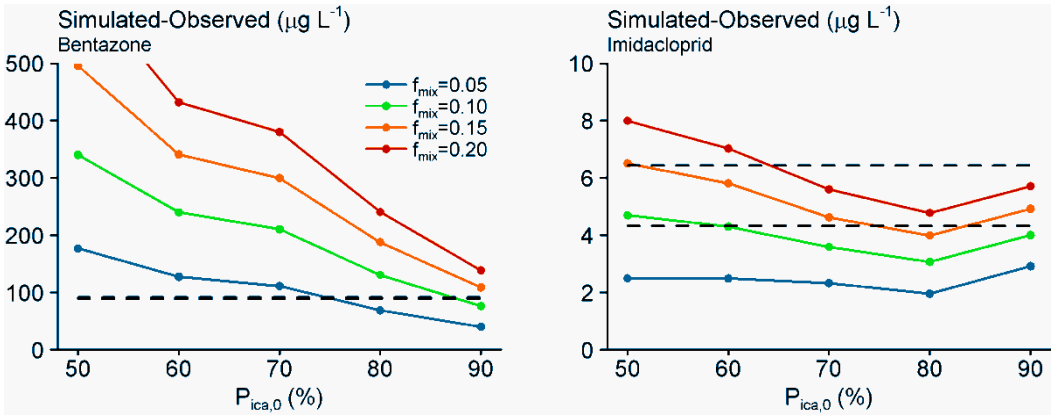

Figure 11 Comparison of the simulated and observed maximum concentration of bentazone (left) and imidacloprid (right) for 20 combinations of the fraction of the internal catchment domain ($P_{ica,0}$) and the runoff extraction ratio ($f_{mix.}$). The dashed lines represent the measurements (for bentazone, there is only one line, because the two drain sets are very close to each other).

4.5 Results

4.5.1 Water flow

Figure 12 and 13 show the results before and after calibration of the macropore parameters. As f_{mix} has no effect on water flow, the differences between the two runs are solely attributable to the difference between the values of $P_{ica,0}$ (0.5 before calibration and 0.9 after calibration). The calibration had a small effect on the simulated groundwater levels (Figure 12) but reduced the cumulative drainage fluxes by approximately 25 per cent (so the increase in volume of the internal catchment domain led to more retention of water in the soil matrix, as might be expected). Nevertheless, both runs were within the range of observed drainage fluxes. At the same time there were large differences in the simulated concentrations in drainage water, as shown in section 4.5.2. This means that it was only possible to obtain a unique calibration of the macropore parameters if measured pesticide concentrations in drainage water were used additionally. Sequential calibration strategies (Vanclooster et al., 2000), in which first the water flow model and then the pesticide fate model is calibrated, may therefore be less suitable for preferential flow models.

Groundwater levels were generally well simulated by the model (Figure 12). This was to be expected as the lower boundary condition of the model was based on observed hydraulic heads in the underlying aquifer (Section 4.3). Up to day 240, the groundwater level is below drain depth (80 cm). As a result, almost no drainage is simulated until this day, except for a small drainage event at day 115 (too small to be seen in Figure 13).

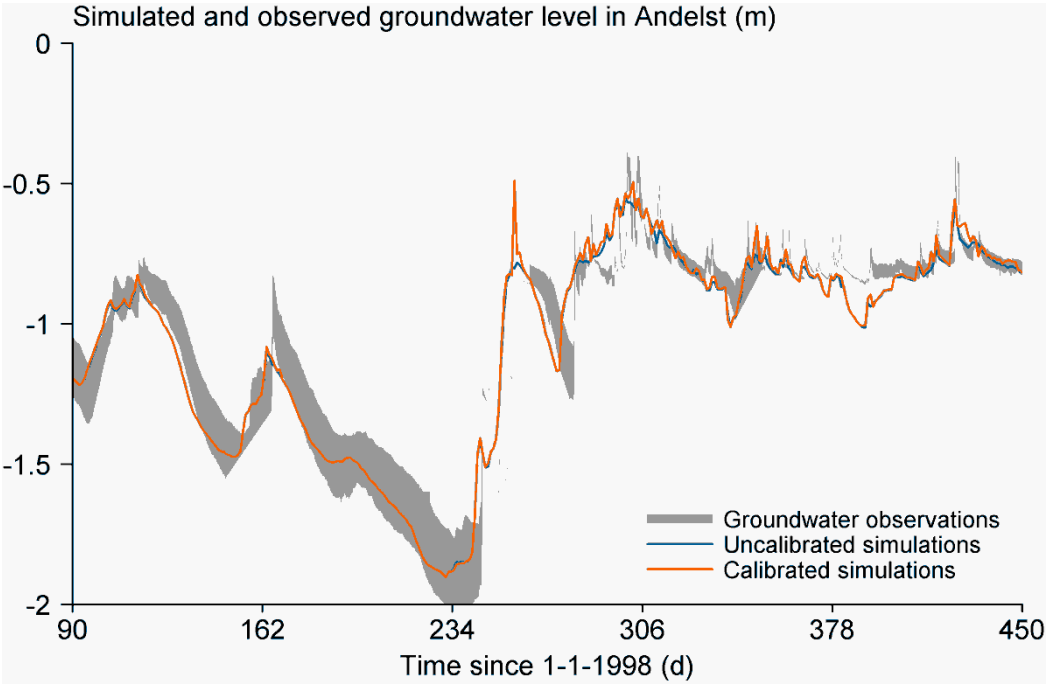

Figure 12 Simulated and observed groundwater levels at the experimental site Andelst. Groundwater levels were measured in duplo; the grey area represents the range of these duplo's.

Drainage fluxes appear to be slightly overestimated during periods with high fluxes and underestimated during periods with low fluxes (Figure 13). The reason for this is the nonlinearity visible in the drainage flux – groundwater level

relationship (Ter Horst et al. 2006 p. 17) for groundwater levels just above the drainage base. This nonlinearity can be partly explained by the geometry of the drain set. Each drain set is actually a set of three connected drainpipes (Section 4.2). Each pipe drain will start draining at a different time. In addition, the drainpipes are tilted, so the effective drain length, i.e. the part of the drain contributing to drainage, will also change with time. This could be solved by using a stepwise linear model to describe the relationship between the groundwater level and drainage fluxes (Kroes et al. 2008). This model, however, is not used within PEARL as information to parameterise this stepwise linear model is generally not available when extrapolating model results to different locations.

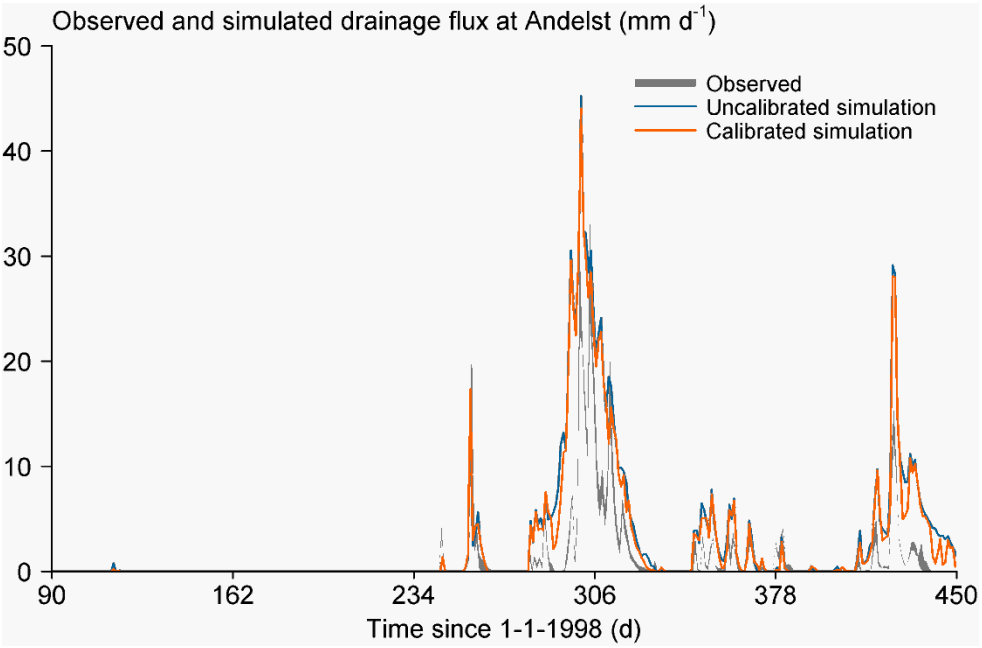

Figure 13 Simulated and observed drainage fluxes at the experimental site Andelst. The red and blue lines represent the simulations before and after calibration of the fraction of the internal catchment domain, respectively. Drainage was measured in two drain sets; the grey area represents the range of these measurements.

Soil moisture profiles that represent almost the full range of the moisture profiles of all sampling dates are shown in Figure 14. The simulations describe the measurements reasonably well. Scorza Júnior and Boesten (2005) showed that the correspondence between measured and simulated soil moisture profiles can be improved by calibration of the soil water retention characteristics. Their justification was that the hydraulic characteristics were measured in samples obtained from one soil pit, which may not be representative for the entire 1.2-ha field. Their calibration increased the saturated hydraulic conductivity to values that are not representative for the matrix of clay soils. If this value had been used in the preferential flow version of PEARL, no surface runoff and preferential flow would have been simulated. For this reason, the original uncalibrated hydraulic characteristics (Table 2) were used in our simulations. It should also be noted that the area in Figure 14 is the average plus and minus two times the standard error. The uncertainty in the individual soil moisture profiles is four times larger, because the standard error is inversely proportional to the square root of the number of samples (i.e. 16). If the standard errors of the

measurements in Figure 14 are multiplied by four, the simulations will be closer to the range of the measurements, but systematic differences will remain.

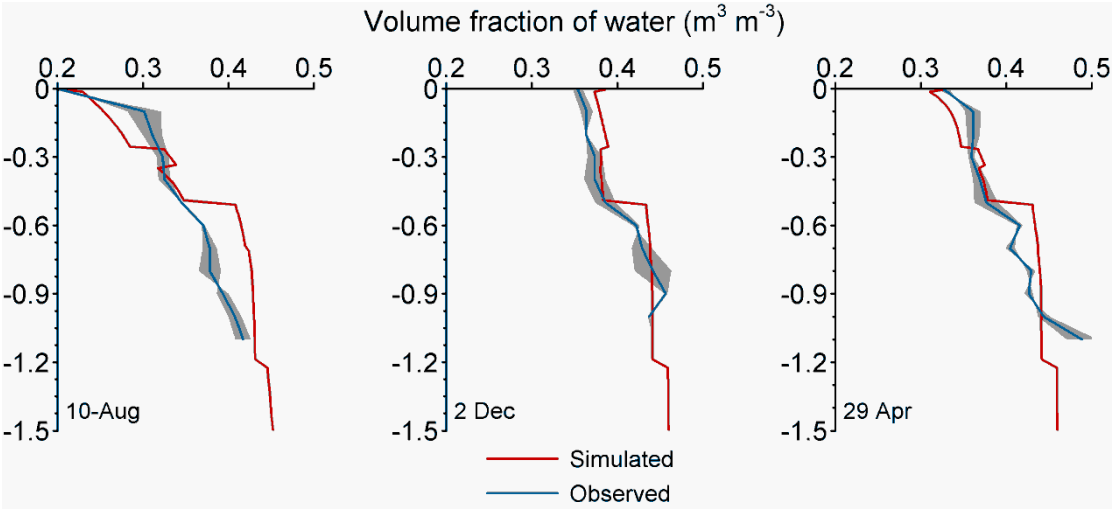

Figure 14 Measured and simulated moisture profiles at the experimental field in Andelst at April 29, June 15, August 10 and December 2. The area is the range of the measured averages plus and minus two times the standard error.

4.5.2 *Substance fate*

Both the measured and the simulated concentration profiles show that the movement of bentazone and imidacloprid in soil is fast owing to preferential flow (Figures 15 and 16). For example, bentazone is found at depths over 100 cm within three weeks after application. For both pesticides, the simulated concentration profiles show peaks at two or three depths (including the one at soil surface). Double or multi peaks in breakthrough of solutes indicate the presence of preferential flow when the solute is applied as a pulse (Villholth et al. 1998, Jury et al. 1991), which is the case in the Andelst experiment. Although the measured concentration profiles show no clear evidence of this multi peak behaviour because of lack of measurements at the depth (120-160 cm) of the deepest simulated peak, it is confirmed by the measured and simulated fast breakthrough and high concentrations in groundwater at that depth (filter 2 in Figure 18).

Breakthrough of bentazone in drain water is extremely fast (Figure 17) and occurs in a small volume (0.30 – 0.44 mm) of water (too small to be seen in Figure 13). The fast breakthrough is due to 6 mm of rain that fell shortly after application, plus an additional 55 mm that fell in the first 3 weeks after application of bentazone. Because the measurements were carried out in duplo, we are confident that these high values were not caused by measurement errors. The model could reproduce this observed fast breakthrough of bentazone well (Figure 17). High concentrations of imidacloprid (4 µg/l in drain set 1 and 6 µg/l in drain set 2) were measured during the first drainage event after imidacloprid application (which was about 2 months later than bentazone application as indicated in Figure 17). The predicted maximum concentration of 4.2 µg/l corresponds well to the initial concentration of imidacloprid measured in drain set 1. Figure 17 demonstrates that the calibration strategy based on the maximum concentration in the drainpipe worked well (Figure 11). After

calibration of the maximum concentrations of both bentazone and imidacloprid, the course of time of the drainpipe concentrations was simulated quite well.

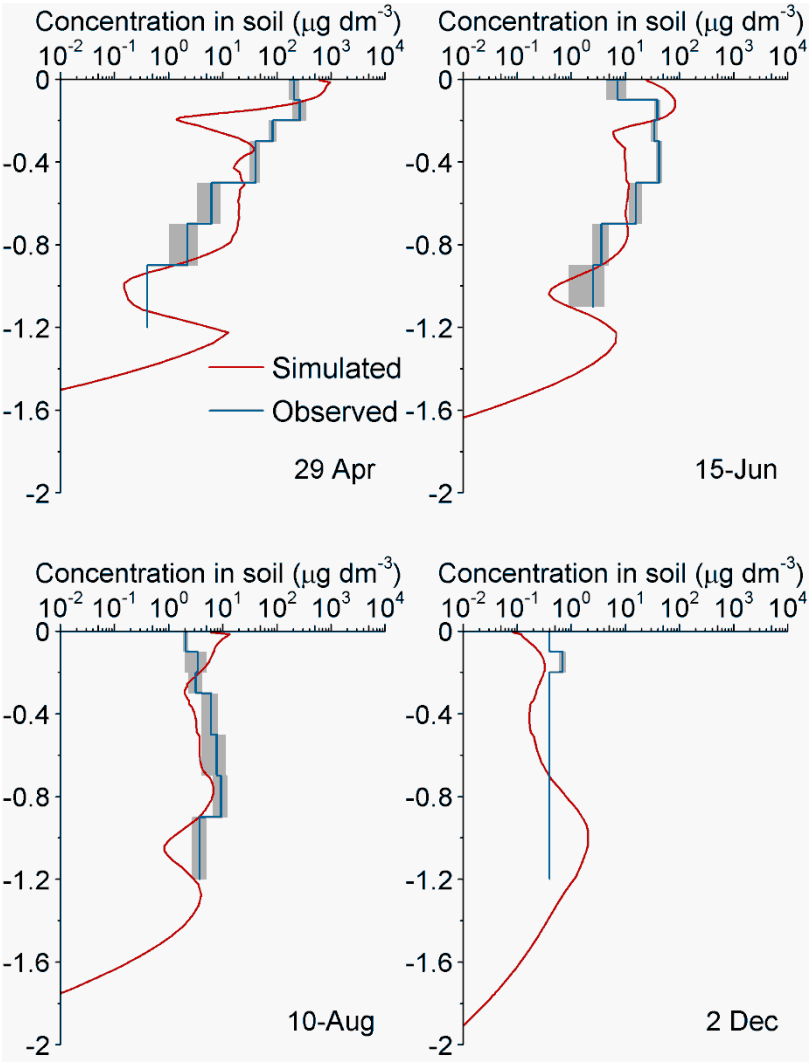

Figure 15 Measured and simulated bentazone concentration profiles at the experimental field Andelst on four sampling dates. The grey area is the range of measured averages plus and minus twice the standard error

Scorza Júnior and Boesten (2005) applied the earlier chromatographic flow version of PEARL to the Andelst field study and were not able to simulate the rapid breakthrough of bentazone and the initial drainage of imidacloprid. Also, with the PEARL parameterisation described in this chapter, the chromatographic flow version of the model could not reproduce the measured rapid movement of the two substances. For example, at the time of the initial peak in drainage water (day 119), bentazone moved to a depth of only 40 cm, which is far above the depth of the drainage system. Also, at the end of the experiment (day 449), imidacloprid moved to a depth of only 50 cm. Scorza Júnior and Boesten (2005) further showed that the concentration profile of bentazone could be described with the chromatographic flow version if an increased but physically unrealistic value of the dispersion length was used (61 cm instead of 5 cm). However, with this increased dispersion length, the movement of imidacloprid was

overestimated. Preferential flow phenomena can therefore not be adequately described with an adapted parameterisation of the convection-dispersion equation, which is in agreement with results obtained by Parker and Valocchi (1986).

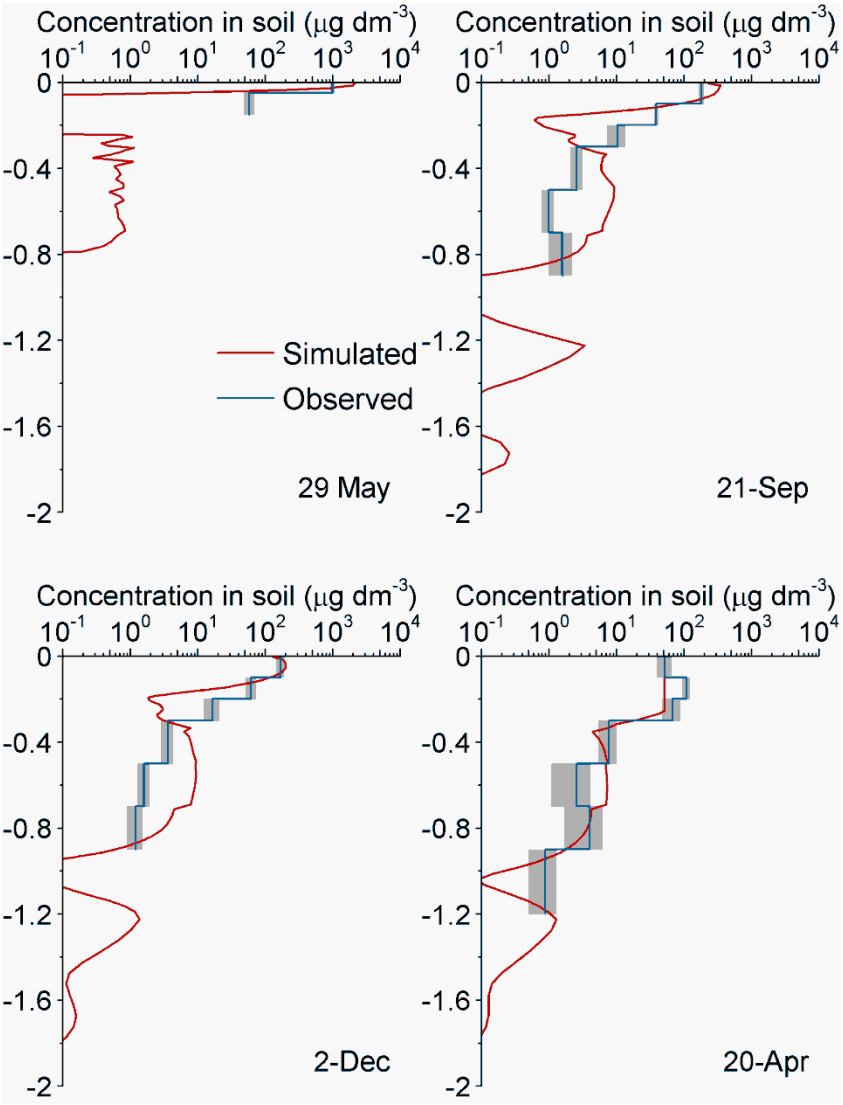

Figure 16 Measured and simulated imidacloprid concentration profiles at the experimental field Andelst on four sampling dates. The grey area is the range of measured averages plus and minus twice the standard error.

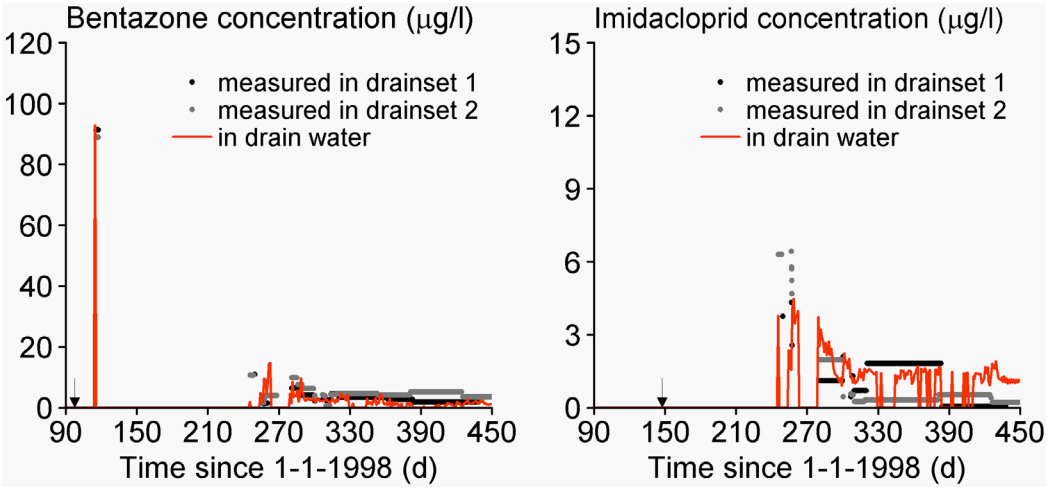

Figure 17 Measured and simulated concentration of bentazone (left) and imidacloprid (right) in drain water for both drain sets as a function of time at the experimental field site Andelst. The arrows indicate the application times of bentazone and imidacloprid.

A parameter that may affect the leaching of sorbing substances is the fraction of sorption sites in contact with the macropores. As noted before, we decided not to calibrate this parameter because Scorza Júnior et al. (2005) found a very small response of the simulated drainage concentration to this parameter. To check if this finding also applies to the PEARL model, we varied the fraction of sorption sites in contact with macropores between 0.01 and 0.04 (the lower and higher limits of the range given by Dubus et al. (2000)). Increasing or decreasing this parameter indeed changed the concentration of imidacloprid by only a few percentage points.

Bentazone was already observed in the shallow groundwater (1.0-1.2 m depth) at 22 days after application (Figure 18). The observed concentration was 16 µg/l. On that day, bentazone concentrations in soil below 0.9 m depth were below the limit of quantification of 0.8 µg dm^{-3} (Figure 15), which corresponds to a maximum bentazone concentration of 2 µg/l in the pore water of the soil matrix. This indicates that the groundwater samples are a mixture of macropore water and micropore water. This is likely to be caused by the sampling procedure: directly before sampling, the filters were pumped dry three times. The fresh water infiltrating into the tubes was sampled. It is unlikely that this water was in full equilibrium with the soil matrix.

The simulated concentration of bentazone in the bypass domain shows a fast increase followed by a rapid decrease (upper left-hand panel of Figure 18). The simulated concentration of bentazone in the liquid phase of the soil matrix at 1.0 - 1.2 m depth shows a more gradual increase (lower left-hand panel of Figure 18). This more gradual response is caused by exchange between the two flow domains, which is a rate-limited process. The maximum concentration of bentazone in the bypass domain is 125 µg/l, which is almost eight times higher than the observed value. However, in the simulations, the peak concentration was reached earlier, so it is not clear whether the predicted peak concentration is wrong. Also, as mentioned above, the observed groundwater concentration is likely to be a mixture of micropore water and macropore water. The predicted concentration of pesticide in the deeper filter is higher than the predicted

concentration of pesticide in the shallow filter, which is a result of preferential flow when the substance is applied as a pulse (Villroth et al. 1998, Jury et al. 1991).

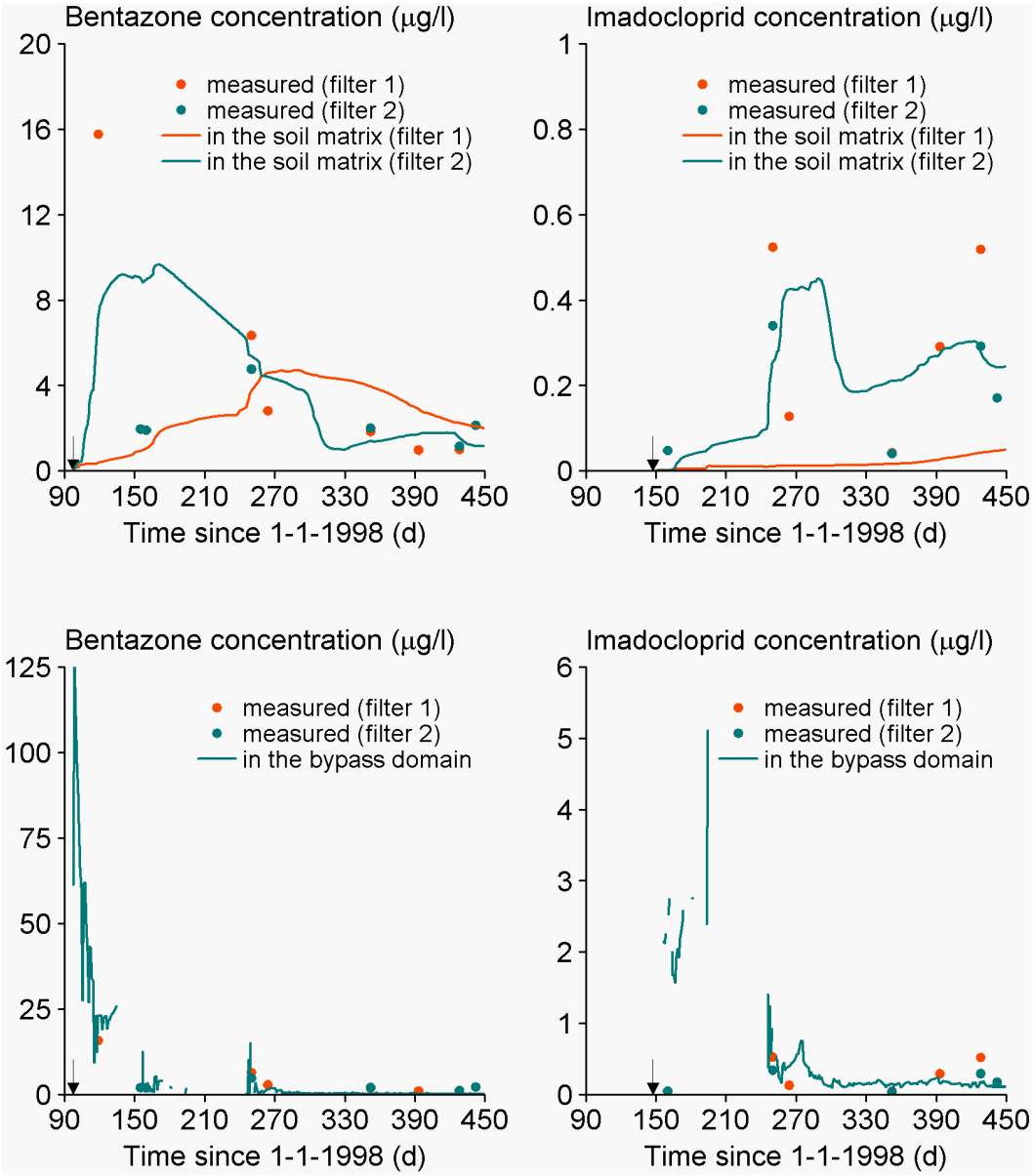

Figure 18 Measured and simulated concentration of bentazone (left) and imidacloprid (right) in groundwater from two different screen depths (1.0-1.2 m depth (filter 1) and 1.3-1.5 m depth (filter 2)). The arrows indicate the application times of bentazone and imidacloprid. The upper panel shows the concentration in the liquid phase of the soil matrix and the lower panel shows the concentration in the main bypass domain.

4.6 Conclusions

The preferential flow version of PEARL was tested against results of a field leaching study on a cracking clay soil with a mobile substance (bentazone) and a moderately sorbing, persistent substance (imidacloprid). PEARL could only correctly describe the decline of the areic mass of bentazone in the field

correctly when the degradation half-life was lowered from 30 days to 14 days. In contrast, the persistence of imidacloprid was described well. The shorter half-life of pesticides under field conditions has been reported earlier (e.g. Beulke et al. 2000), and shows that calibration of the degradation half-life is necessary in many cases.

Most preferential flow parameters could be obtained from field measurements, pedotransfer functions and general soil structural knowledge; only three preferential flow parameters (the fraction of the internal catchment domain at soil surface, the volume of macropores at soil surface and the runoff extraction ratio) needed calibration. A simple sensitivity analysis showed that the drainage concentration was almost insensitive to the volume of macropores at soil surface, so that only two sensitive calibration parameters remained. After calibration, PEARL was able to simulate the rapid breakthrough of bentazone and imidacloprid in drainage water well. This was not possible with the chromatographic flow version of PEARL, even when the dispersion length and soil physical characteristics were set to physically unrealistic values (Scorza Júnior and Boesten 2005).

For an adequate simulation of the concentration in drainage water, a high value for the fraction of the internal catchment domain was necessary. This implies that a large fraction of water entering the macropore system must re-infiltrate into the soil matrix, thus reducing the fraction of rapid flow. The importance of the internal catchment domain was also shown by Van Schaik et al. (2010).

The simulated substance concentration in the soil matrix of the saturated zone increases with depth. This is probably due to the assumption of perfect mixing of the substance in the macropore. This is a strong simplification because the macropores will usually be filled with water between drain depth (0.8 m) and the bottom depth of the permanent macropores (1.6 m) and because there seems to be no mechanism that could be responsible for this perfect mixing. So the model needs further development to be able to simulate groundwater concentrations realistically. For the drainpipe this is not a problem because the water in the drainpipe is a mixture of the liquid phase of depths between groundwater level and 1.6 m.

Following Vanclooster et al. (2000), we started with using a sequential calibration strategy, so first the water flow model was calibrated and then the pesticide fate model. The calibration parameters of the preferential flow model had only a small effect on the simulated drainage fluxes and groundwater levels. These parameters had, however, a large effect on the simulated substance concentration in drain water, so calibration of the preferential flow module was impossible without using the concentration in drain water. This complicates the calibration, as the drainage concentration is also dependent on substance properties that may need calibration, such as the degradation half-life. In this study, a manual calibration procedure was applied, in which first the degradation half-life was calibrated and then the preferential flow parameters. A Bayesian calibration method could be considered in future applications, because this is more objective and also gives insight into parameter sensitivity and uncertainty.

5 Parameterisation of the Andelst scenario

5.1 Introduction

The Andelst dataset covers a period of approximately one year. Because the exposure assessment should be carried out for multiple years (Chapter 1), the dataset was extended to a 15-year period using data from a weather station at a distance of 40 km and from a neighbouring groundwater observation well. How this was done, is described in Section 5.2. Section 5.3 describes the effect of the crop parameterisation on the simulated drainage concentration. Section 5.4 presents example calculations with bentazone and imidacloprid (i.e. the test substances described in Chapter 4). Appendix 1 gives an overview of all scenario parameters.

5.2 Extension of the Andelst dataset to a 15-year dataset

To extend the Andelst dataset to a long-term dataset, additional data are needed on the lower boundary condition of SWAP (the hydraulic head of the first aquifer) and weather conditions (daily minimum and maximum temperature, daily precipitation, daily rainfall duration and potential evapotranspiration). In the Andelst scenario, it was further assumed that winter wheat was grown each year (emergence date October 27 and harvest date August 20). To avoid ploughing the field when the crop was present, the ploughing date was changed from December 8 in the Andelst field study to October 15 in the Andelst scenario. The plough depth was set to 20 cm, because this is the plough depth used in GeoPEARL. Moreover, the PPR-Panel considered 20 cm a representative value for European agricultural practice (EFSA 2010). Table 4 lists the differences between the Andelst field dataset and the Andelst scenario.

Observations of hydraulic heads are available in the DINO ('Data en Informatie van de Nederlandse Ondergrond') database (www.dinoloket.nl). We checked all bore holes within 5 km of the Andelst field site for suitable data and selected bore hole B39H0311, which is situated at approximately 1 km from the field site. In this bore hole, hydraulic heads were available for the period 1991-2005. For the year 1998, the hydraulic heads obtained in bore hole B39H0311 showed the same temporal pattern as the measurements at the Andelst field site, but the mean value was 13 cm lower (Figure 19). This difference is likely to be caused by differences in altitude between the two fields. After correction of the dataset for this altitude difference, the dataset was judged acceptable for extrapolating the Andelst data set. The full dataset is shown in Figure 20.

Daily weather data from station 260 'De Bilt' (at a distance of 40 km from the field site) was downloaded from the website of the Royal Netherlands Meteorological Institute (www.knmi.nl) and converted to the format needed by PEARL. The preferential flow version of PEARL needs information on precipitation events (i.e. start and end time of a precipitation event and amount of precipitation). The KNMI dataset gives the daily rainfall duration only. We therefore made the simplifying assumption that all rain fell in the first hours of the day, with the number of hours being equal to the rainfall duration.

Following FOCUS (2000), a warm-up period was added to the dataset. For this purpose, the data for the period 2001-2005 was copied to the period 1986-1990 (after correction for leap years), so the total length of the dataset is 20 years.

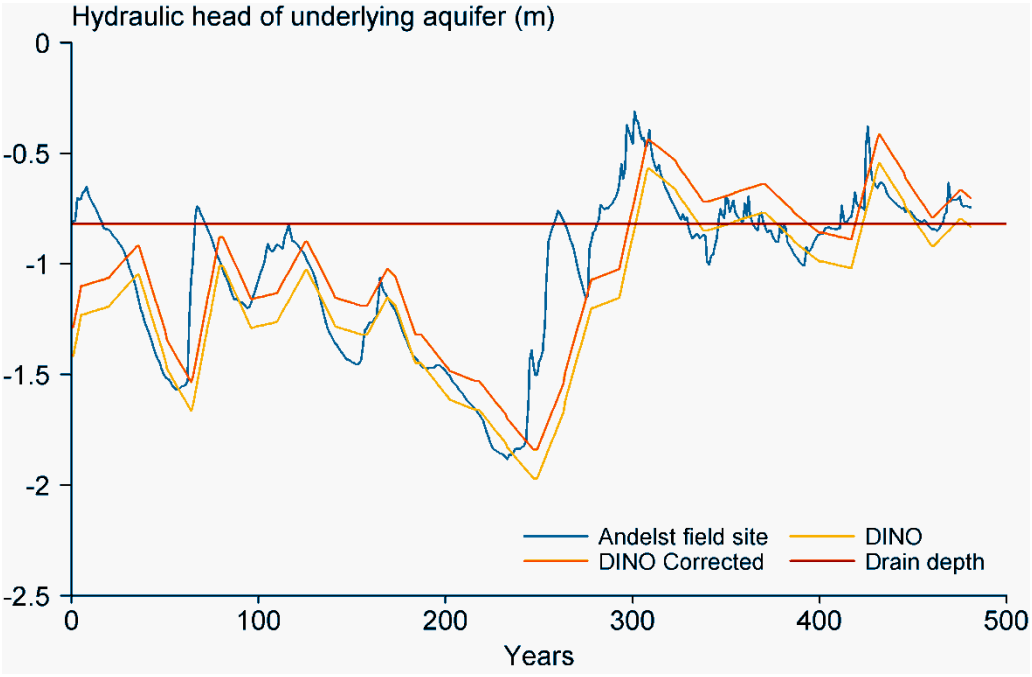

Figure 19 Hydraulic head observed at the Andelst field site and at DINO bore hole B39H0311. The yellow line shows the original observations, the red line shows the hydraulic head corrected for the altitude difference.

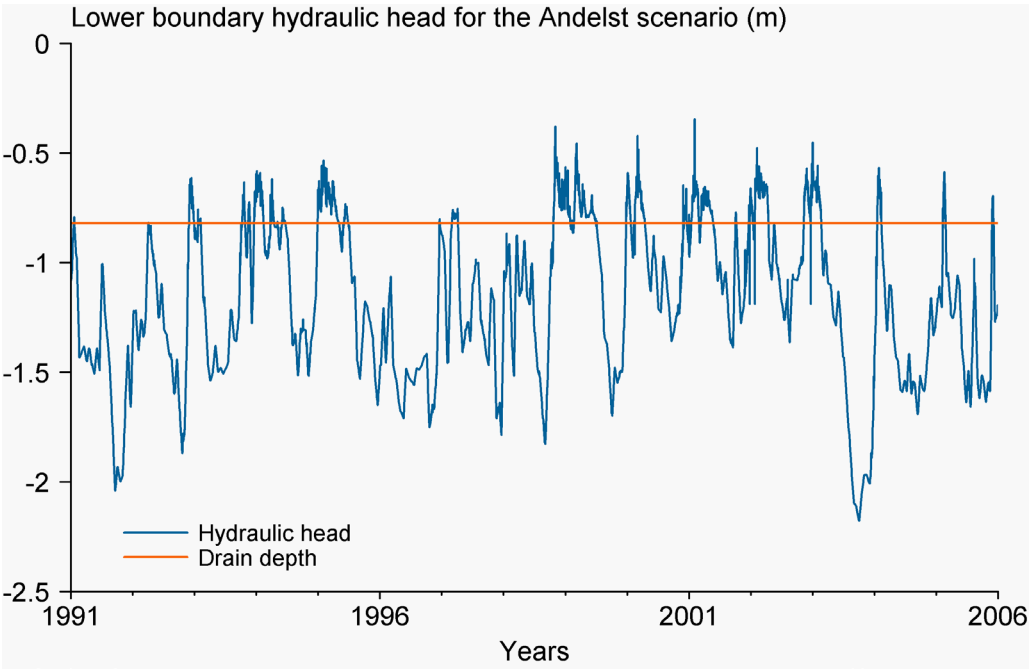

Figure 20 Hydraulic head as a function of time observed in DINO groundwater well B39H0311 after correction for altitude differences. This observation well is situated at approximately 1 km from the Andelst field site. Monitoring data were available for the period 1991-2005. The period 1986-1990 (not shown) is a copy of the period 2001-2005, and is used as a warm-up period.

Table 4 Overview of differences between the Andelst field dataset and the Andelst scenario. Resulting peak concentrations are discussed in Section 5.3.

Property	Andelst field dataset*	Andelst scenario
Time period	April 1998 until April 1999	1991-2005 (first five years copied to obtain a warm-up period).
Weather data	Rainfall measured on-site, other parameters from weather station Wageningen at 10 km from site.	Weather station De Bilt at 40 km from site. Rainfall assigned to first hours of day.
Hydrological lower boundary condition	Measured on-site.	Fortnightly measurements from a groundwater bore hole at 1 km from site.
Plough date and depth	December 8, 26 cm	October 15 each year, 20 cm
Root density distribution	As observed at Andelst site	Conform FOCUS (2000), i.e. uniform.
Pesticide applications	One pesticide application.	Annual applications of pesticide.
1998 peak concentration in drainpipe (µg L^{-1}).		
bentazone	92 (measured 89-91)	20
imidacloprid	4.3 (measured 4-6)	9

*) original calibration, see Section 5.3 for details.

Table 5 shows the mean annual water balance for the Andelst scenario. Actual evapotranspiration is 405 mm a^{-1}, which is judged plausible for winter wheat in the Netherlands. Actual transpiration, however, is low. This is caused by the shallow rooting depth observed at the Andelst field site (Chapter 4). As a result of this shallow rooting depth, transpiration is reduced by low soil water pressure heads that occur frequently in the top soil. Transpiration reduction for this site is, however, not plausible as sufficient water is available in the deeper parts of the soil profile. It is generally acknowledged that plants preferentially take up water from moist soil layers, hence optimising crop water use (Tiktak and Bouten 1994, Javaux et al. 2011, Attinger and Hildebrandt 2011). The effect of the shallow root density distribution was confirmed in an additional run in which a homogeneous (and therefore deeper) root density distribution was assumed. This run showed a transpiration of 170 mm a^{-1} which is close to the potential reference transpiration (183 mm a^{-1}) and therefore a more realistic value. The working group therefore decided that a uniform root density distribution should be the basis for the crop parameterisation in the scenario.

Drainage is dominated by rapid flow (bypass drainage is approximately 280 mm a^{-1} and matrix drainage 70 mm a^{-1}), which means that preferential flow through macropores is the dominant flow mechanism in this soil. The matrix still plays an important role in this scenario, however, as 458 mm a^{-1} infiltrates into the internal catchment domain and only 53 mm into the bypass domain. Water captured in this domain must infiltrate into the soil matrix before it can reach the drainpipe. Notice that the water balance of the macropores is hardly affected by the root length distribution. This was expected as the water balance of the macropores is strongly influenced by top surface processes (runoff into the macropores).

Table 5 Water balance (mm a^{-1}) for the period 1991-2005. Lines in italics represent internal balance terms. The adapted run refers to a run with a uniform root length distribution (see text).

Balance term (mm a^{-1})	Original	Adapted
Precipitation	860	860
Seepage at lower boundary	102	42
Evaporation of intercepted water	28	27
Soil evaporation	277	270
Transpiration	110	170
Drainage from soil matrix	70	67
Drainage from macropore domain	281	283
Infiltration into the soil matrix	*322*	*322*
Runoff into internal catchment domain	*415*	*415*
Runoff into bypass domain	*47*	*47*
Precipitation into the internal catchment domain	*43*	*43*
Precipitation into the bypass domain	*6*	*6*
Flux from internal catchment domain into micropore domain	*481*	*481*
Flux from micropore domain into internal catchment domain	*23*	*23*
Flux from bypass domain into micropore domain	*167*	*170*
Flux from micropore domain into bypass domain	*397*	*402*

The transient boundary condition shown in Figure 20 causes a large variability of the annual drainage fluxes across the years (Figure 21). In 20 per cent of the years (1991, 1996 and 1997), drainage towards the field ditch is close to zero. The maximum value of the annual drainage flux is 940 mm a^{-1}. This value is higher than the annual precipitation rate for that year, which is caused by upward seepage from the regional groundwater system. Upward seepage causes dilution of drainpipe water, which implies that the highest discharge of water towards field ditches does not necessarily coincide with the highest discharge of substances (Figure 24).

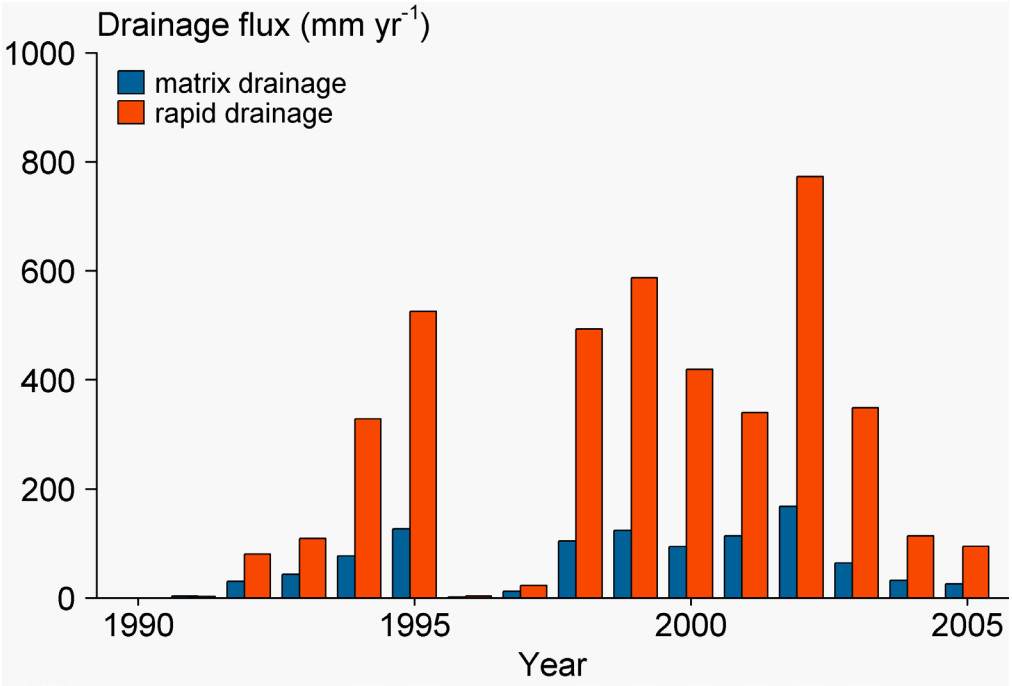

Figure 21 Flux of water towards the field ditch in the drainpipe exposure scenario.

5.3 Crop parameterisation

The simulations described in this report considered winter wheat only, because that was grown at the Andelst field site. However, the working group considered simulations with winter wheat not appropriate in all cases, because many plant protection products are applied in spring when winter wheat is already well developed. For this reason, the final scenario will be run in combination with crops described by FOCUS (2000, 2011). We selected the Hamburg scenario for this purpose, because this scenario is in the same FOCUS climatic zone as the Andelst scenario. All crop properties were taken from the FOCUS database, except for the crop factor which was recalculated to match Makkink reference evapotranspiration (Feddes 1987). This means that the crop factors were multiplied by a factor of 1.0-1.3, depending on the time in the growing season (cf. Table 5 in Feddes 1987). Resulting crop factors are shown in Table 6.

Table 6 Crop factors relative to Makkink reference evapotranspiration (f_{crp}) as a function of crop development stage (DVD) for five FOCUS crops. The dates are the emergence and harvest date, respectively.

Winter cereals (01-Nov to 10-Aug)		Spring cereals (01-Apr to 20-Aug)		Maize (05-May to 20-Sep)		Sugar beet (15-Apr to 08-Oct)		Potatoes (10-May to 15-Sep)	
DVD	f_{crp}	DVD	f_{crp}	DVD	f_{crp}	DVD	f_{crp}	DVD	f_{crp}
0.00	0.0	0.00	0.0	0.00	0.0	0.00	0.0	0.00	0.0
0.65	0.2	0.47	0.9	0.63	1.2	0.78	1.2	0.56	0.7
0.75	1.1	1.00	0.9	1.00	1.2	1.00	1.2	1.00	0.7
1.00	1.1								

In contrast to the Andelst crop parameterisation, FOCUS assumes a uniform distribution of roots with depth. In Section 5.2, we demonstrated that a uniform root density distribution leads to more efficient crop water use. Simulations with a uniform root length distribution lead to higher substance concentrations in the drainpipe (125 µg L^{-1} for bentazone and 6 µg L^{-1} for imidacloprid). These concentrations are still close to the range of observed values. Results of this recalibration exercise are shown in Figure 22.

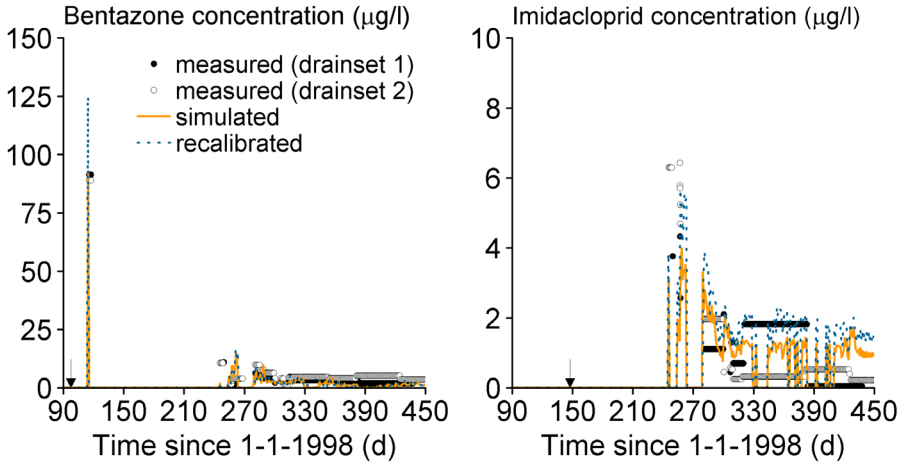

Figure 22 Measured and simulated concentration of bentazone (left) and imidacloprid (right) in drain water for both drain sets as a function of time at the experimental field site Andelst. The arrows indicate the application times of bentazone and imidacloprid. The original simulation is the simulation described in Chapter 4. The blue dashed line refers to the simulation with a uniform root density distribution.

The effect of crop type on the simulated water balance for five FOCUS crops (winter cereals, spring cereals, maize, sugar beet and potatoes) is shown in Table 7. Transpiration of the FOCUS crops ranges from 164 mm a^{-1} for winter cereals to 210 mm a^{-1} for spring cereals. The higher transpiration is generally compensated for by a lower bottom boundary flux. Effect of crop type on drainage is generally small.

Table 7 Water balance (mm a^{-1}) simulated for five FOCUS Hamburg crops and for the original Andelst winter wheat crop for the period 1991-2005.

Crop	P	Q_{bot}	E_{int}	E_{sol}	E_{trp}	Dr_{mat}	Dr_{byp}
Andelst, original	860	102	28	268	110	71	280
Andelst, adapted	860	42	27	270	170	67	283
Winter cereals	860	35	23	284	164	68	286
Spring cereals	860	19	29	260	210	68	274
Maize	860	39	28	269	171	69	283
Sugar beet	860	28	34	255	196	70	277
Potatoes	860	39	28	269	171	69	283

P is precipitation, Q_{bot} is bottom boundary flux, E_{int} is evaporation of intercepted water, E_{sol} is soil evaporation, E_{trp} is transpiration, Dr_{mat} is drainage from soil matrix and Dr_{byp} is drainage from bypass domain.

5.4 Example calculations

Example calculations were carried out with the two test substances that were applied in the Andelst field study, i.e. bentazone and imidacloprid. Calculations were done with the adapted crop parameterisation for the Andelst field site, so a uniform root density distribution was assumed. The substances were surface applied annually (in accordance with FOCUS 2000). Dosage and application times were kept at the values used in the Andelst field study, so bentazone was applied each year on 7 April (dosage 1.4 kg ha^{-1}) and imidacloprid on 27 May (dosage 0.55 kg ha^{-1}).

Effect of boundary conditions

To investigate the effect of using a different lower boundary condition, we performed a simulation with only one substance application. Application rates and times were equal to the application rates and times for the Andelst field study, the on-site measured meteorological data was used, and no warm-up period was assumed. Results shown in Figure 23 indicate that the bentazone peak directly after application is not simulated. The reason is that the groundwater level is not above drain depth on that particular day. Observations at the DINO bore hole have a lower temporal resolution (they are done on a fortnightly basis, whereas the on-site observation are done at a daily basis). Results further show that a peak is simulated for both substances around day 160. On this day, the simulated groundwater level is above drain depth when using the DINO lower boundary condition. The different boundary conditions cause different values of the peak concentration for the year 1998 as shown in Table 4.

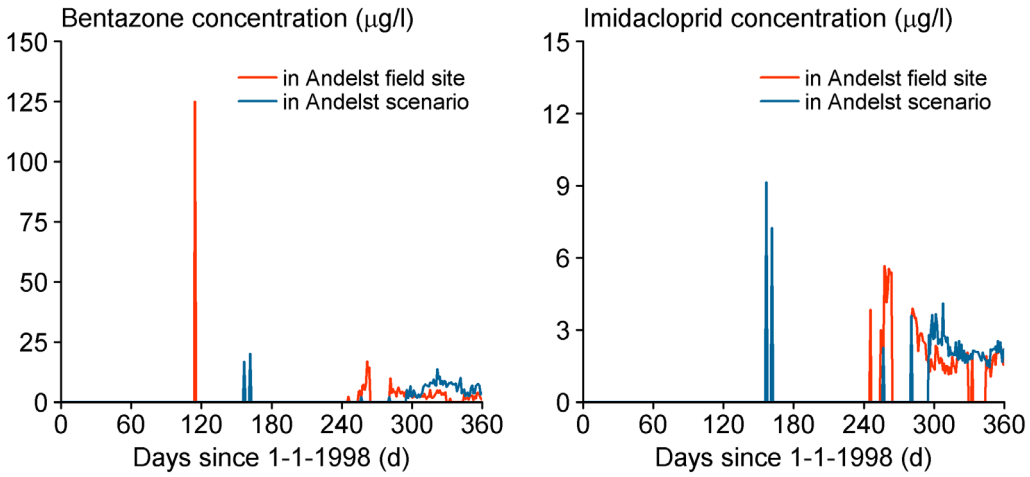

Figure 23 Simulated concentration of bentazone (left) and imidacloprid (right) in drain water as a function of time at the experimental field site Andelst. The blue line indicates the simulation with the lower boundary condition observed at the field-site, the red line indicates the simulation with the lower boundary condition observed at the DINO bore hole. In the simulations the substances were applied only in 1998.

Although the model calibration and the scenario selection were carried out with great care and although this work took considerable research efforts over a period of several years, the uncertainty in the predicted peak concentrations in the Andelst scenario is still considerable: the results in Table 4 suggest that the true peak concentrations may be several times higher or lower than the predictions.

Comparison of Figure 23 and Figure 24 reveals that the concentration of imidacloprid in drainage water is higher in the long-term simulations than in the short-term simulations. This effect is not found for bentazone, and can be explained by the longer degradation half-life of imidacloprid. In contrast to bentazone, this substance slowly accumulates in the soil system (Table 8). Because of the rapid exchange between the substance and the macropores, this results in increased drainage concentrations in the long-term simulations.

Results of long-term simulations

Results of the long-term simulations in Figure 24 indicate that the maximum concentration of bentazone in drain water is higher than the maximum concentration of imidacloprid in drain water (130 versus 23 µg/l). However, in eight out of fifteen years, the concentration of imidacloprid in drain water is higher. Corrected for the difference in dosage (1.4 kg ha^{-1} for bentazone and 0.55 kg ha^{-1} for imidacloprid), these differences are even higher. This somewhat counterintuitive behaviour can be explained from the substance balance (Table 8), which shows that drainage is dominated by transport through the macropores. Substances can enter the macropores in two ways, i.e. runoff and exchange between the soil matrix and the macropores. Runoff can only occur if the substance is still present in the mixing layer. Due to the short degradation half-life and the low K_{om} value, bentazone has often disappeared from the top 1 cm before the first runoff event. Imidacloprid has a longer half-life and is less mobile, so its residence time in the mixing layer is longer. As a result, runoff of imidacloprid into the macropores is generally higher than bentazone runoff. Comparable results were obtained by Larsson and Jarvis (2000). They observed

that leaching of some very mobile compounds was actually reduced by macropore flow.

Substance that has entered the internal catchment domain cannot reach the drainpipe without re-infiltration into the soil matrix. Again, the short degradation half-life of bentazone causes rapid removal of the substance that re-infiltrates into the soil matrix at shallow depths and, hence, reduces drainage. Part of the substance in the internal catchment domain, however, re-infiltrates the soil matrix at greater depths (the maximum depth of the internal catchment domain is at drain depth). Substance that re-infiltrates at these depths is assumed not be degraded. Because the soil is often near-saturated at drain depth, there is a strong interaction between the soil matrix and the macropores at this depth. Therefore, exfiltration from the internal catchment domain enhances drainage through the bypass domain. Moreover, the current version of PEARL assumes no degradation in the macropores.

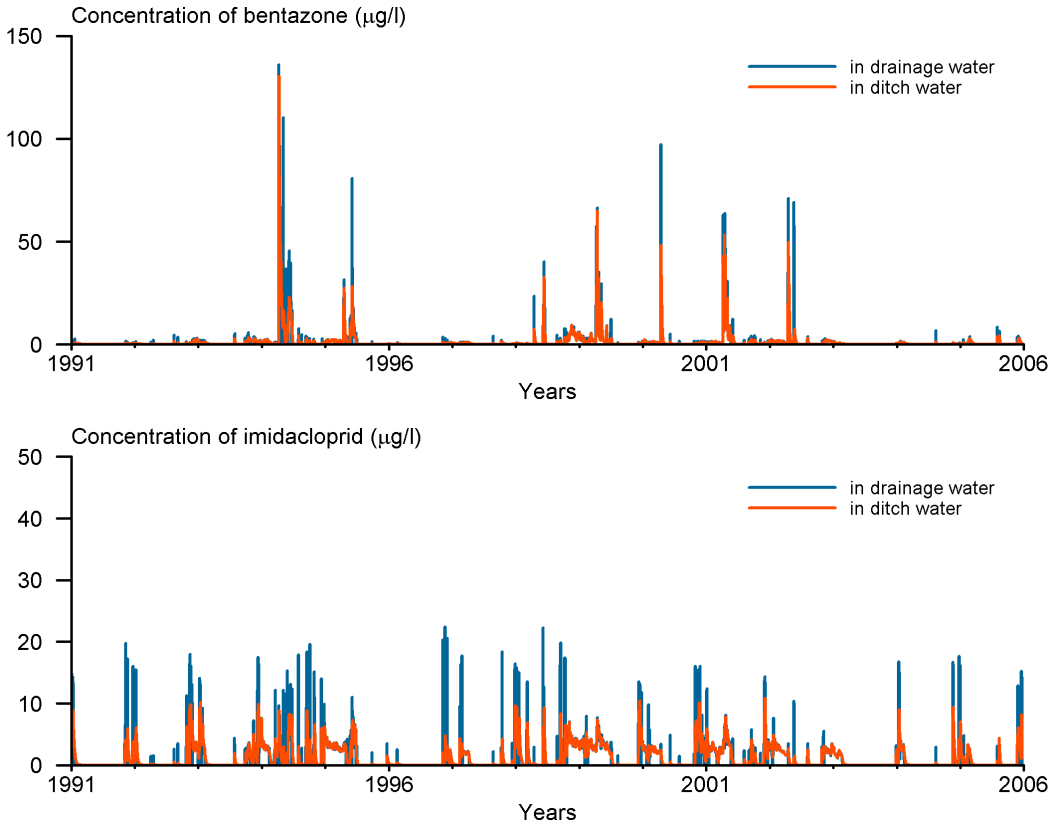

Figure 24 Predicted concentration of bentazone (upper panel) and imidacloprid (lower panel) in the drainpipe exposure scenario. The substances are applied annually. The blue line shows the concentration in drainage water, the red line shows the predicted initial concentration in the adjacent ditch, using the TOXSWA metamodel.

Figure 24 can be used to derive the maximum annual concentrations in drain water. This results in 15 peak concentrations that can be used to construct a temporal cumulative distribution function (Figure 25). Results in figure 25 show that the temporal distribution function of bentazone is more skewed than the frequency distribution function of imidacloprid, which confirms the findings above. The absolute difference between the two substances is also influenced by

the different dosage of the two substances (1.4 kg ha^{-1} for bentazone and 0.55 kg ha^{-1} for imidacloprid).

Figures 24 and 25 show also the predicted initial concentration in the adjacent ditch calculated with the TOXSWA metamodel. Metamodel parameters were set to the values in Section 3.5, so a treatment ratio of 100 per cent was assumed. The volume of the ditch followed from the scenario selection of the drift exposure scenario (Tiktak et al. 2012b), and was set to 0.55 m^3 m^{-1}. Figure 25 shows a dilution factor of 30-50 per cent, indicating that the maximum concentration often occurs during relatively small drainage events.

Table 8 Substance balance (% of the applied dosage) for the period 1991-2005 for the substances bentazone and imidacloprid. Lines in italics represent internal balance terms.

Balance term (% of the applied dosage)	Bentazone	Imidacloprid
Storage change	0.00	0.20
Degradation	77.27	94.52
Uptake	22.16	3.15
Drainage from micropore domain	0.08	0.41
Leaching	0.01	0.00
Drainage from macropore domain	0.48	1.73
Runoff into internal catchment domain	*6.53*	*9.99*
Runoff into bypass domain	*0.73*	*1.12*
Flux from internal catchment domain into micropore domain	*6.59*	*10.84*
Flux from micropore domain into internal catchment domain	*0.06*	*0.86*
Flux from bypass domain into micropore domain	*0.85*	*1.88*
Flux from micropore domain into bypass domain	*0.61*	*2.49*

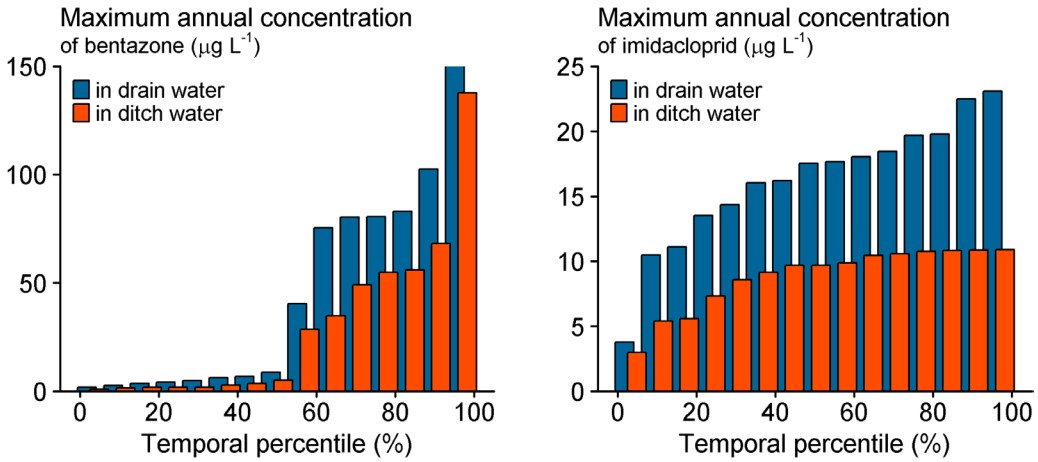

Figure 25 Predicted cumulative distribution function of the maximum annual peak concentration for bentazone (left panel) and imidacloprid (right panel). The blue bars show the concentration in drain water, the red bars show the predicted concentration in the adjacent ditch, using the TOXSWA metamodel.

Effect of crop type

Figure 26 shows the effect of crop type on the simulated temporal frequency distribution of bentazone and imidacloprid in ditch water. In contrast to the previous paragraphs, application was carried out on the date of crop emergence and ploughing was done one month before crop emergence. So the two substances were applied in autumn in the case of winter wheat and in spring in

the case of the other four crops. As a result, the simulated concentrations are higher for winter wheat than for the other four crops.

Winter cereals and sugar beet were considered the most appropriate crops, because these two crops are predominantly grown on soils where preferential flow is important. Also, the crop factors for these two crops are relatively close to the crop factor of winter wheat at the Andelst field site.

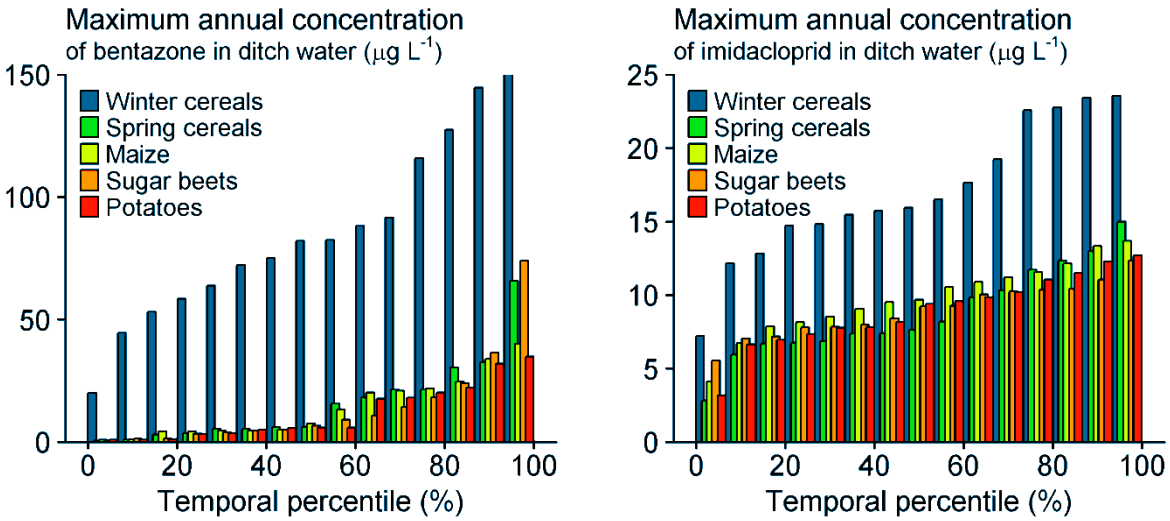

Figure 26 Predicted cumulative distribution function of the maximum annual peak concentration for bentazone (left panel) and imidacloprid (right panel) in ditch water for five FOCUS crops. The cumulative distribution functions were derived from the 15 maximum annual concentrations according to the procedure described above Figure 25. Substances were applied one day before crop emergence.

6 Calculation of the overall 90th percentile with GeoPEARL

In the previous chapters, we have shown that the exposure assessment for the Andelst scenario gives 15 annual maximum concentrations. The spatially distributed pesticide fate model GeoPEARL is used to determine which of these annual peak concentrations corresponds best to the 90th percentile of the exposure concentration in all ditches. This chapter describes the parameterisation and application of the preferential flow version of GeoPEARL.

6.1 Model parameterisation

A standard GeoPEARL assessment consists of PEARL simulations for 6 405 map units (Tiktak et al. 2002, 2003). These map units (also called 'plots') are characterised by unique combinations of climatic district, hydrotype, groundwater depth class, land-use type, and soil type (Figure 27). The bottom boundary condition of the hydrological sub-model SWAP consists of a long-term average soil water flux on which a sine-function with a fixed amplitude is imposed (Kroon et al. 2001). This flux is obtained from a link between the stationary regional groundwater model NAGROM and SWAP.

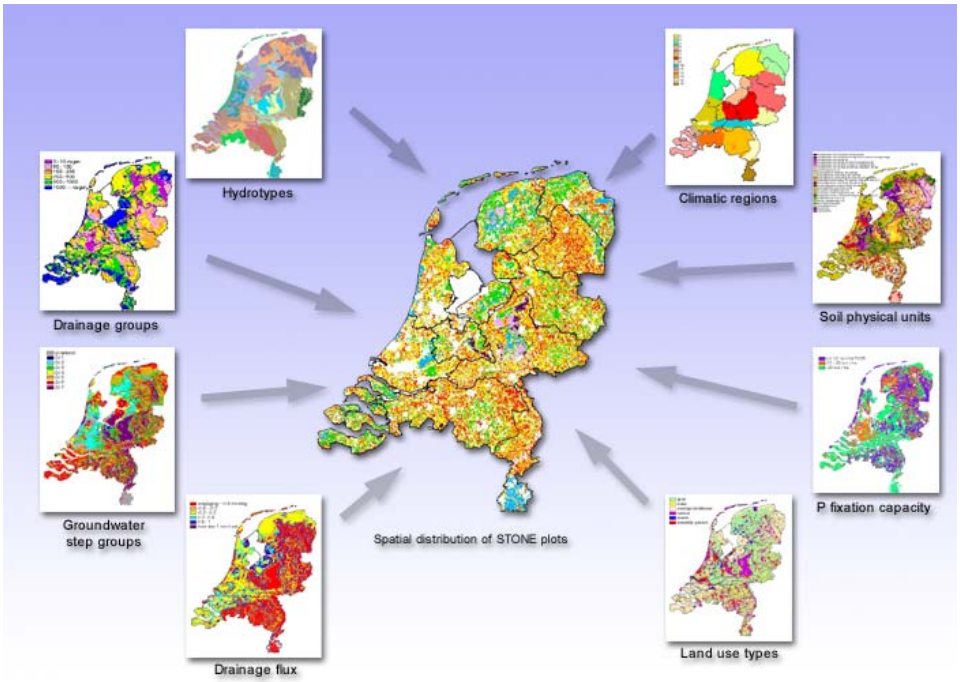

Figure 27 Procedure for creating the spatial schematisation for GeoPEARL. This procedure was originally developed for the Dutch Model for Emission of Nutrients, STONE (Kroon et al. 2001).

Parameters of the preferential flow module had to be assigned to all these map units. Because direct measurements of these parameters were not available at the regional scale, pedotransfer functions were developed. These pedotransfer functions relate the characteristics of the macropore system to generally available data, particularly clay content, organic matter content, soil moisture characteristics and the mean lowest groundwater level. Experimental results from nine locations (Bronswijk and Evers-Vermeer 1990, Smelt et al. 2001,

Scorza Júnior 2004, Van der Salm et al. 2006, Van Beek et al. 2008) were available for the construction of these pedotransfer functions.

Some macropore parameters were only available where high quality field experiments were conducted (Andelst (Smelt et al. 2001, Scorza Júnior et al. 2004), De Bouwing (Hendriks et al. 1999) and Waardenburg (Van der Salm et al. 2006, Van Beek et al. 2008)). The most crucial dataset was the Andelst field experiment. This field-scale experiment was conducted in a pipe-drained cracking clay soil to study the movement of water and two PPPs with contrasting mobility (bentazone and imidacloprid).

6.1.1 *Basic data*

The macropore pedotransfer functions relate the characteristics of the macropore system to generally available spatially-distributed parameters, particularly clay content, organic matter content and mean lowest groundwater level. The mean pipe drain-depth is another important parameter, because rapid drainage cannot occur if the groundwater level is below the depth of the drainpipes. These four parameters are available in the GeoPEARL database (Figure 28). Only drained soils are shown, because the population of interest is limited to these soils (Chapter 1).

Clay and organic matter
We started the construction of the macropore pedotransfer functions with the assumption that all static macropores are structural shrinkage cracks due to ripening of clay (Section 6.4). Clay content is therefore a crucial soil parameter. In the Netherlands, drained soils can roughly be subdivided into two groups based on clay content, i.e. rigid, non-shrinking sandy soils with a clay content less than 8 per cent and shrinking clayey soils with a clay content over 8 per cent (Figure 28). The clayey soils can further be distinguished into fluvial clays in the centre of the country and maritime clays in the coastal regions. Highest clay contents (> 50 per cent clay) are found in fluvial deposits. Organic matter content is strongly correlated with clay content, so highest organic matter contents are generally found in areas with high clay contents.

Groundwater level and pipe drain depth
The Mean Lowest Groundwater Level (*MLG*) is another important parameter, because formation of shrinkage cracks is generally limited to this depth (Section 6.1.4). Mean lowest groundwater level is generally shallow (80-100 cm) in the river Rhine region and deep in the coastal clay region. Pipe drain-depth follows roughly the same spatial pattern, with the deepest drains occurring in recently reclaimed polders.

6.1.2 *Macropore geometry*

In PEARL, macropore geometry is described with six parameters (Figure 7), i.e. the depth of the plough layer (Z_{Ah}), the bottom depth of the internal catchment domain (Z_{Ica}), the bottom depth of the permanent macropores (Z_{Sta}), the volume fraction of permanent macropores in the bypass domain at soil surface ($V_{Sta,byp,0}$) the volume fraction of permanent macropores in the internal catchment domain at soil surface ($V_{Sta,ica,0}$), and the shape parameter m. Parameters are further needed for the polygon diameter and the shrinkage characteristics.

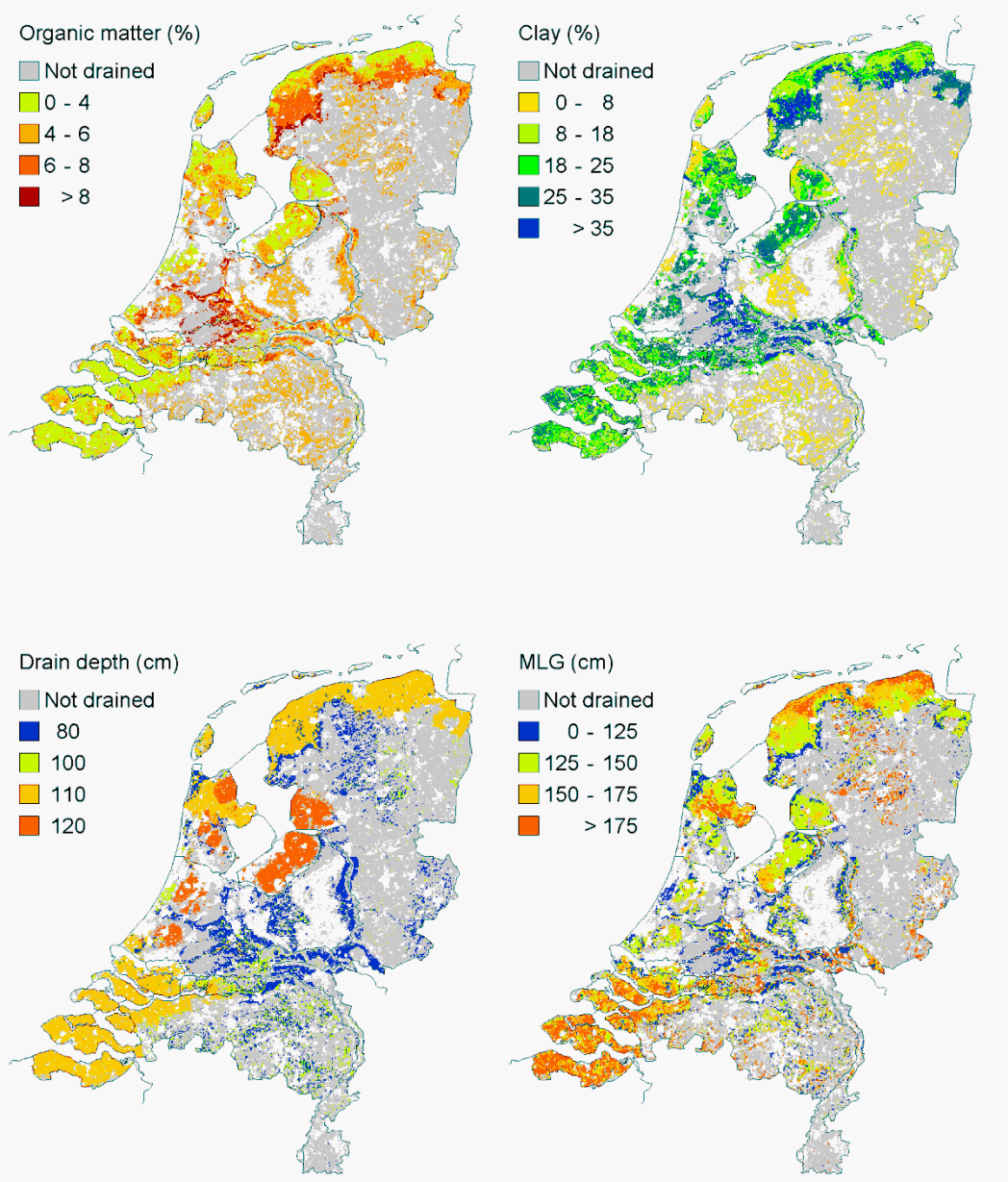

Figure 28 Basic data for the macropore pedotransfer functions. Basic soil properties were derived from the GeoPEARL schematisation (Tiktak et al. 2002). MLG refers to the Mean Lowest Groundwater Level. Only areas with pipe drained soils are shown.

Depth distribution of macropores

The depth of the plough layer, Z_{Ah}, is set to 30 cm. This depth corresponds to the depth of the top soil in the Staring Series (Wösten et al. 1994, 2001). The bottom depth of the permanent macropores, Z_{Sta}, is assumed to be equal to the depth of average deepest groundwater level. At this level, the formation of structural shrinkage cracks due to ripening of clay will be limited (Hendriks et al. 1999). Also, biological macropore initiating processes such as the formation of holes by roots, worms, insects and small mammals are likely to be negligible (Lindahl et al. 2009). The bottom depth of the internal catchment domain is set equal to the depth of the mean highest groundwater table. Above this depth, there is generally no direct contact between the macropores and the saturated

zone, so water must always infiltrate into the soil matrix. The assumptions for the bottom depth of the two macropore domains were confirmed at two field studies in cracking clayey soils (Hendriks et al. 1999).

Volume fraction of static macropores at soil surface
The estimation of the total volume fraction of static macropores at soil surface started with the assumption that all static macropores are structural shrinkage cracks due to ripening of clay. Starting from this simple assumption, we further assumed that the magnitude of structural shrinkage is proportional to the shrinkage potential of all clays. Shrinkage potential can be expressed as the *COLE* (-), the coefficient of linear extensibility for a certain moisture content range of a clay soil (Bronswijk and Evers-Vermeer 1990):

$$COLE = \left(\frac{V_{wet}}{V_{dry}} \right)^{1/3} - 1 \qquad (47)$$

in which V_{wet} (m^3) is the volume of a soil aggregate in wet state and V_{dry} (m^3) is the volume of a soil aggregate in dry state. The USA soil classification system (Soil Survey Staff 1975) defines V_{wet} as the volume of a soil aggregate at a pressure head of -333 cm. This definition is, however, not useful in Dutch conditions, because Dutch soils are usually wetter than moisture contents corresponding to a pressure head of -333 cm. Therefore, we chose the range from saturation to oven dry, because this range gives good information about swelling and shrinkage potential to be expected under Dutch conditions.

For this *COLE* a pedotransfer function was derived by multiple regression, with explanatory variables clay and organic matter content:

$$COLE = -0.02094 + 0.003311 f_{clay} + 0.009051 f_{om} \quad (n = 37; R^2_{adj} = 0.81) \qquad (48)$$

where COLE (-) is the coefficient of linear extensibility for drying from saturation to oven dry, f_{clay} (per cent) is clay content, f_{om} (per cent) is organic matter content, and *N* is the number of samples. Data were taken from nine different locations (Bronswijk and Evers-Vermeer 1990, Smelt et al. 2001, Van der Salm et al. 2006). Figure 29 gives a comparison between measured and predicted COLE for these data.

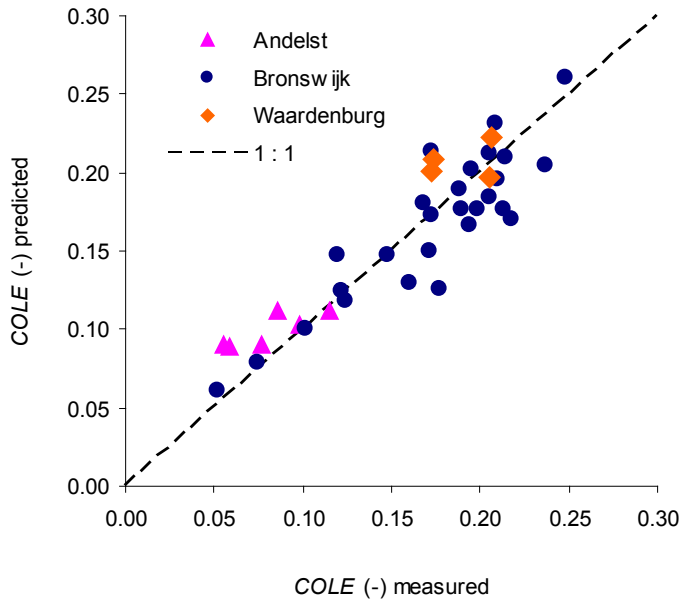

Figure 29 Scatter plot of measured versus predicted COLE. 'Bronswijk' refers to the seven locations reported in Bronswijk and Evers-Vermeer (1990). Andelst refers to the Andelst field study and Waardenburg refers to the Waardenburg field study reported by Van Beek et al. (2008). Predictions were made with Eqn. 48.

In order to obtain the relation between the static macropore volume at soil surface ($V_{sta,0}$) and the *COLE* of Eqn. 48, linear regression was conducted between this COLE and available data on $V_{sta,0}$ (Figure 30). Only two values $V_{sta,0}$ were available, i.e. one for location Andelst and one for location De Bouwing (Hendriks et al., 1999). It was further assumed that for *COLE* zero $V_{sta,0}$ is zero as well (thus intercept = 0). With this assumption, lines were plotted from point (0,0) through each of the two points (*COLE*,$V_{sta,0}$). The two slopes obtained in this way (0.374 for Andelst and 0.393 for De Bouwing) were averaged, yielding the equation:

$$V_{sta,0} = 0.384COLE \qquad (49)$$

Observations of the volume of static macropores at the two sites also included macropores with a biological origin (worm holes), so Eqn. 49 describes both classes of macropores (i.e. structural cracks and macropores with a biological origin). The spatial distribution of the volume of static macropores at soil surface is shown in Figure 31.

The distribution of the total macropore volume over the two macropore domains is specified by parameter $P_{ica,\,0}$, the volumetric proportion of the internal catchment domain at the soil surface. This parameter was obtained by calibration to the Andelst dataset and was set to 0.9.

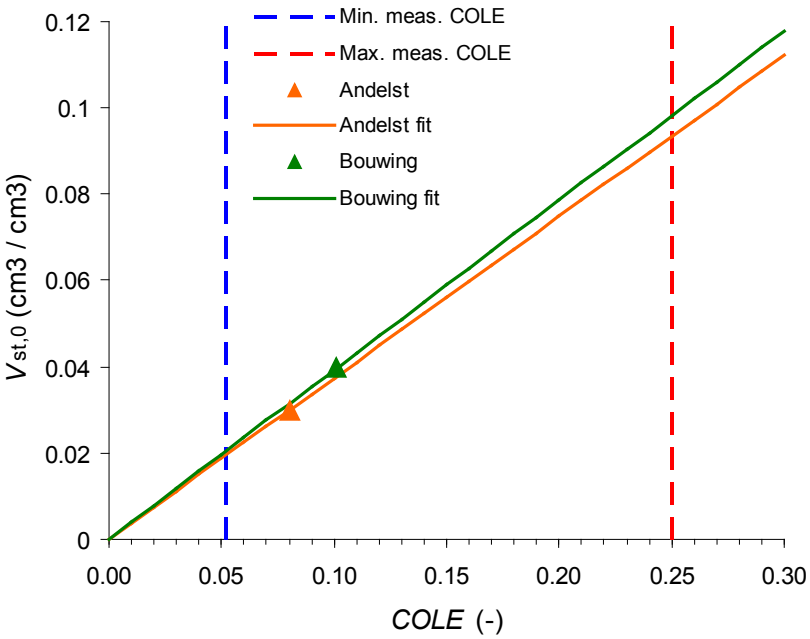

Figure 30 Fits of $V_{sta,0}$ versus COLE for Andelst and De Bouwing. Min. and max. measured COLE refers to the minimum and maximum values in Figure 29.

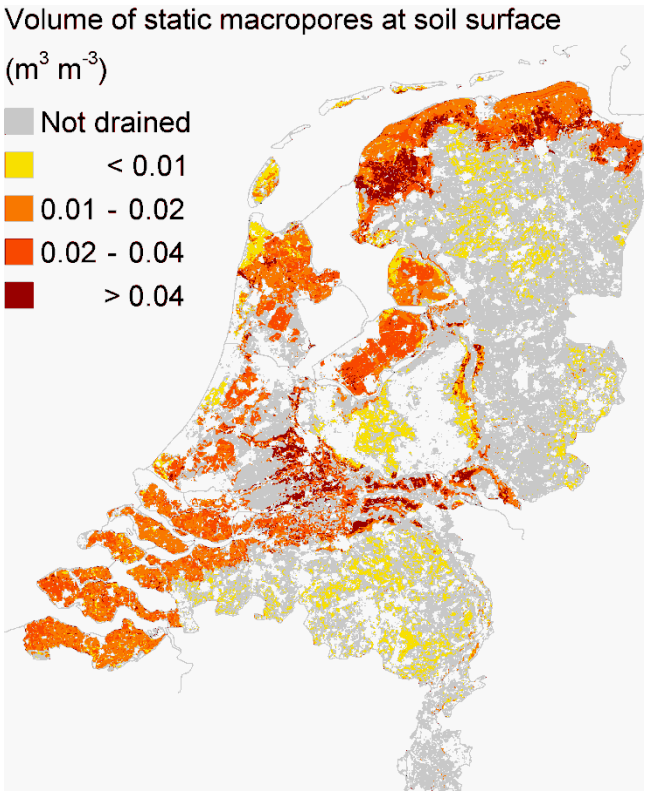

Figure 31 Volume of static macropores at soil surface, predicted with Eqn. 48 and 49.

Shrinkage characteristics
Pedotransfer functions have been developed for the two typical points in Figure 8, i.e. the void ratio at moisture ratio zero (e_0) and the moisture ratio at transition of residual to normal shrinkage (φ_a):

$$e_0 = \frac{(78.1198 - 0.7496 f_{clay} - 1.7823 f_{om}) \frac{\theta_s}{1-\theta_s}}{100} \qquad N = 37;\ R^2_{adj} = 0.79 \qquad (50)$$

$$\phi_a = \frac{(97.9423 - 0.8834 f_{clay} - 1.252 f_{om}) \frac{\theta_s}{1-\theta_s}}{100} \qquad N = 37;\ R^2_{adj} = 0.83 \qquad (51)$$

where f_{clay} (per cent) is the clay content, f_{om} (per cent) is the organic matter content, and θ_s ($m^3\ m^{-3}$) is the volume fraction of water at saturation. With these two points, SWAP generates the entire shrinkage characteristic as represented by the equation of Kim (1992). The use of one pedotransfer function was justified by the relative homogeneous mineralogical composition of Dutch clayey soils (Breeuwsma 1985, Breeuwsma et al. 1986).

Effective polygon diameter
In SWAP, the effective polygon diameter d_{pol} plays a role in the calculation of the exchange of water between macropores and the soil matrix (Eqn. 12 and 13). Polygon diameter is depth dependent (Eqn. 6). Both the minimum value and the maximum value of the effective soil matrix polygon diameter at soil surface were calculated with a pedotransfer function by Jarvis et al. (2007):

$$d_{pol} = 2 * 10^{(0.409 - 0.133 f_{om}/1.724 + 0.034 f_{clay})} \qquad (52)$$

where d_{pol} (mm) is the soil matrix polygon diameter, f_{om} (per cent) is organic matter content of the top soil, and f_{clay} (per cent) is the clay content of the topsoil. Notice that we introduced a factor 2 into Eqn. 52. This factor has been introduced because the original pedotransfer function gives an expression for the effective diffusion path length in the MACRO model. It is assumed that this path length equals half the effective matrix polygon diameter d_{pol}.

It should be noted that parameter d_M that is obtained by using the pedotransfer function of Jarvis et al. (2007) does not strictly have the same meaning as half of the polygon diameter d_{pol} in SWAP. In MACRO the path-length d_M (cm) is considered to be 'an effective aggregate half-width'. Its function in the calculation of water exchange between macropores and micropores is:

$$S_w = \frac{G_f D_w \gamma_w}{d_M^2} \qquad (53)$$

where S_w ($m^3\ m^{-3}\ d^{-1}$) is volumic volume rate of water exchange rate between macropores and the matrix, G_f (-) is a geometry factor for shape of matrix polygon, D_w ($cm^2\ d^{-1}$) is the effective water diffusivity, γ_w (-) is a scaling factor to match the approximate and exact solution to the diffusion problem, θ_b ($m^3\ m^{-3}$) is the volume fraction of water at the micropore-macropore boundary, and θ_{min} ($m^3\ m^{-3}$) is the volume fraction of water in the micropores.

In the original formulation of Eqn. 53 by Gerke and van Genuchten (1993), d_M has the theoretical meaning of the 'half width of a matrix block' or the path-length from the wall of a rectangular soil slab to the middle of this slab. The practical meaning of this parameter is an 'effective' half width or path-length, as in reality not all aggregates are shaped in the same way. On the basis of this meaning of d_M we could conclude that there is a clear relation between the two effective path-length parameters in MACRO and SWAP:

$$d_{pol} = 2d_M \tag{54}$$

However, Eqn. 53 uses two scaling factors. Gerke and van Genuchten (1993) conclude that 'for extension of the dual-porosity model to other geometries than rectangular slabs, and also mixtures of aggregates of different shapes and sizes (...) one could also treat the dual-porosity model in a more pragmatic manner by considering the geometry factor G_f, or better perhaps the entire term $G_f \gamma_w / d_M^2$, as an essentially empirical quantity which must be calibrated to observed field data.'

According to Jarvis et al. (2007), G_f is 'set to 3 internally' in MACRO, and according to Scorza Júnior et al. (2007): 'In MACRO, γ_w is set at an average value of 0.8', with reference to the MACRO Technical description. This implies that the calibration of 'the entire term $G_f \gamma_w / d_M^2$, as an essentially empirical quantity' comes down to calibration of d_M, as this is the only variable within this 'entire term.' This also implies that d_M has lost its original, strict meaning of a half-width, and implicitly includes the variation in parameters G_f and γ_w. The consequence is that the Jarvis pedotransfer function will yield reasonable estimates for half of d_{pol} for structured clay soils to which the constant values of parameters G_f and γ_w in MACRO apply.

6.1.3 *Water flow*

The macropore version of PEARL needs only a few new parameters for soil water flow, i.e. Philip's sorptivity and the drainage resistance of the macropore system. Some parameters, such as the soil hydraulic characteristics, needed re-evaluation, however.

Rainfall intensity
Runoff occurs at short time-scales, so correct simulation of runoff requires realistic rainfall intensities (Kroes et al. 2008). Rainfall intensity was calculated from the daily rainfall depth and daily rainfall duration. In GeoPEARL, the rainfall was assigned to the first hours of the day.

Hydraulic characteristics of the soil matrix
The hydraulic conductivity of the soil matrix controls both surface runoff flux and exchange between the macropores and the matrix. In GeoPEARL, pedotransfer functions are used to predict the parameters of the Mualem-van Genuchten hydraulic functions (Wösten et al. 2001). These pedotransfer functions do, however, apply to the entire soil and not only to the soil matrix. Direct application of these pedotransfer functions would therefore lead to underestimation of surface runoff and hence of macropore flow, because the hydraulic conductivity is known to increase rapidly across a small pressure head range as saturation is approached (Jarvis and Messing 1995). To account for this effect, we defined a boundary pressure head, h_b, and calculated the corresponding water content θ_b and hydraulic conductivity K_b to represent the saturated state of the soil matrix (conform Jarvis et al. 1991):

$$\theta_b = \theta_r + \frac{\theta_s - \theta_r}{[1 + (\alpha \mid h_b \mid)^n]^m} \quad (55)$$

and

$$K_b = K_s S_e^{\lambda} \left[1 - \left(1 - S_e^{1/m}\right)^m\right]^2 \quad (56)$$

where θ_s (m^3 m^{-3}) is the saturated volume fraction of water, θ_r (m^3 m^{-3}) is the residual volume fraction of water, α (m^{-1}) reciprocal of the air entry value, K_s (m d^{-1}) saturated hydraulic conductivity, n (-) and λ (-) are parameters, m = 1-1/n, and S_e (-) is the relative saturation, which is given by:

$$S_e = \frac{\theta_b - \theta_r}{\theta_s - \theta_r} \quad (57)$$

The boundary pressure head, h_b, was set to -5 cm, which corresponds to a pore diameter of 0.5 mm according to the Young Laplace relation. This value is in the range proposed by Jarvis and Messing (1995). A map of the so-obtained boundary hydraulic conductivity is shown in Figure 32.

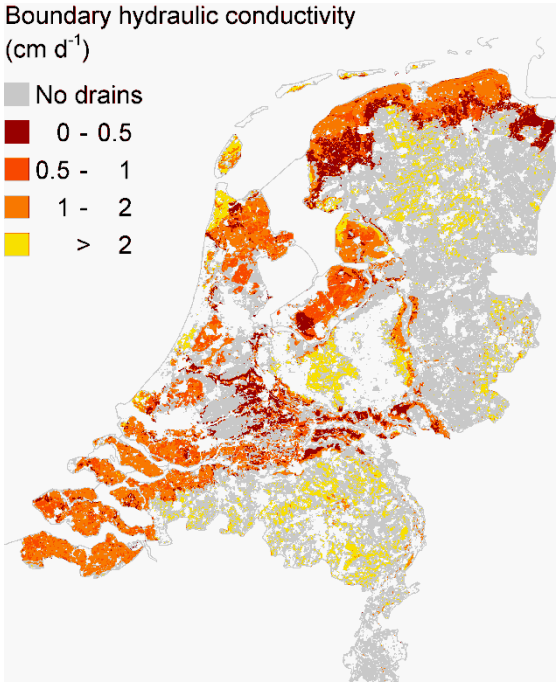

Figure 32 Boundary hydraulic conductivity representing the saturated state of the soil matrix based on a boundary pressure head of -5 cm.

Philip's sorptivity

Philip's sorptivity, S_p, is used in the calculation of infiltration from macropores into the soil matrix (Eqn. 12). S_p is a function of initial moisture content, θ_0. Because measured sorptivities were not available, we derived the sorptivity as a function of water content from the soil hydraulic characteristics (Parlange 1975). A factor for modifying the theoretical sorption function of Parlange may be introduced. This factor reflects the influence of water repellent coatings on the surface of clay aggregates, which may hamper infiltration into these aggregates

(Dekker and Ritsema 1996). In PEARL, this factor is set to 1 by default, which implies no hampering effect on infiltration of these coatings.

Properties of the drainage system
Rapid drainage towards drainpipes is controlled by the depth of the drainage system and the drainage resistance (Eqn. 15). In GeoPEARL, the depth of the pipe-drainage system was set to 0.8-1.2 m, depending on land-use and soil type (Kroon et al. 2001). The corresponding drainage resistance can be calculated on the basis of the desired maximum groundwater level midway between two drains and the desired maximum discharge ('design discharge'):

$$\gamma_{dr} = \frac{h_{design} - h_{dr}}{q_{design}} \tag{58}$$

where γ_{dr} (d) is the drainage resistance, h_{design} (m) is the desired maximum groundwater level midway between two drains, h_{dr} (m) is the drainage depth, and q_{design} (m d^{-1}) is the design discharge. In arable land, usually a design discharge of 7 mm d^{-1} is chosen in combination with a desired maximum groundwater level midway between two drains of 0.5 m below the soil surface (Cultuurtechnisch Vademecum 1998). This implies a maximum convexity of 0.30-0.70-m above drain level h_{dr}. The resulting drainage resistance is 43 d in the case of a drain depth of 80 cm and 100 d for a drain depth of 120 cm. These values are introduced into the new GeoPEARL version.

In the case of a macroporous soil, the so-obtained drainage resistance was assigned to the rapid drainage system (i.e. the macropores). Because the drainage resistance of the soil system as a whole (i.e. macropores and soil matrix) should have approximately the same value, we assigned a high drainage resistance of 10 times the rapid drainage resistance to the matrix drainage resistance. Following the rule of parallel resistances, the overall drainage resistance amounts to:

$$\gamma_{dr} = \frac{1}{1/\gamma_{rd} + 1/\gamma_{mi}} \tag{59}$$

where γ_{rd} (d) is rapid drainage resistance and γ_{mi} (d) is resistance for drainage through the soil matrix.

6.1.4 *Substance transport*

The substance transport module contains only two adjustable preferential flow parameters, i.e. the thickness of the mixing layer and the runoff extraction ratio (Eqn. 27-29). The thickness of the mixing layer was set to 1 cm, which is the mean of the values proposed by Sharpley (1985). The runoff extraction ratio was set to 0.125. This value was obtained by calibration of PEARL to the drain water concentration observed at the Andelst field site (Chapter 4).

6.1.5 *Parameterisation of the TOXSWA metamodel*

To calculate the concentration in the ditch, GeoPEARL is combined with a metamodel of TOXSWA (Section 3.5). For each plot, the following parameters are needed: (i) the area of the adjacent field per unit ditch length, (ii) the area of the upstream catchment per unit ditch length, (iii) the fraction of the upstream catchment that is treated, and (iv) the volume of the ditch per unit ditch length (lineic volume).

The area of the adjacent field was obtained from an overlay of the land-use map and the watercourses map on the 1:10,000 topographical map of the Netherlands (TOP10). The average size of the adjacent field emerged as approximately 100 m^2 m^{-1}. The overlay further showed little variation across the country, so we decided to use this mean value for the entire country.

The fraction of the upstream catchment that is treated was set to 100 per cent (conservative assumption). Eqn. 35 shows that for a treatment ratio of 100 per cent, the area of the upstream catchment does not affect the peak concentration in the water course. We therefore decided to use one value of the area of the upstream catchment for the entire country, i.e. 200 m^2 m^{-1}.

The initial ditch volume was calculated with Eqn. 37. Based on field inventories, Massop et al. (2006) showed that there is a good correspondence between geohydrological characteristics of the subsoil and ditch properties. Geohydrological characteristics of the subsoil are available for 22 so-called hydrotypes. Because the hydrotype is one of the basic map-layers in GeoPEARL, assignment of ditch volume to GeoPEARL units has become straightforward (Figure 33). Results indicate a plausible pattern with high ditch volumes in the clay region and low ditch volumes in the sand region.

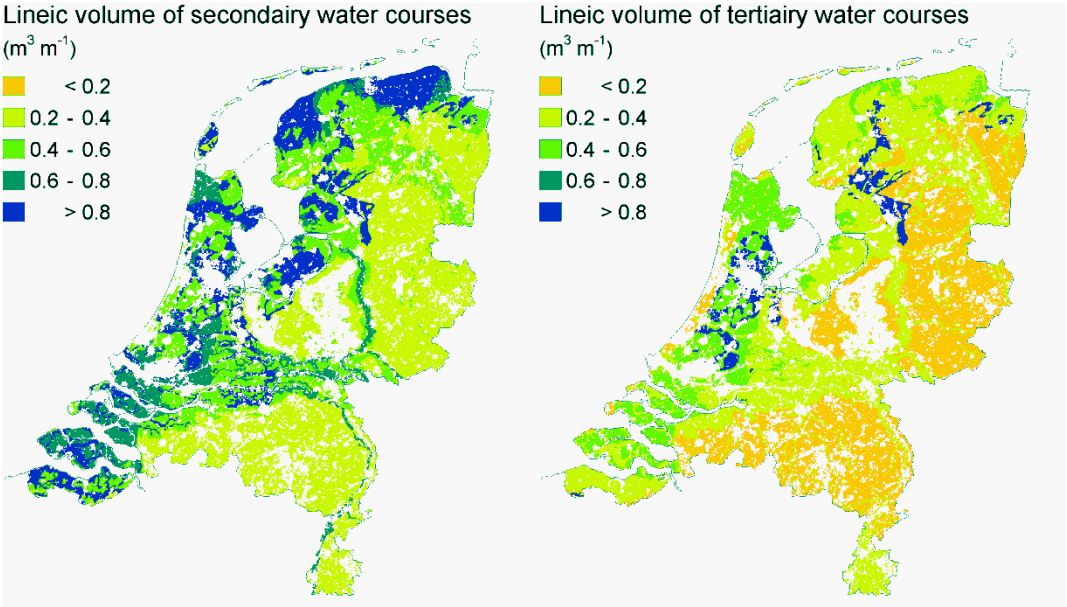

Figure 33: Lineic volume of secondary water courses (left) and tertiary water courses (right). Values apply to a 'wet-winter period'.

6.1.6 *Test of the TOXSWA metamodel*

The TOXSWA metamodel was tested at the Andelst field site for 39 theoretical substances (Table 9). The crop selected was sugar beet and the substances were applied on April 7 at a dose of 0.55 kg ha^{-1}. To make the comparison possible, drift deposition was set to zero in TOXSWA. Furthermore, the $DegT50_{water}$ and $DegT50_{sediment}$ were set to 1000 d and sorption to sediment and suspended solids were set to zero.

Table 9 Substances included in the calculation of the target temporal percentile (green is included, grey is not included). The numbers in the table are the substance IDs.

	K_{om} (L/kg)						
DegT50 (d)	10	20	30	60	120	240	480
10	**1**	**4**	**8**	**13**	**19**	**26**	**33**
20	**2**	**5**	**9**	**14**	**20**	**27**	**34**
30	**3**	**6**	**10**	**15**	**21**	**28**	**35**
60		**7**	**11**	**16**	**22**	**29**	**36**
120			**12**	**17**	**23**	**30**	**37**
240				**18**	**24**	**31**	**38**
480					**25**	**32**	**39**

For each substance, 15 annual maximum concentrations are simulated with both TOXSWA and the TOXSWA metamodel as included in PEARL. This results in a dataset of 15x39=585 maximum annual concentrations. The correlation is generally good (r^2 = 0.93; Figure 34).

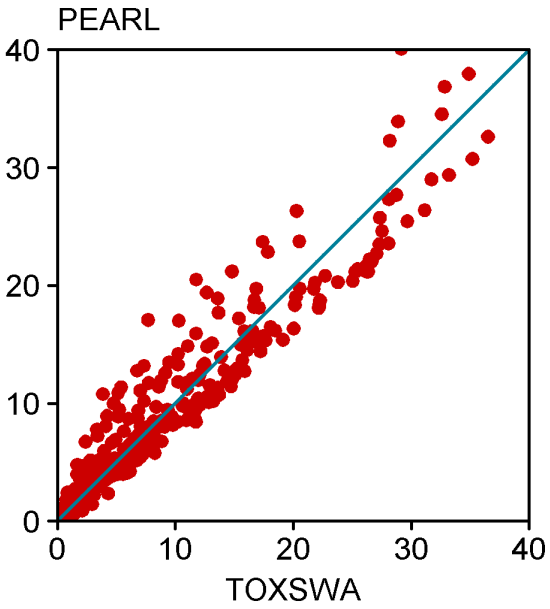

Figure 34 Comparison of the maximum annual concentration in ditch water as simulated with TOXSWA and the TOXSWA metamodel as included in PEARL. The blue line is the 1:1 line.

In this study, the relative ranking of the 15 simulated maximum annual concentrations is important (see further chapter 7). For this reason, we performed a Spearman rank test for each of the 39 substances, using the simulated maximum annual concentrations from the metamodel and TOXSWA. Results are shown in Figure 35. The figure shows that, for most substances, Spearman's rank coefficient is above 0.7. In some cases, however, the rank coefficient is low. Further investigation revealed that this is the case if the differences between the 15 maximum annual concentrations are small, so a small difference (in absolute terms) between the metamodel and the original model results in a completely different rank. This can be seen in Figure 45 for substance 30 with a K_{om} of 240 and a half-life of 120. For this substance, a difference of only a few per cent results in a completely different temporal percentile (i.e. rank). The conclusion is that in the majority of the cases

Spearman's rank coefficient is sufficiently high (> 0.7). Furthermore, in cases with low Spearman's rank coefficients, the predicted maximum annual concentration does not show much variation between the years.

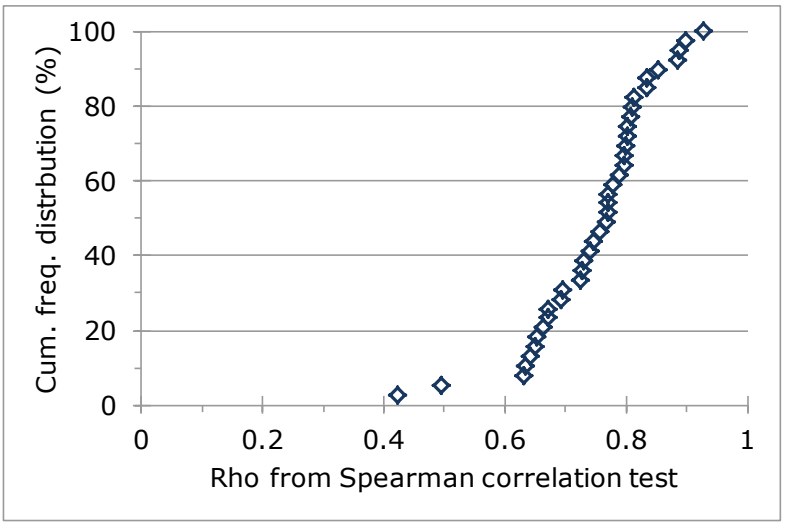

Figure 35 Cumulative frequency distribution of Spearman's rank coefficient (rho) for each of the 39 sets of maximum annual concentrations.

6.2 Results

The endpoint of the drainpipe exposure assessment is the 90th percentile of the annual maximum concentration in all ditches that potentially receive PPPs from tile drains (Chapter 2). This implies that the peak concentration must be simulated for all ditches adjacent to pipe drained soils. In this section the most important results are presented. Firstly, the most important pathways are discussed (Section 6.2.1). Then, in Section 6.2.2, simulation results for six hypothetical substances are presented. Properties of these substances are given in Table 10. In this section, all simulations were carried out with a dosage of 1 kg ha^{-1} at the soil surface on April 7.

Table 10 Sorption coefficient to organic matter and degradation half-life for six hypothetical substances.

Substance number	K_{om} (L kg^{-1})	*DegT50* (d)
1	10	10
2	70	40
3	25	50
4	50	50
5	75	50
6	200	120

6.2.1 Main flow pathways

Drainage to field ditches consists of two terms, i.e. rapid drainage due to macropore flow, and slow drainage due to matrix flow. In clayey soils, rapid drainage is the dominant term with a mean annual drainage flux of 376 mm a^{-1} (Table 11). In sandy soils, this rapid drainage does not occur at all. Water can enter the macropores by surface runoff or by exfiltration from the soil matrix. In the clayey soils ninety per cent of the runoff water is routed into the internal catchment domain (349 mm to the internal catchment domain and 40 mm to

the bypass domain). This is caused by the calibrated value for $P_{ica,0}$ of 0.9. In these soils the 349 mm runoff into the internal catchment infiltrates into the matrix and a large portion of this (330 mm) flows from the matrix to the bypass domain. The rapid drainage is 376 mm whereas the runoff into the bypass domain is only 40 mm. So most of the rapid drainage water is caused by the 330 mm of water that flowed from the matrix to the bypass domain. This means that the pathway internal catchment domain – soil matrix – bypass domain is the dominant flow pathway in these soils.

Table 11 Water balance (mm a^{-1}) for the 20-year simulation period. Balance terms are averages of all soils in the sand region and in the clay region. Lines in italics represent internal balance terms.

Balance term (mm yr^{-1})	Sand region†	Clay region†
Precipitation and irrigation	816	828
Seepage at lower boundary‡	90	-64
Evapotranspiration	481	426
Matrix drainage	242	90
Rapid drainage	0	376
Infiltration of precipitation into the soil matrix	*816*	*439*
Runoff into bypass domain	*0*	*40*
Runoff into internal catchment domain	*0*	*349*
Flow from the matrix to the bypass domain	*0*	*330*
Flow from the internal catchment domain to the matrix	*0*	*349*

† Sand region: regions with sandy soils, i.e. soils with a clay content < 8%. Clay region: region with clayey soils, i.e. soils with a clay content > 8%.

‡ Positive values refer to downward flow; negative values to upward flow.

The spatial pattern of the runoff flux into macropores in Figure 36c shows a strong correspondence with the clay content in Figure 28. The runoff flux is controlled by the boundary hydraulic conductivity (K_b): low K_b values correspond with high runoff fluxes. The consequence is that the boundary hydraulic conductivity (and indirectly clay content) is an important driver for the rapid drainage flux, which is in line with results from a study with the MACRO model by Stenemo and Jarvis (2007).

In recently reclaimed polder areas, exfiltration from the soil matrix into the macropores is the most important term (these areas are indicated by red colours in Figure 36d). These polder areas are low lying areas compared to their surroundings, causing regional groundwater flow towards these polders. This regional groundwater flow causes upward seepage followed by exfiltration from the saturated soil matrix into the macropores and, finally, rapid drainage. Large areas with upward seepage are found in sandy soils as well. This net upward seepage is the main cause of the high values of slow matrix drainage in those regions (Figure 36b). Upward seepage results in input of uncontaminated water into the soil profile, which means that a high value of the drainage flux is not necessarily an indicator of high vulnerability to pesticide leaching.

In most clayey soils net-flow is from the macropores into the soil matrix (green colours in Figure 36d). In these soils, flow at the lower boundary is generally downwards. Net-flow from the macropores into the soil matrix is primarily caused by infiltration from the internal catchment domain. A large proportion of water that has infiltrated into the soil matrix then exfiltrates into the bypass domain (Table 11), leading to enhanced rapid drainage.

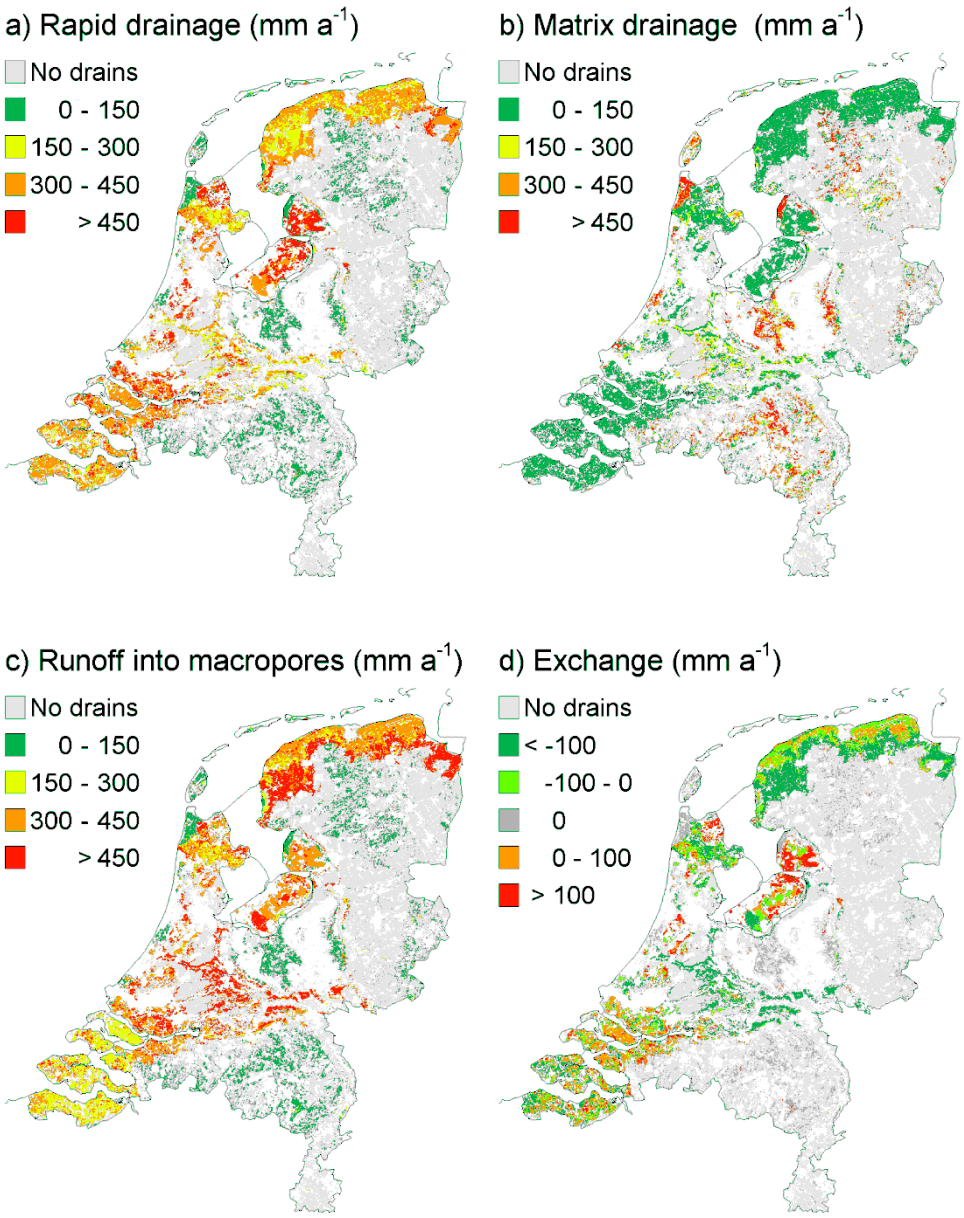

Figure 36: Simulated mean annual water balance of the macropore domain. Areas without pipe drains are not shown. (a) Rapid drainage flux due to macropore flow. (b) Drainage flux resulting from matrix flow. (c) Runoff into macropores. (d) Net water flux from the soil matrix into the macropores, positive values indicate that the net flow direction is towards the macropores.

6.2.2 *Drainage of substances to surface water*

Figure 37 shows the drainage flux of substance 1 to the surface water. The other five substances are not shown, because their predicted spatial patterns are comparable.

Both the predicted mass flux in rapid drainage and matrix drainage are high in clayey soils and low in sandy soils. This seems to be in contradiction with the opposite spatial pattern of the volume fluxes of drainage in Figure 36. This is, however, not the case, but can be explained by transport through the internal catchment domain. Based on findings in the Andelst field experiment

(Chapter 4), 90 per cent of the runoff volume is assumed to enter the internal catchment domain. Substance that enters the internal catchment domain is forced to infiltrate the soil matrix at greater depths, thus bypassing the reactive part of the soil matrix. In the saturated part of the soil column, macropores and micropores are well connected throughout, which implies that this mechanism can enhance both rapid drainage and matrix drainage.

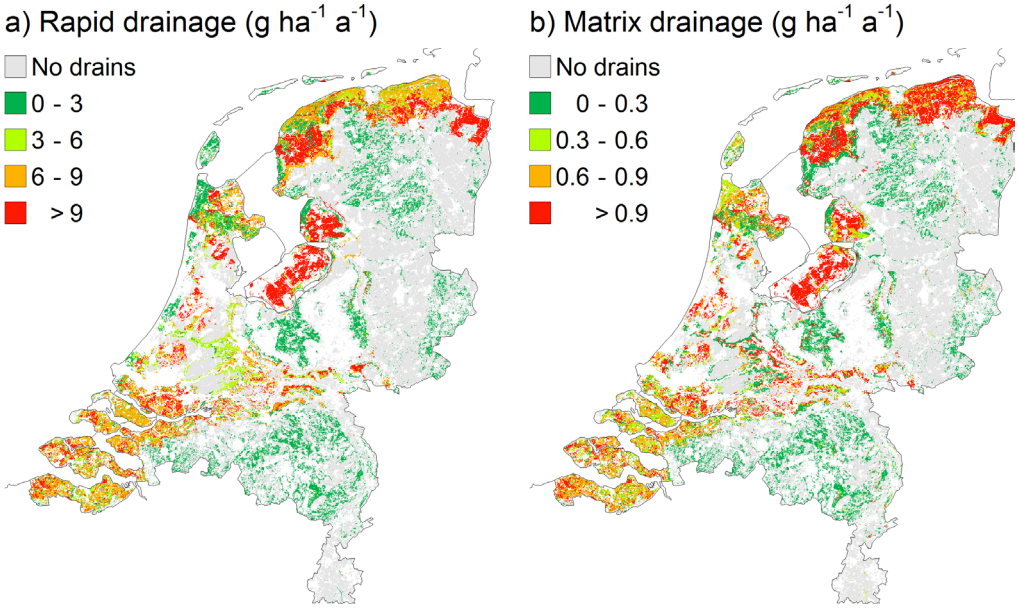

Figure 37 Drainage of an example substance to the surface water. The left-hand panel shows the rapid drainage flux, the right-hand panel shows the drainage through the saturated part of the soil matrix (matrix drainage). Notice the different scales of the two maps.

GeoPEARL is run for a period of 20 years, so 20 annual maximum concentrations in ditch water are calculated for each map unit. Figure 38 shows the median value of these 20 concentrations for the six example substances. As expected, the concentration in ditch water is generally high in clayey soils and low in sandy soils. Substance properties do have an effect on the predicted concentrations. The highest drainage concentrations are predicted for substances 3 and 4. The degradation half-life of these substances is 50 days, and their sorption coefficients are moderate (25-50 L/kg). Apparently, the combination of the two substance properties is such that they are not degraded nor leached from the mixing layer before the first runoff event takes place. The lowest concentration is predicted for substance 1. This is in line with findings in Chapter 5, where it was shown that substances with a short degradation half-life may be dissipated before the first runoff event.

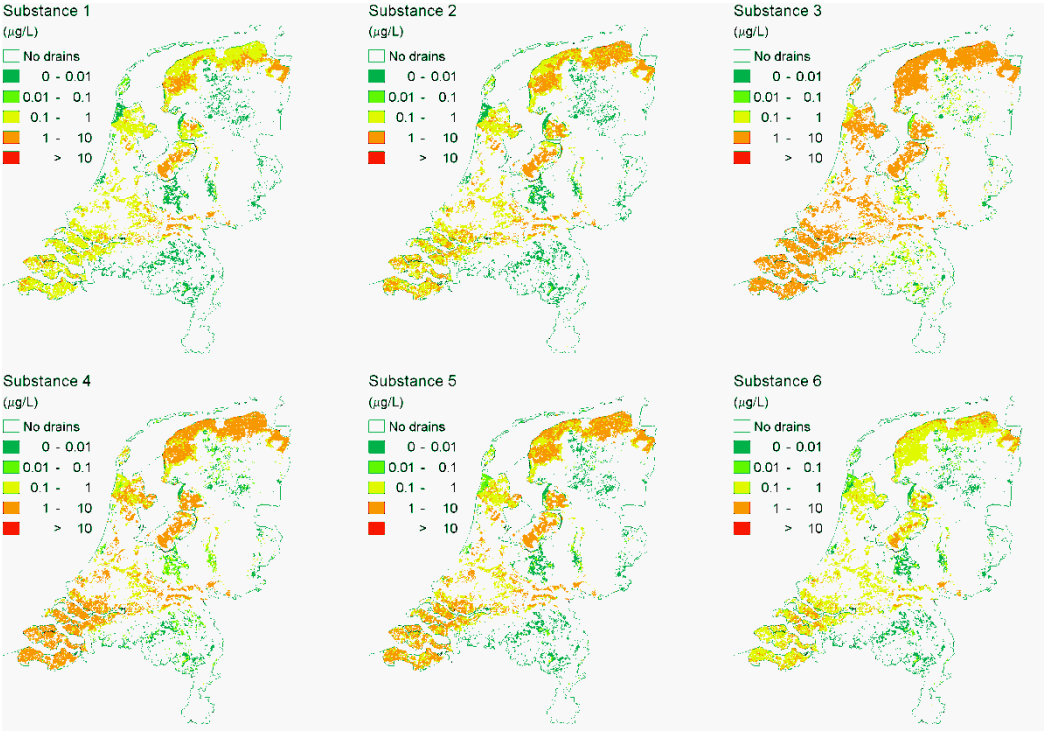

Figure 38 Median value of the predicted maximum annual concentration of the six example substances in secondary ditches (see Table 10 for substance properties).

In this study, GeoPEARL is primarily used for scenario selection, so we are interested in the relative vulnerability. To get a picture of the relative vulnerability of locations, we ranked the concentrations in Figure 38 on a scale of 0-100 per cent (Figure 39). The six maps are comparable with high concentrations in clayey soils and low concentrations in sandy soils. This general trend is confirmed in Figure 40, which shows the effect of organic matter content and clay content of the top 30 cm of the soil on the simulated maximum concentration in ditch water. Both figures show considerable scatter, which is due to other factors such as the hydrological boundary condition. Nevertheless, the concentrations generally increase with increasing clay content (R^2=0.45 for both substances). Organic matter does not show a significant trend, but this is probably caused by cross correlations with other factors. For example, clay content and organic matter content are correlated (organic matter content is generally higher in clayey soils than in soils with a lighter texture). This cross correlation also explains the decrease of the ditch concentration at high clay contents: organic matter content of these soils is generally greater than 10 per cent.

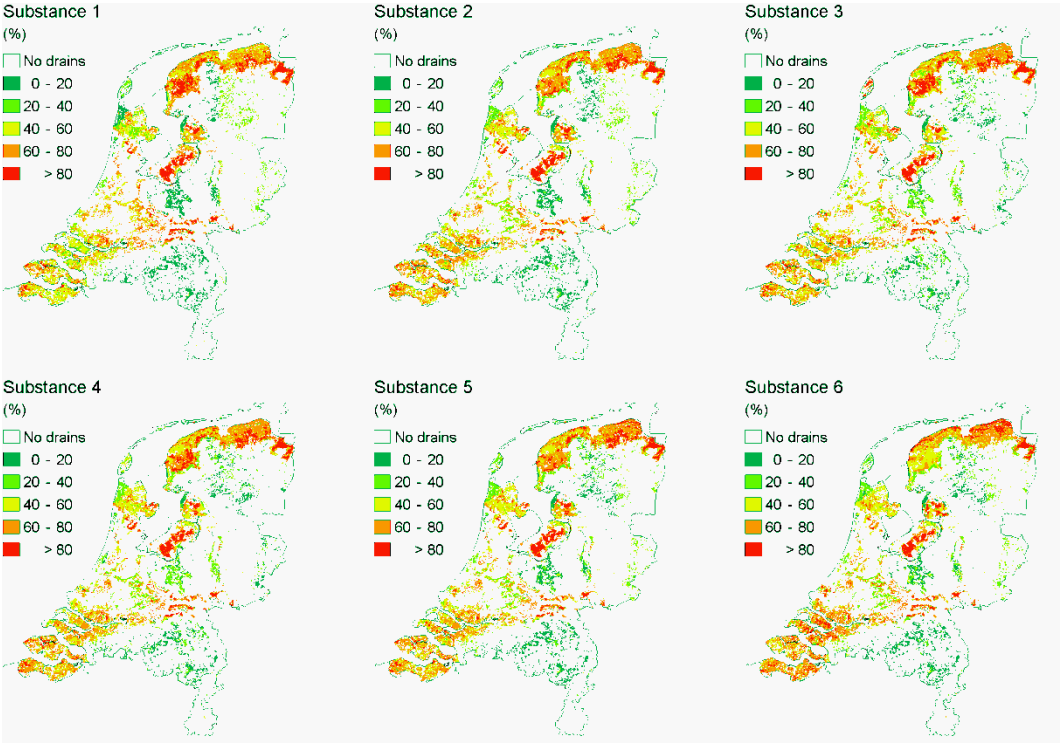

Figure 39 Ranking of the median value of the maximum annual concentration of the six example substances in secondary ditches.

Figure 40 shows that the response of the ditch concentration to these two soil properties is substance dependent. For example, the weakly sorbing substance in the upper panel of the figure shows larger differences of the ditch concentration between sandy soils and clayey soils than the moderately sorbing substance in the lower panel of the figure. This different response also explains why there are differences between the maps of the relative concentration shown in Figure 39. In the Northern clay area, for example, the predicted relative vulnerabilities of the weakly sorbing substance 1 and the strongly sorbing substance 6 show opposite spatial patterns. In this region, both organic matter content and clay content increase from North to South. As a consequence, the boundary hydraulic conductivity (an important trigger for the generation of surface runoff), decreases from North to South. Apparently, for weakly sorbing substances, the boundary hydraulic conductivity is an important driver and for strongly sorbing substances, the organic matter content is also important.

The lesson from these maps is that the ranking of locations is substance dependent. A scenario that is sufficiently conservative for one substance may therefore not be sufficiently conservative for another substance. The consequence is that this substance dependence must be dealt with in the scenario selection procedure.

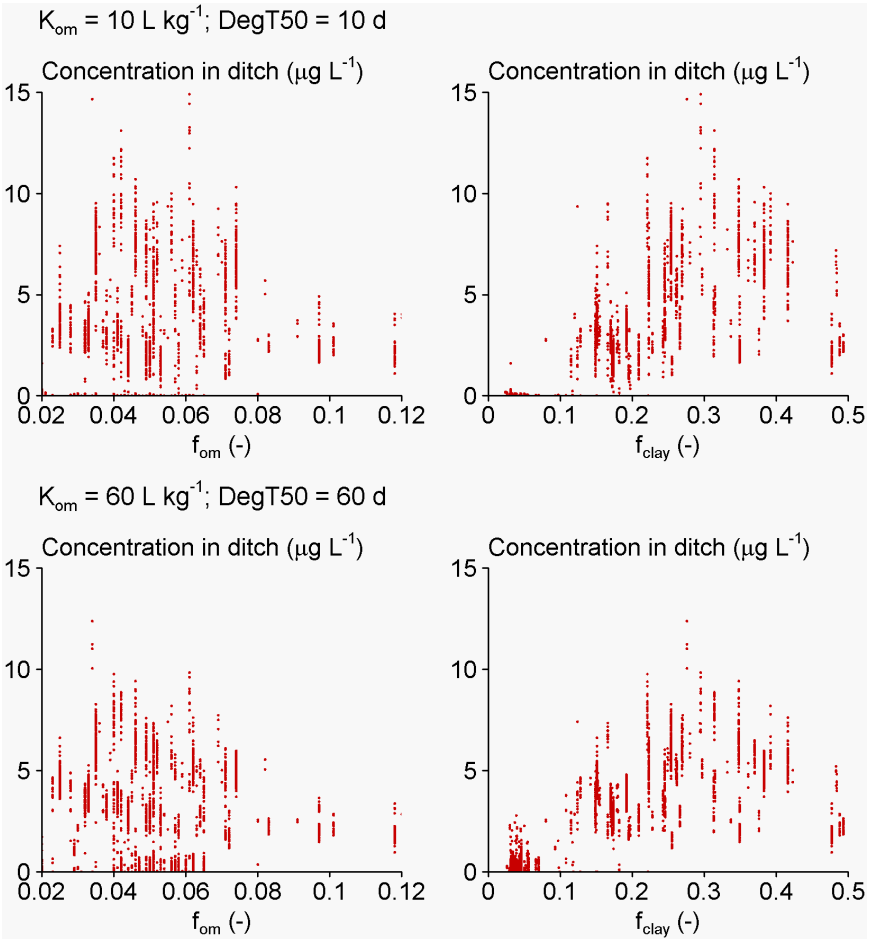

Figure 40 Effect of organic matter content (left) and clay content of the top 30 cm (right) on the simulated maximum concentration of two example substances in ditch water.

6.2.3 *Cumulative distribution function*

GeoPEARL results can be used to calculate the overall cumulative frequency distribution function of the concentration in adjacent ditches. Within each GeoPEARL map-unit, three ditch types may be present, i.e. primary water courses, secondary water courses and tertiary water courses. Massop et al. (2006) showed that drainpipes are generally not connected to primary water courses, so primary water courses were discarded from the population of relevant ditches. The number of annual peak concentrations per map unit was therefore 2 (the number of ditch types that potentially receive input from drainpipes) × 20 (the number of simulation years). The total number of map units is 6405, so the frequency distribution function consists of 256,200 data points.

Weighting factors were assigned to each data point, based on the lineic length of the water courses (Figure 41). An additional weighing factor is introduced to account for the fraction of arable land within each map unit. This was considered necessary because the population should include arable land only, and the map units are generally not homogeneous with respect to land-use. So, the weighing factor can be written as:

$$f_{i,j,k} = \frac{f_{D,i} f_{A,i} L_{i,j}}{\sum_{i=1}^{6405} \sum_{j=1}^{2} \sum_{k=1}^{20} f_{D,i} f_{A,i} L_{i,j}} \quad (60)$$

where $f_{i,j,k}$ (-) is a weighing factor for plot i, ditch type j, and year k, $l_{i,j}$ (m) is the ditch length, $f_{A,i}$ (-) is the fraction of arable land within a map unit and $f_{D,i}$ (-) is a factor describing the presence of a drainpipe system in a map unit. The factor $f_{D,i}$ can only have two values, i.e. 0 (no drainpipe system present) or 1 (drainpipe system present). The aim of this factor is to exclude plots that are not pipe drained. Notice that there is no weighing factor for the year, which means that each year has been given the same weight.

The cumulative frequency distribution function can be used to calculate the overall 90th percentile of the concentration in the adjacent ditch. Results for 39 hypothetical substances are shown in Figure 42. The overall 90th percentile increases with increasing *DegT50* and decreases with increasing K_{om}. A similar trend is found in models based on the convection-dispersion equation (Boesten and Van der Linden 1991). They observed that the leaching concentration in groundwater differed by four orders of magnitude in a smaller range of *DegT50* and K_{om} values. Compared to those differences, the observed differences in Figure 42 are small. The maximum concentration in drain water is primarily caused by preferential flow, where the substance bypasses most of the reactive part of the soil. (The mixing layer and the sorption sites in the macropores are the most important reactive compartments that need to be passed.)

Results in Figure 37 are not directly used in the drainpipe assessment, because the final assessment is based on the Andelst field-site. How this is done is described in Chapter 7.

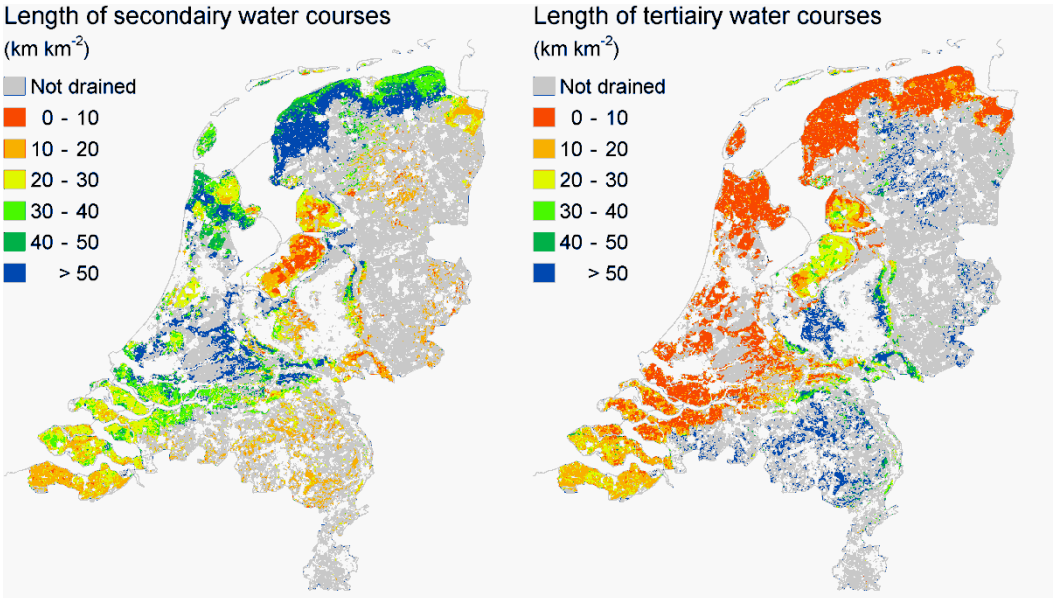

Figure 41 Length of secondary water courses (left) and tertiary water courses (right). The figure shows regions with pipe drained soils only.

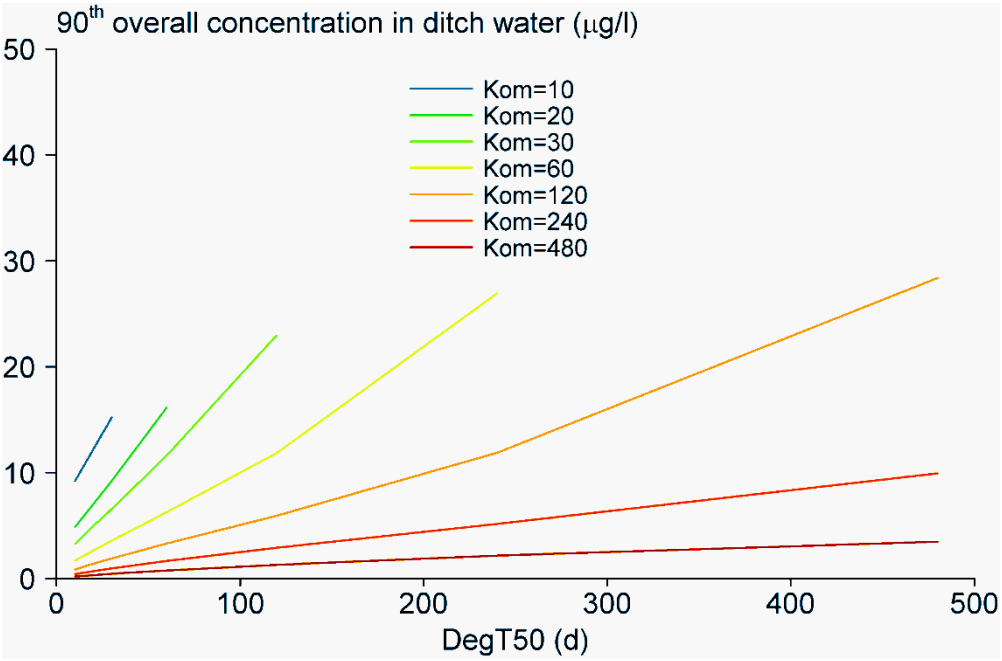

Figure 42 Overall 90th percentile of the peak concentration in the adjacent ditch. The figure is based on simulations with 39 hypothetical substances with properties shown in Table 9.

6.3 Discussion and conclusions

Using information available in generally available databases, we have successfully applied a spatially distributed pesticide fate model that includes a description of macropore flow. Based on common knowledge of this process, the predicted spatial pattern can be judged 'plausible'. Nevertheless, the model predictions are subject to a high degree of uncertainty. Errors result from the way in which the system is conceived (conceptual errors) and from the way in which the model parameters have been generated.

The seasonal dynamics of the groundwater table is an important factor for the simulation of drainage fluxes (Chapter 4). In the Netherlands, the groundwater dynamics are described by so-called ground water depth classes. Overbeek et al. (2002) showed that the ground water depth classes are generally well described by the model. This conclusion applies, however, only to the long-term average groundwater dynamics and not to individual years. In GeoPEARL, the bottom boundary condition is obtained from a link between a stationary regional groundwater model and SWAP; it consists of a long-term average soil water flux on which a sine-function with a fixed amplitude is imposed (Kroon et al. 2001). The resulting variation of the groundwater table between the years shows a somewhat averaged behaviour. As the pesticide concentration in drain water is extremely sensitive to the groundwater level (Chapter 4), the differences between the years may therefore be slightly underestimated. This could be resolved by combining SWAP with a transient groundwater flow model such as MODFLOW as done in the Netherlands Hydrological Instrument (NHI).

The second limitation is that the current model does not include an explicit description of the abundance of macropores with a biological origin, such as channels made by deep-burrowing (anecic) earthworms. Lindahl et al. (2009) showed that in loamy soils, earthworm channels are more abundant than

structural cracks. In the Netherlands, loess soils are primarily situated in Southern Limburg. Loess soils are usually not pipe drained, and are therefore not relevant to the current study. The loess soils are extremely vulnerable to groundwater leaching, however. For this reason, there is scope for extension of GeoPEARL with a description of the presence of earthworm channels. The pedotransfer functions by Lindahl et al. (2009) could be considered for this purpose.

The parameterisation of the macropore parameters in GeoPEARL is based on two sources, i.e. a series of pedotransfer functions and two field experiments. The pedotransfer functions developed in this study are obtained from a wide range of clay soils. Given the good correlation between soil structural parameters and basic soil properties, we believe that these pedotransfer functions form a solid basis for the parameterisation of the model. This good correlation was probably caused by the relatively constant mineralogical composition of soils in the Netherlands. For this reason, care should be taken when extrapolating these pedotransfer functions to soils outside the Netherlands, as their mineralogical composition may be completely different.

An important limitation of the current model parameterisation is that three macropore flow related parameters could only be obtained by calibration at the Andelst field site. Two of these parameters (the fraction of the internal catchment domain and the runoff extraction ratio) are extremely important for the peak concentration in drain water. Application of PEARL to more field experiments should therefore be an important research topic for the upcoming years.

The resolution of the GeoPEARL schematisation with 6405 map units is lower than the resolution of the land-use maps that were used for filtering arable land. The consequence is that map units with non-arable soil properties may be included in the assessment. For example, the high clay contents in Figure 40 are typical for grassland soils in the river Rhine delta. Despite the use of a detailed land-use mask, these map units were not removed from the population (apparently, within these map units arable land is present as well). We reduced the effect of the mismatch between the GeoPEARL schematisation and the land-use mask by giving map units with a low proportion of arable land less weight (Chapter 7). Nevertheless, there is scope for the development of a better schematisation, based on arable soils only.

7 Selection of the target temporal percentile

7.1 Introduction

The previous chapter showed that GeoPEARL can be used to generate maps of the concentration of PPPs in ditch water. The most straightforward way to obtain the exposure scenario would be to select one of the GeoPEARL map-units and base the exposure assessment directly on simulations for this single map unit. As discussed in Chapter 1, we considered this approach not appropriate. Instead, we will base the exposure scenario on the Andelst field site. This assessment results in 15 annual maximum concentrations (Figure 25). GeoPEARL was used to determine which of these 15 annual peak concentrations corresponds to the 90th percentile of the exposure concentration in all ditches (the target temporal percentile). How this is done is described in Section 7.2.

7.2 Procedure

As discussed in Chapter 5, simulations with the Andelst scenario (see Appendix 1 for scenario properties) give 15 annual peak concentrations. GeoPEARL was used to determine which of these annual peak concentrations corresponds to the 90th percentile of the exposure concentration in all ditches. This was done as follows:

1. GeoPEARL was run for a 20-year period, so 20 annual peak concentrations were obtained for each map unit;
2. A cumulative distribution function (cdf) of all annual peak concentrations was constructed in which each peak concentration was given a weight proportional to the total ditch length associated with the corresponding GeoPEARL plot, and the 90th percentile was calculated from this overall cdf (red line in Figure 44);
3. For the Andelst scenario, a cumulative distribution function of the 15 annual maximum concentrations was created (green line in Figure 44);
4. The target temporal percentile is the temporal percentile that predicts the same concentration as the 90th percentile of the overall cdf. This percentile can be looked up by following the arrows A, B and C in Figure 44. In our example, the target temporal percentile to be used in the exposure assessment is 20 per cent.

The spatial percentiles can only be calculated in an appropriate way if the differences between the GeoPEARL runs and the Andelst scenario are as small as possible. Therefore, in both the GeoPEARL runs and the runs for the Andelst scenario, substances were annually applied to the soil surface on April 7. All substance properties (except DegT50 and K_{om}), were set equal to the default value of FOCUS substance D as reported in FOCUS (2000). Furthermore, the depth dependence of degradation (f_z) was set to the FOCUS default values. Finally, no crop interception was assumed. In this chapter, the runoff extraction ratio was set to 0.125 (i.e. the value obtained for the calibration at the Andelst field site, see Chapter 4).

The organic matter content for the Andelst scenario is 2.1 per cent, which is a typical value for calcareous clayey soils in arable land (De Vries 1999). This value is lower than most values in the GeoPEARL database (Figure 40). This is likely to be caused by scale differences: the Andelst scenario represents a single field, whereas the soil properties in the GeoPEARL database are nominal values

for 456 soil types at the 1:50.000 soil map (De Vries 1999). Organic matter content is extremely variable within these soil types (Figure 43). Part of this variability is caused by differences in land-use within a soil type. De Vries (1999) showed, for example, that calcareous clayey soils have a mean organic matter content of 2.3 per cent when situated in arable land (which is quite close to the value for the Andelst scenario) and 6.2 per cent when situated in grassland. To account for this systematic effect of land-use within a GeoPEARL soil type on the organic matter content, we have used the 10th percentile of the organic matter content within a soil type to estimate the organic matter content of the arable land within this soil type. This is a best-guess solution given the limited time available. It is not clear whether this proposal will overestimate or underestimate the actual organic matter content of arable land.

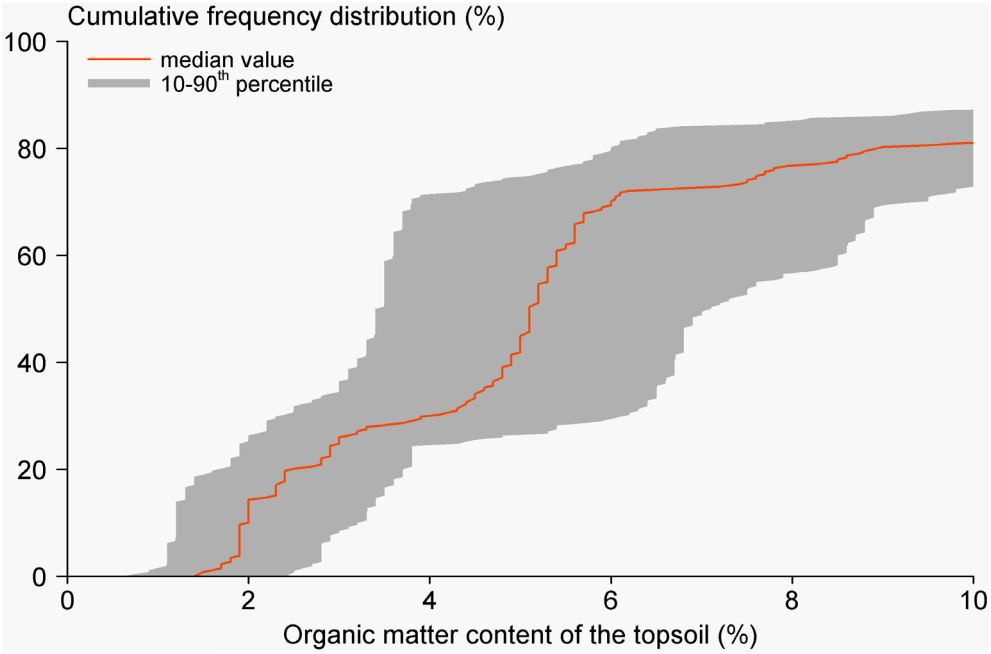

Figure 43 Cumulative frequency distribution of organic matter in the topsoil. The red line is the median value as present in the GeoPEARL database. The grey area is the interval bounded by the 10th and the 90th percentile within each map unit.

To make the comparison between the Andelst scenario and the soils present in the GeoPEARL database as pure as possible, the organic matter content of the Andelst scenario was multiplied by 1.56. This factor corresponds to the average ratio of the median value of organic matter within each soil type and the 10th percentile of organic matter within each soil type. By multiplying the organic matter content of the Andelst soil by this factor, a soil profile is created that has an organic matter content typical of the nominal value within GeoPEARL. Please notice that this scaling has been done only for the purpose of the calculation of the temporal percentiles. In the final simulations, the organic matter content was kept at its original value of 2.1 per cent, which is, as indicated, typical of an arable soil.

The calculations with the Andelst scenario are performed for winter wheat. The GeoPEARL calculations are done for maize, grass, winter wheat or potatoes. For each GeoPEARL plot, the calculation is performed for the most dominant of these four crops. The selection of the target temporal percentile is based on

comparison of the results of the Andelst scenario with the results from GeoPEARL. This comparison should in principle be as pure as possible. The difference between the crops that were used in Andelst and GeoPEARL, is therefore undesirable. However, it is difficult to perform GeoPEARL calculations with for example only winter wheat because the bottom boundary condition in GeoPEARL has been calibrated using calculations with these four crops. It would require considerable research efforts to recalibrate this bottom boundary condition using only winter wheat.

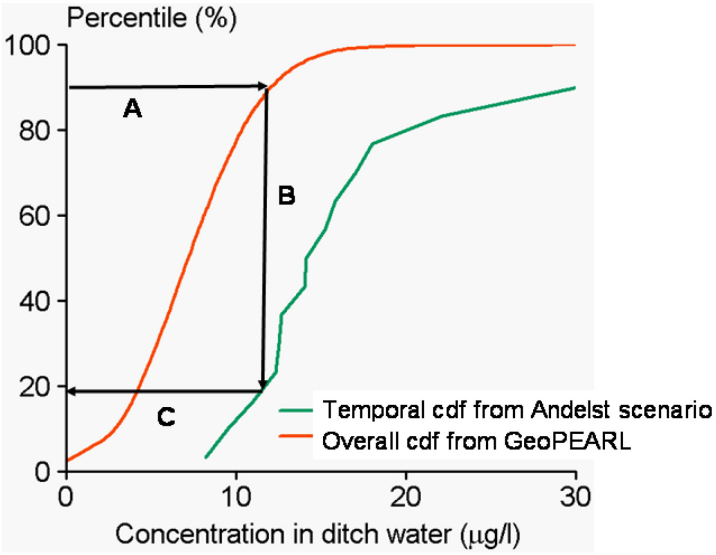

Figure 44 Procedure to derive the target temporal percentile to be used in the exposure assessment. For the Andelst scenario, the target temporal percentile predicts the same concentration as the 90th percentile of the overall cumulative distribution function (red line).

The selected temporal percentile should be sufficiently conservative for all relevant substances. However, due to the non-linearity of the relation between soil parameters, substance properties and predicted environmental concentrations, the ranking of climate and soil property combinations is different for different substances. As a consequence, a temporal percentile derived for one substance may not be sufficiently conservative when applied to another substance. To overcome this problem, the target temporal percentile was calculated for 39 substances with different degradation half-lives and sorption coefficients (Table 9).The temporal percentile to be used within DRAINBOW will be based on the temporal percentiles derived for the 39 substances.

7.3 Target temporal percentiles

We started the analysis with a visual comparison of the two cumulative frequency distribution functions, i.e. the overall cumulative frequency distribution of the predicted concentration in ditch water calculated with equation 60, and the temporal frequency distribution of the predicted concentration at the scaled Andelst scenario.

Results for six example substances are shown in Figure 45. These results show that the cumulative frequency distribution functions are generally steeper for

substances with a high K_{om} value (a steeper frequency distribution function means that the differences between the years and/or locations are smaller). A similar conclusion was drawn for the temporal frequency distribution function of bentazone and imidacloprid at the Andelst field site (see Chapter 4).

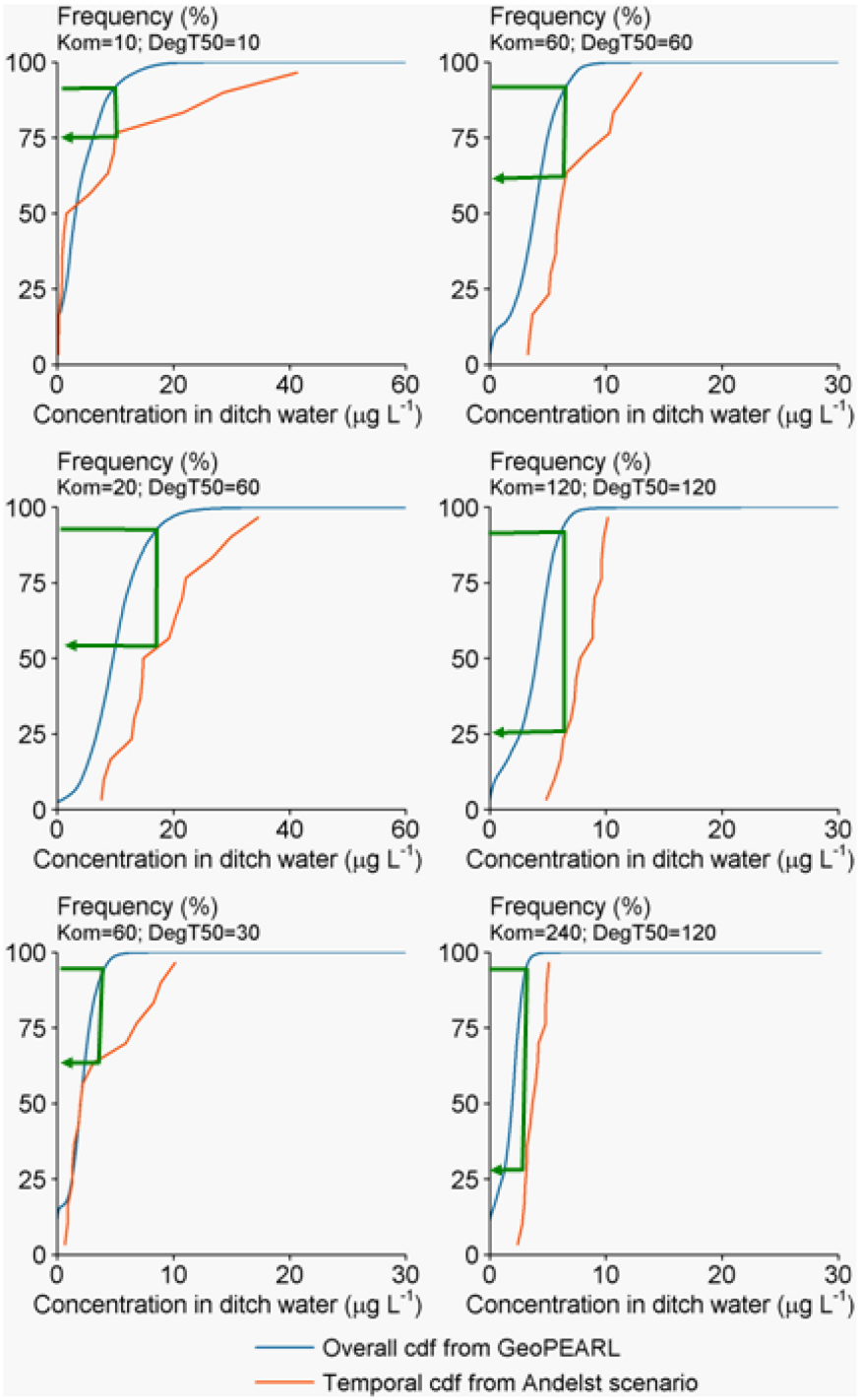

Figure 45 Comparison of the overall cumulative distribution function (cdf) from the GeoPEARL run and the temporal distribution function for the 15 weather years at the scaled Andelst scenario (i.e. organic matter multiplied by 1.56). The green lines indicate the target temporal percentile (see Section 7.2 for procedures). The green arrows are only indicative, see table 12 for exact values.

The temporal frequency distribution function at the scaled Andelst scenario shows a stronger response to substance properties than the overall cumulative distribution. This is caused by the fact that the sensitivity to substance properties is location dependent. Because the overall distribution consists of a large number of locations, the overall distribution will still show significant variability, even if the variability at individual locations is negligible.

Figure 45 can be used to calculate the target temporal percentile. The target temporal percentile is the temporal percentile at the scaled Andelst scenario that predicts the same concentration as the 90th percentile of the overall cdf. This percentile can be looked up by following the green arrows in Figure 45 (see also Section 7.2). Results for all 39 substances are shown in Table 12. As expected from Figure 45, the target temporal percentile decreases with increasing K_{om} and with increasing *DegT50*. For substances with a high K_{om} and DegT50, the target temporal percentile is zero. This means that for these substances, the target concentration will be higher than the 90th overall concentration. Why this is the case is explained in Section 7.4.

Table 12 Target temporal percentile for the 39 example substances. The target temporal percentile is the temporal percentile at the scaled Andelst scenario that predicts the same concentration as the 90th percentile of the overall frequency distribution function.

	K_{om} (L/kg)						
DegT50 (d)	10	20	30	60	120	240	480
10	77.8	75.6	75.1	65.8	59.5	56.7	50.3
20	77.8	73.6	70.9	65.2	59.2	56.7	43.4
30	77.6	72.6	70.7	65.8	50.5	56.8	43.4
60	-	55.3	55.8	65.3	59.9	55.8	50.9
120	-	-	35.0	22.9	25.5	28.0	14.4
240	-	-	-	37.9	9.5	4.9	3.5
480	-	-	-	-	50.9	6.9	0.0

7.4 Spatial percentile for the scaled Andelst scenario

As mentioned before, the overall 90th percentile consists of a spatial component and a temporal component. With the procedure above, the temporal percentile is fixed for each substance. As the spatial percentile and the temporal percentile are uniquely linked, the spatial percentile for the Andelst scenario is also fixed for each substance. This can be shown with a contour diagram (Figure 46). The X-coordinate in such a contour diagram corresponds with the percentile of the cumulative distribution of the predicted concentrations due to spatial variability that is obtained for the median weather year. The Y-coordinate corresponds with the percentile of the cumulative probability density function resulting from the 20 weather years at a given location. The contour lines correspond with the overall percentiles taken from the frequency distribution function obtained with Eqn. 60. The example contour diagrams in Figure 46 show that a low temporal percentile must be compensated for by a high spatial percentile and vice versa. For substance 1, the target temporal percentile is 78 per cent (Table 12), which implies that the corresponding spatial percentile is 85 per cent. For substance 30, the target temporal percentile is 28 per cent, so the corresponding spatial percentile is 98 per cent. Generally it can be stated that the spatial percentile for the Andelst scenario is between 85 and 100 per cent. For substances with a high K_{om} and DegT50, the soil is an extremely worst-case soil.

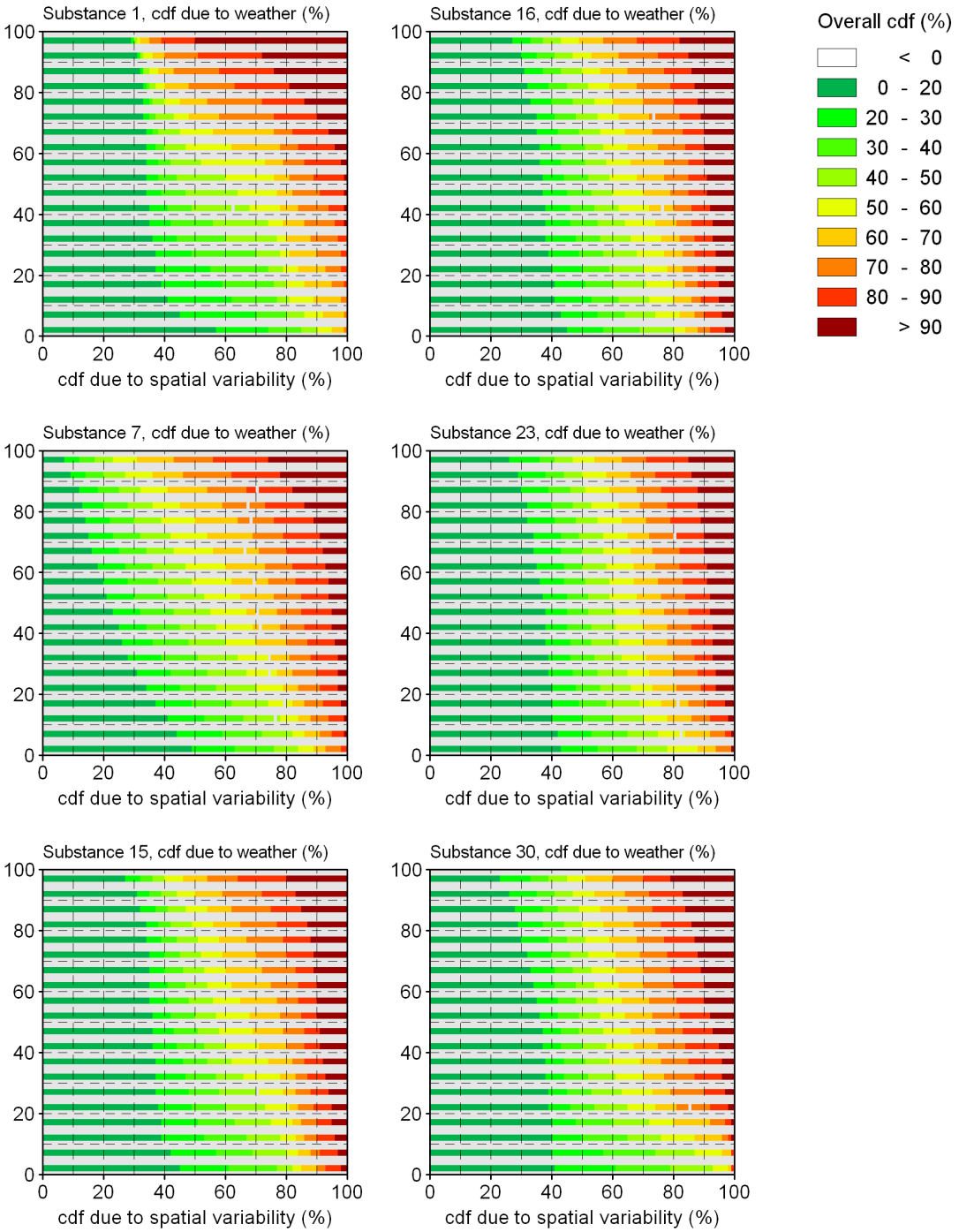

Figure 46 Contour plot of the overall percentiles of the annual maximum concentration in the adjacent ditch for six example substances (see Table 9 for substance properties). The X-coordinate corresponds with the percentile of the spatial cumulative distribution function (cdf) and the Y-coordinate with the percentile of the cdf due to weather (i.e. the temporal percentile).

The fact that, for many substances, the spatial percentile for the Andelst scenario is greater than 90 per cent is confirmed by comparing the mean soil properties of ten map units around the 90th overall percentile predicted with GeoPEARL with the soil properties of the Andelst scenario (Figure 47). For most substances, the clay content of the Andelst scenario is higher than the clay

content of the map units around the 90th percentile predicted by GeoPEARL. As shown in Figure 40, a higher clay content also implies a higher concentration in the field ditch (with the exception of very high clay contents). For many substances, the organic matter content of the Andelst scenario is lower than the mean organic matter content of the map units around the 90th percentile. Although the relation between organic matter and the ditch concentration shown in Figure 40 is weak, Figure 42 indicates that a lower organic matter content should also cause a higher ditch concentration, as the concentration in the ditch decreases with increasing K_{om}. With a constant value of K_{om}, one may therefore also expect a decrease of the ditch concentration with increasing organic matter. Both the organic matter content and the clay content corresponding to the overall 90th percentile are plausible for a Eutric Fluvisol, which is the soil type of the Andelst scenario (De Vries 1999).

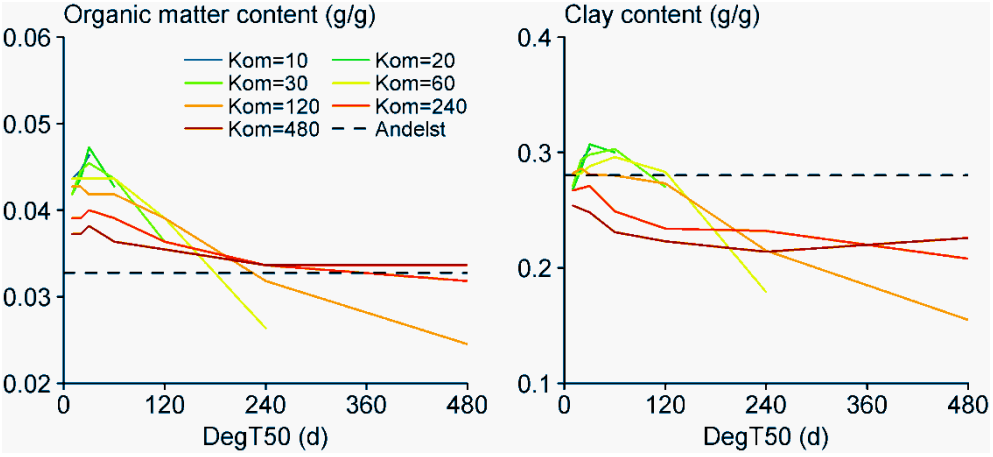

Figure 47 Mean organic matter content (left) and clay content (right) of ten map units for which the concentration in the field ditch is simulated to be around the 90th percentile of the overall distribution.

7.5 Temporal percentile to be used in DRAINBOW

As shown in Section 7.3, the target temporal percentile is substance dependent. One possible solution would be to include all these temporal percentiles in the software tool DRAINBOW and let the software tool automatically select the temporal percentile. There are, however, uncertainties in the selection of the temporal percentile. One uncertainty results from the use of the simplified lower boundary condition in GeoPEARL: it consists of a long-term average soil water flux on which a sine-function with fixed amplitude is imposed (Kroon et al. 2001). Additional analyses showed that due to the use of fixed lower boundary conditions, the differences between the years were underestimated. In view of this uncertainty, the working group considered it more appropriate to use only one temporal percentile in DRAINBOW. This temporal percentile should be sufficiently conservative for the majority of substances. Figure 48 shows the ratio between the predicted concentration for a certain temporal percentile at the Andelst scenario and the overall 90th percentile concentration predicted by GeoPEARL. This figure shows that the use of the 63rd temporal percentile is sufficiently conservative for most substances. The working group judged the overestimation of the exposure concentrations for substances with high K_{om} and high DegT50 acceptable because this is a limited number of substances and because of the uncertainties associated with (i) the selection of the

10th percentile of the organic matter content within map units and (ii) the effect of the lower hydrological boundary condition.

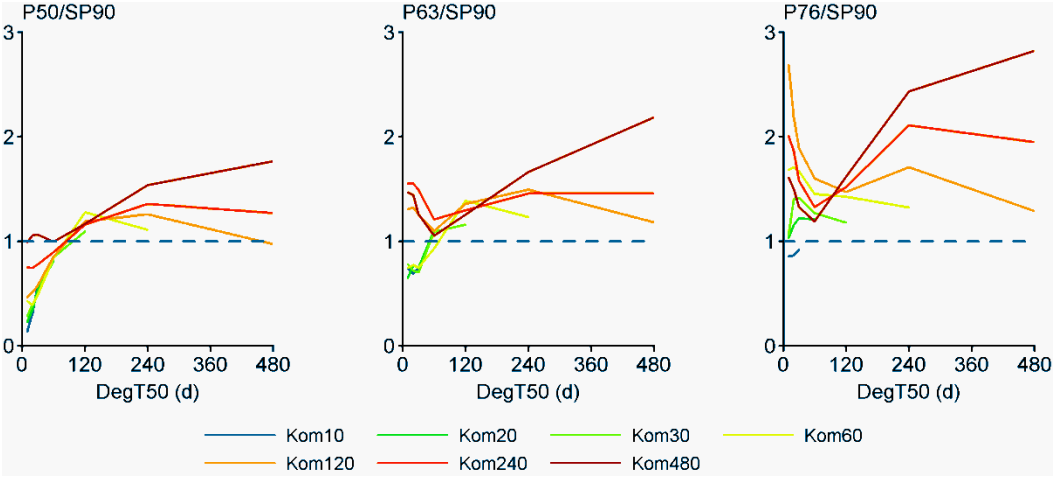

Figure 48 Ratio of the predicted concentration for a certain temporal percentile at the Andelst scenario and the overall 90th percentile concentration predicted by GeoPEARL.

The 63rd temporal percentile of the predicted peak concentration is up to two times higher than the overall 90th percentile simulated with GeoPEARL (Figure 42 and Figure 49). Taking the 63rd percentile instead of the overall 90th percentile is the first reason. The second reason is the scaling of organic matter, which results also in higher predicted concentrations.

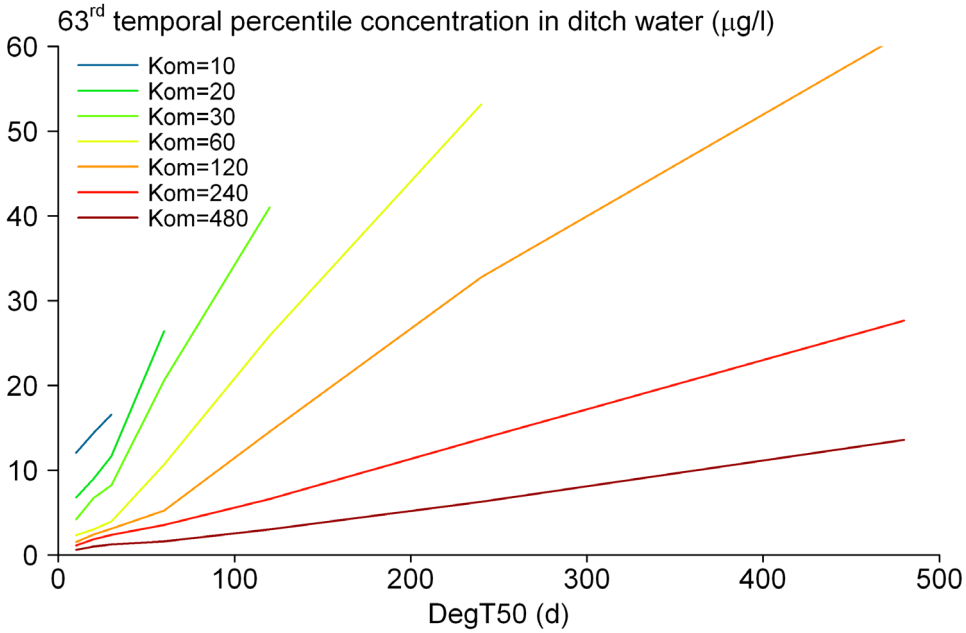

Figure 49 63rd temporal percentile of the peak concentration in the adjacent ditch. The figure is based on simulations with 39 hypothetical substances with properties shown in Table 9.

8 Conclusions and recommendations

8.1 Conclusions

As part of the proposed revised assessment procedure of exposure of aquatic organisms, a drainpipe exposure scenario was developed that corresponds to the 90th overall percentile of the exposure concentration in Dutch ditches that potentially receive input from drainpipes. This scenario is based on data from an experimental field site on a cracking clay soil.

The peak concentration in the ditch is considered to be the most important exposure endpoint for assessing the effects on aquatic organisms. The peak concentration in drain water is primarily affected by preferential flow through macropores, so we extended the Dutch pesticide leaching model PEARL with a preferential flow module. Central to this new model is a description of the geometry of the macropores and the presence of a so-called internal catchment domain. This internal catchment domain consists of macropores that end above drain depth.

The model concepts were tested at the Andelst field site. We showed that most parameters could be obtained from direct measurements or from commonly available data sources using pedotransfer functions; only three macropore flow related parameters needed calibration, i.e. the volume of macropores at soil surface, the fraction of the internal catchment domain at soil surface and the runoff-extraction ratio. The concentration in drain water appeared to be rather insensitive to the volume of macropores at soil surface, so only two important calibration parameters remained. The fraction of the internal catchment domain had to be increased to 90 per cent, indicating that a significant part of the substances still had to move through the soil matrix. The value of the runoff extraction ratio was 0.1, which is the average of values suggested in the literature. After calibration, the leaching and drainage of two substances was fairly well described by the model.

The Andelst dataset was used to build the Andelst exposure scenario. The Andelst dataset covered a period of approximately one year. To minimise the effect of application time on the predicted exposure concentration, we decided that the exposure assessment should be carried out for a long-term period. The Andelst dataset was therefore extended to a 15-year dataset, using data from a weather station at a distance of40 km and from a neighbouring groundwater bore hole. This resulted in 15 annual maximum concentrations. The peak concentration of a weakly sorbing and quickly degrading substance showed much more variability between the years than the peak concentration of a moderately sorbing and somewhat persistent substance. As a consequence, the frequency distribution function of the annual maximum concentration was steeper for the first substance. This behaviour was judged plausible and is related to the short residence time of the substance in the mixing layer.

The assessment for the Andelst scenario resulted in a temporal frequency distribution function consisting of 15 annual peak concentrations. The temporal percentile that predicts the same concentration as the overall 90th percentile of the exposure concentration was called the target temporal percentile. The overall 90th percentile was obtained with the spatially distributed leaching model GeoPEARL. This model was combined with a metamodel of TOXSWA, so that it

was possible to simulate the maximum concentration in all Dutch ditches. Nearly all preferential flow parameters could be obtained from generally available data sources using pedotransfer functions. Three macropore related parameters had to be taken directly from the Andelst field site. (These are the same parameters that also needed calibration at the Andelst site.) Two of these parameters (the fraction of the internal catchment domain and the runoff extraction ratio) are extremely important for the peak concentration in drain water. We consider this an important limitation of the current parameterisation, because it is uncertain whether this single field site is sufficiently representative for the entire area of drained arable soils.

The simulated spatial pattern was judged plausible with high predicted peak concentrations in clay soils and low peak concentrations in sandy soils. The simulations showed that not only the rapid drainage fluxes were enhanced by preferential flow; also the predicted mass fluxes in matrix drainage were enhanced. This was caused by transport through the internal catchment domain, which causes substances to bypass the most reactive part of the soil profile.

The predicted spatial pattern of the peak concentration was substance dependent. For weakly sorbing substances, drainage conditions appeared to be optimal if the boundary hydraulic conductivity was low, whereas for moderately sorbing substances low organic matter content was also necessary.

The target temporal percentile was substance dependent. Its value ranged from 78 per cent for weakly sorbing and quickly degrading compounds to 0 per cent for strongly sorbing and persistent compounds. Contour diagrams showed that the spatial percentile for the Andelst scenario ranged from approximately 85 per cent to 100 per cent. This means that for strongly sorbing and persistent compounds, the Andelst scenario is more worst-case than the overall 90^{th} percentile. In view of uncertainties in the estimation of the temporal percentiles, the working group proposes using one single temporal percentile for all substances. The 63^{rd} temporal percentile appeared to be the best compromise.

The target maximum concentration (i.e. the concentration in ditch water for the year corresponding to the target percentile) increased with increasing *DegT50* and decreased with increasing K_{om}. The predicted differences of the target maximum concentration were small compared to the difference of the leaching concentration predicted by the convection-dispersion equation. This was judged plausible, because the maximum concentration is primarily caused by preferential flow where the substance bypasses most of the reactive part of the soil profile.

Although the model calibration and scenario selection were carried out with great care and although this work took considerable research efforts over a period of several years, the uncertainty in the predicted peak concentrations in the Andelst scenario is still considerable: the results in Table 4 suggest that the true peak concentrations may be several times higher or lower than the predictions.

8.2 Recommendations

The Andelst field experiment has played a crucial role in the development of the drainpipe exposure scenario. It is currently the only Dutch dataset where sufficient data is available to parameterise and test all modules of the preferential flow version of PEARL. Additional field experiments should be carried

out to get more confidence in the model. Additional field experiments also increase the quality of the GeoPEARL parameterisation, because two important macropore flow related parameters could only be obtained from calibration at the Andelst field site.

In view of the available time, a manual calibration method was used. The calibration should be repeated using a Bayesian calibration method. Such a calibration method is more objective and also provides more insight into the propagation of uncertainty to the predicted concentrations.

The current version of GeoPEARL is less suitable for predicting the absolute concentration in drain water, because the lower boundary condition of the model is extremely simplified. A more detailed transient boundary condition is delivered by the Netherlands Hydrological Instrument (www.nhi.nu). We therefore recommend coupling GeoPEARL to the NHI.

The resolution of the GeoPEARL schematisation with 6 405 map units is lower than the resolution of the land-use maps that were used for filtering arable land. The consequence is that map units with non-arable soil properties may be included in the assessment. For example, the high clay contents in Figure 40 are typical for grassland soils in the river Rhine delta. Despite the use of the detailed land-use mask, these map units were not removed from the population (apparently, within this map unit arable land is present as well). We reduced the effect of the mismatch between the GeoPEARL schematisation and the land-use mask by giving map units with a low proportion of arable land less weight (Chapter 7). Despite this, the organic matter content of arable soils is underestimated in GeoPEARL. This was allowed for in an ad-hoc way when estimating the temporal percentiles to be used in the exposure assessment. There is considerable uncertainty in this ad-hoc correction procedure. The development of a purer spatial schematisation based on arable soils only will avoid these problems.

As described before, only one drainpipe scenario was developed for the entire area of arable land (excluding grassland) in view of the available time. The maps in Figure 38 showed that there are considerable regional differences in ditch concentrations within the Netherlands. Therefore we expect that there will be considerable differences between the 90^{th} percentile ditch concentrations for different crops (for example between crops such as flower bulbs which are not grown on clayey soils and crops such as winter wheat which are grown on such soils). We recommend developing crop-specific drainpipe scenarios because they are likely to lead to significant refinement of the exposure assessment.

Preliminary analyses showed that GeoPEARL generates differences between yearly peak concentrations that are smaller than those in the Andelst scenario. This is probably caused by the difference in the lower hydrological boundary condition (fixed sine-function for the flux in GeoPEARL and the DINO time series of the hydraulic head shown in Figure 19). This difference between GeoPEARL and the Andelst scenario was one of the main arguments for proposing a fixed temporal percentile (63^{rd}) which is, for most substances, on the conservative side. We therefore recommend analysing the effect of this difference in the lower hydrological boundary condition more in depth in a future study.

The PEARL model assumes that no degradation occurs in the macropore domain. This is a conservative assumption. One may expect that there is microbial activity within the macropore domain and that in reality degradation does occur.

Therefore we recommend performing a sensitivity analysis for a number of substances to check whether this assumption has indeed a negligible effect on the drainpipe concentrations.

MACRO is currently the only preferential flow model that is used for the evaluation of active substances at the EU-level. A benchmark of PEARL with MACRO is necessary to increase confidence in the two models.

This study revealed that the sensitivity of the model to the new model parameters is complex and not yet fully understood. A stochastic uncertainty analysis of the new GeoPEARL version should therefore be carried out to gain insight into the propagation of parameter uncertainty to the predicted drainage and leaching concentration. This study should also reveal to what extent the overall 90^{th} percentile of the drainage concentration as predicted by GeoPEARL shifts towards higher values.

List of abbreviations

cdf	Cumulative distribution function
COLE	Coefficient of Linear Extensibility
Ctgb	Board for the Authorisation of Plant Protection Products and Biocides
DINO	Data and Information of the Dutch Soil
DRAINBOW	Drainage and Spray Drift Burden Of Water
EFSA	European Food Safety Authority
ELINK	Linking aquatic exposure and effects
ERC	Ecotoxicologically Relevant Type of Concentration
EU	European Union
FOCUS	FOrum for the Co-ordination of pesticide fate models and their USe
GeoPEARL	The spatially distributed version of the PEARL model
KNMI	Royal Dutch Meteorological Institute
MACRO	A pesticide fate model with a description of preferential flow
MLG	Mean Lowest Groundwater level
MODFLOW	A commonly used modular groundwater flow model.
NHI	Netherlands Hydrological Instrument
PBL	Netherlands Environmental Assessment Agency
PEARL	Pesticide Emission At Regional and Local Scales. The pesticide leaching model used in this study
PEC	Predicted Environmental Concentration
PPP	Plant Protection Product
RETC	Retention curve program for unsaturated soils.
RIVM	National Institute for Public Health and the Environment
STONE	Dutch National Nutrient Emission Model
SWAP	Soil Water Atmosphere Plant model. The water flow model used in PEARL
TOXSWA	Toxic Substances in Water. Model that simulates pesticide fate in surface water
TWA	Time Weighted Average
WFD	Water Frame Directive

References

Adriaanse, P.I. 1996. Fate of pesticides in field ditches: the TOXSWA simulation model. SC-DLO rerport 90, Wageningen, the Netherlands, 241pp.

Ahuja, L.R., A.N. Sharpley and O.R. Lehman. 1982. Effect of soil slope and rainfall characteristics on phosphorous in runoff. J. Environ. Qual. (11):9-13.

Allaire, S.E, S. Roulier and A.J. Cessna, 2009. Quantifying preferential flow in soils: A review of different techniques. J. Hydrol. (378):179-204.

Algoazany, A.S., P.K. Kalita, G.F. Czapar and J.K. Mitchell. 2007. Phosphorus transport through subsurface drainage and surface runoff from a flat watershed in East Central Illinois, USA. J. Environ. Qual. (36):681-693.

Attinger, S., and A. Hildebrandt. 2011. A critique on combining the water stress function with root density distributions to find vertical water uptake profiles in SVAT models. Geophysical Research Abstract

Beltman, W.H.J., and P.I. Adriaanse. 1999. Proposed standard scenarios for surface water model in the Dutch authorization procedure of pesticides; method to define standard scenarios for determining exposure concentrations simulated by the TOXSWA model. SC-DLO report 161, Wageningen, the Netherlands, 90pp.

Beulke, S., I.G. Dubus, C.D. Brown and B. Gottesbüren. 2000. Simulation of pesticide persistence in the field on the basis of laboratory data – a review. J. Environ. Qual. (29):1371-1379.

Boesten, J.J.T.I. 1986. Behaviour of herbicides in soil: simulation and experimental assessment. Doctoral thesis. Institute for Pesticide Research, Wageningen, 263 pp.

Boesten, J.J.T.I., and A.M.A. van der Linden. 1991. Modeling the influence of sorption and transformation on pesticide leaching and persistence. J. Environ. Qual. (20):425-435.

Boesten, J.J.T.I., and L. Stroosnijder. 1986. Simple model for daily evaporation from fallow tilled soil under spring conditions in a temperate climate. Neth. J. Agric. Sci. (34):75-90.

Boesten, J.J.T.I., and L.J.T. van der Pas. 2002, Movement of water, bromide and the pesticides ethoprophos and bentazone in a sandy soil: the Vredepeel dataset. Agric. Water Manag. (44):21-42.

Bouma, J., and J.L. Anderson. 1973. Relationships between soil structure characteristics and hydraulic conductivity. In: R.R. Bruce (ed.). Field soil moisture regime. SSSA Special Publ. No. 5. Am. Soc. of Agron. Madison, Wisconson, USA.

Breeuwsma, A. 1985. Kleimineralogische en chemische karakteristieken van zeeklei, rivierklei en beekklei. STIBOKA report 1869, STIBOKA, Wageningen, the Netherlands.

Breeuwsma, A, R. Zwijnen and W. Balkema. 1986. Kleimineralogische samenstelling van Kwartaire en Tertiaire kleiafzettingen in Nederland. STIBOKA report 1850, STIBOKA, Wageningen, the Netherlands.

Brock, T., A. Alix, C. Brown, E. Capri, B. Gottesbüren, F. Heimbach, C. Lythgo, R. Schulz and M. Streloke. 2009. Executive summary and recommendations. EU and SETAC Workshop on Linking Aquatic Exposure and Effects in the registration procedure of plant protection products (ELINK). SETAC Press and CRC Press, Taylor & Francis Group.

Bronswijk, J.J.B., and J.J. Evers-Vermeer. 1990. Shrinkage of Dutch clay soil aggregates. Neth. J. Agric. Sci. (38):175-194.

Cultuurtechnisch Vademecum. 1998. Handboek inrichting en beheer landelijk gebied. Werkgroep Herziening Cultuurtechnisch Vademecum. Cultuurtechnische Vereniging, Utrecht.

Dekker, L.W., and C.J. Ritsema. 1996. Preferential flow paths in a water repellent clay soil with grass cover. Water Resour. Res. (32):1239-1249.

De Vries, F. 1999. Een fysisch-chemische karakterisering van de bodemeenheden van de Bodemkaart van Nederland, schaal 1:50 000, met onderscheid naar grondgebruik. DLO-Staring Centrum rapport 286, Wageningen, the Netherlands.

Dubus, I.G., S. Beulke and C.D. Brown. 2000. A briefing document on the application of inverse modelling techniques to pesticide leaching models. Rep. PL0528. SSLRC,Cranfield Univ., Silsoe.

EFSA (2010). Selection of scenarios for exposure of soil organisms to plant protection products. EFSA Journal 2010; 8(6):1642. doi:10.2903/j.efsa.2010.1642.

Feddes, R.A. 1987. Crop factors in relation to Makkink reference crop evapotranspiration. In Evaporation and Weather, TNO Committee on Hydrological Research. Proc and Information (39), the Hague, The Netherlands, pp. 33-46.

Feddes, R.A., P.J. Kowalik and H. Zaradny. 1978. Simulation of field water use and crop yield. Simulation Nomographs. Pudoc. Wageningen, The Netherlands. pp. 189.

FOCUS. 2001. FOCUS Surface Water Scenarios in the EU Evaluation Process under 91/414/EEC. Report of the FOCUS Working Group on Surface Water Scenarios, EC Document Reference SANCO/4802/2001-rev.2. 245pp.

Gerke, H.H., and M.T. van Genuchten. 1993. Evaluation of a first-order water transfer term for variably-saturated dual-porosity flow models. Water Resources Research (29):1225-1238.

Greco, R., R.F.A. Hendriks and W. Hamminga. 1997. Clay soil aggregate sorptivity measurements under different water contents. Proceedings of the National Hydraulics Conference, Turin, Italy, November 1996.

Gouy, V., J-C Dur, R. Calvet, R. Belamie and V. Chaplain. 1999. Influence of adsorption-desorption phenomena on pesticide run-off from soil using simulated rainfall. Pestic. Sci. (55):175-182.

Halbertsma, J.M., and G.J. Veerman. 1997. Determination of the unsaturated conductivity and water retention characteristic using the Wind's evaporation method. p. 46-55. In J. Stolte (ed.). Manual for soil physical measurements, Version 3.0. Technical Document 37. DLO Winand Staring Centre, Wageningen, the Netherlands.

Hendriks, R.F.A., K. Oostindië and P. Hamminga. 1999. Simulation of bromide tracer and nitrogen transport in a cracked clay soil with the FLOCR/ANIMO model combination. J. Hydrol. (215):94-115.

Hendriks, R.F.A. 2009. Absorption of macropore water into the unsaturated matrix in SWAP. Working document. Available at http://www.pearl.pesticidemodels.eu.

Heuvelink, G.B.M., S.L.G.E. Burgers, A. Tiktak and F. van den Berg. 2010. Uncertainty and stochastic sensitivity analysis of the GeoPEARL pesticide leaching model. Geoderma (155):186-192..

Ippisch, O., H.-J. Vogel and P. Bastian. 2006. Validity limits for the van Genuchten-Mualem model for parameter estimation and numerical simulation. Adv. Water Resour. (29):1780-1789.

Javaux, M., X. Draye, V. Couvreur, H. Vereecken and J. Vanderborght. 2011. How relevant are 1D models for predicting root water uptake processes. Geophysical Research Abstracts.

Jarvis, N.J., M. Larsbo, S. Roulier, A. Lindahl and L. Persson. 2007. The role of soil properties in regulating non-equilibrium macropore flow and solute transport in agricultural topsoils. European Journal of Soil Science (58):282-292.

Jarvis, N.J., and I. Messing. 1995. Near-saturated hydraulic conductivity in soils of contrasting texture as measured by tension infiltrometers. Soil Sci. Soc. Am. J. (59):27-34.

Jury, W.A., W.R. Gardner and A.W.H. Gardner. 1991. Soil Physics, fifth ed. John Wiley and Sons, Hoboken, USA.

Van Keulen, H., and J. Wolf. 1986. Modelling of agricultural production: weather, soils and crops. Pudoc, Wageningen, the Netherlands.

Kim, D.J. 1992. Characterization of swelling and shrinkage behaviour, hydraulic properties and modelling of water movement in a physically ripening marine clay soil. Ph.D. Thesis, Catholic University, Leuven, Belgium.

Kroes, J.G., J.G. van Dam, P. Groenendijk, R.F.A. Hendriks and C.M.J. Jacobs. 2008. SWAP version 3.2. Theory, description and user manual. Alterra report 1649, Alterra, Wageningen, the Netherlands.

Kroon, T., P. Finke, I. Peereboom and A Beuzen. 2001. Redesign STONE. De nieuwe schematisatie voor STONE: de ruimtelijke indeling en de toekenning van hydrologische en bodemchemische paramaters. Lelystad, RIZA, rapport 2001.017.

Larsson, M.H., and N.J. Jarvis. 2000. Quantyfying interactions between compound properties and macropore flow effects on pesticide leaching. Pest. Manag. Sci. (56):133-141.

Leistra, M., A.M.A. van der Linden, J.J.T.I. Boesten, A. Tiktak, and F. van den Berg. 2000. PEARL model for pesticide behaviour and emissions in soil-plant systems. Description of processes. Alterra report 013, Alterra, Wageningen, the Netherlands.

Lindahl, A.M.L., I.G. Dubus and N.J. Jarvis. 2009. Site classification to predict the abundance of the deep-burrowing earthworm Lumbricus terrestris L. Vadose Zone J. (8):911-915.

Massop, H.Th.I, J.W.J. van der Gaast and A.G.M. Hermans. 2006. Kenmerken van het ontwateringsstelse in Nederland. Alterra report no. 1397, Alterra, Wageningen, the Netherlands.

Overbeek, G.B.J., A.H.W. Beusen, P.C.M. Boers, G.J. van den Born, P. Groenendijk, J.J.M. van Grinsven, T. Kroon, H.G. van der Meer, H.P. Oosterom, P.J.T.M. Puijenbroek, J. Roelsma, R. Rötter, A. Tiktak and S. van Tol. Plausibiliteitsdocument STONE 2.0. Globale verkenning van de plausibiliteit van het model STONE versie 2.0 voor de modellering van uit- en afspoeling van N en P. RIVM rapport 718501001, RIVM, Bilthoven, the Netherlands.

Parker, J.C., and A.J. Valocchi. 1986. Constraints on the validity of equilibrium and first-order kinetic transport models in structured soils. Water Resour. Res. (22):399-407.

Parlange, J.Y. 1975. On solving the flow equation in unsaturated soils by optimization: horizonal infiltration. Soil Sci. Soc. Am. Proc. (39):415-418.

Philip, J.R. 1957. The theory of infiltratio: 4. Sorptivity and algebraic infiltration equations. Soil Sci. (84):264-275.

Rozemeijer, J.C., and Y. van der Velde. 2008. Oppervlakkige afstroming ook van belang in het vlakke Nederland. H_2O (19):88-90.

Rozemeijer, J.C., Y. van der Velde, F.C. van Geer, M.F.P. Bierkens and H.P. Broers. 2010. Direct measurements of the tile drain and groundwater flow route contributions to surface water contamination: From field-scale concentration patterns in groundwater to catchment-scale surface water quality. Environmental Pollution (158):3571-3579.

Scheffer, F., P. Schachtschabel, H.P. Blume, K.H. Hartge and U. Schwertman. 1979. Lehrbuch der Bodemkunde. 10., durchgesehene Auflage. Enke Verlag, Stutgart, Germany.

Scorza Júnior, R.P., and J.J.T.I. Boesten. 2005. Simulation of pesticide leaching in a cracking clay soil with the PEARL model. Pest. Manag. Sci. (61):432-448.

Scorza Júnior, R.P., N.J. Jarvis, J.J.T.I. Boesten, S.E.A.T.M. van der Zee and S. Roulier. 2007. Testing MACRO (version 5.1) for pesticide leaching in a Dutch clay soil. Pest Manag Sci. (63):1011-1025.

Scorza Júnior, R.P., J.H. Smelt, J.J.T.I. Boesten, R.F.A. Hendriks and S.E.A.T.M. van der Zee. 2004. Preferential flow of bromide, bentazon, and imidacloprid in a Dutch clay soil. J. Environ. Qual. (33):1473-1486.

Sharpley, A.N. 1985. Depth of surface soil-runoff interaction as affected by rainfall, soil slope, and management. Soil. Sci. Soc. Am. J. (49):1010-1015.

Smelt, J.H., R.F.A. Hendriks, L.J.T. van der Pas, A.M. Matser, A. van den Toorn, K. Oostindië and O.M. van Dijk-Hooijer. 2001. Transport of water, bromide ion, nutrients and the pesticides bentazone and imidacloprid in a cracking, tile drained clay soil at Andelst, the Netherlands. Alterra report 289, Wageningen, the Netherlands.

Soil Survey Staff. 1975. Soil taxonomy: a basic system for soil classification for making and interpreting soil surveys. Agric. Handbook 436, US Dept. of Agric. US Govt. Print Off., Washington DC.

Stenemo, F., and N. Jarvis. 2007. Accounting for uncertainty in pedotransfer functions in vulnerability assessments of pesticide leaching to groundwater. Pest Manage. Sci. (63): 867-875

Sukhija, B.S., D.V. Reddy, P. Nagabhushanam and S. Hussain. 2000. Recharge processes: piston flow vs preferential flow in semi-arid aquifers of India. Hydrogeology Journal (11):387-395

Ter Horst, M.M.S., R.F.A. Hendriks and J.J.T.I. Boesten. 2006. Addendum to Alterra report 289 'Transport of water, bromide ion, nutrients and the pesticides bentazone and imidacloprid in a cracking, tile drained clay soil at Andelst, the Netherlands'. Alterra, Wageningen, the Netherlands.

Tiktak, A., R.F.A. Hendriks and J..T.I. Boesten. 2012a. Simulation of pesticide leaching towards surface water in a pipe-drained cracking clay soil in the Netherlands. Pest Manag. Sci. (68):290-302.

Tiktak, A., J.J.T.I. Boesten, R.F.A. Hendriks and A.M.A. van der Linden. 2012c. A spatially distributed model of pesticide movement in Dutch macroporous soils. J. Hydrol. (470-471):316-327.

Tiktak, A., P.I. Adriaanse, W. Beltman, J.J.T.I. Boesten, J. Delsman, C. van Griethuysen, M.M.S. ter Horst, J. Klein, B.H.J. Linders, A.M.A. van der Linden, and J.C. van de Zande. 2012b. Scenarios for exposure of water organisms in the Netherlands. Edge-of-field water courses. RIVM report 607402002/2012. RIVM, Bilthoven, the Netherlands.

Tiktak, A., and W. Bouten. 1994. Soil water dynamics and long-term water balances of a Douglas Fir stand in the Netherlands. J. Hydrology. (156):265-283.

Tiktak, A., D.S. De Nie, A.M.A. van der Linden and R. Kruijne. 2002. Modelling the leaching and drainage of pesticides in the Netherlands: the GeoPEARL model. Agronomie (22):373-387.

Tiktak, A., F. van den Berg, J.J.T.I. Boesten, D. van Kraalingen, M. Leistra and A.M.A. van der Linden. 2000. Manual of FOCUS PEARL version 1.1.1. RIVM report 711401008, RIVM, Bilthoven, the Netherlands.

Tiktak, A, A.M.A. van der Linden and J.J.T.I. Boesten. 2003. The GeoPEARL model. Model description, applications and manual. RIVM report 716601007, RIVM, Bilthoven, the Netherlands.

Vanclooster, M., J.J.T.I. Boesten, M. Trevisan, C.D. Brown, E. Capri, O.M. Eklo, B. Gottesbüren, V. Gouy and A.M.A. van der Linden. 2000. A European test of pesticide-leaching models: methodology and major recommendations. Agric. Water Manag. (44):1-19.

Van den Berg, F., A. Tiktak, D. van Kraalingen, A.M.A. van der Linden and J.J.T.I. Boesten. 2006. Documentation update for PEARL 3.3.3. Working document available at http://www.pearl.pesticidemodels.eu.

Van den Berg, F., D.J. Brus, S.L.G.E. Burgers, G.B.M. Heuvelink, J.G. Kroes, J. Stolte, A. Tiktak and F. de Vries. 2008. Uncertainty and sensitivity analysis of GeoPEARL. Alterra report 1330, MNP report 500123001, Alterra, Wageningen, the Netherlands.

Van der Velde, Y., J.C. Rozemeijer, G.H. de Rooij, F.C. van Geer and H.P. Boers. 2010. Field-scale measurements for separation of catchment discharge into flow route contributions. Vadose Zone Journal (9):25-35.

Vanderborght, J. and H. Vereecken. 2007. Review of dispersivities for transport modelling in soils. Vadose Zone Journal (6):29-52.

Vanderborght, J., A. Tiktak, J.J.T.I. Boesten and H. Vereecken. 2011. Effect of pesticide fate parameters and their uncertainty on the selection of 'realistic worst-case' scenarios of pesticide leaching to groundwater. Pest. Sci. Manag. (67):294-306.

Van der Linden, A.M.A. J.J.T.I. Boesten, A.A. Cornelese, R. Kruijne, M. Leistra, J.B.H.J. Linders, J.W. Pol, A. Tiktak and A.J. Verschoor. 2004. The new decision tree for evaluating pesticide leaching from soils. RIVM report 601450019, RIVM, Bilthoven, the Netherlands.

Van Genuchten, M.Th. 1980. A closed form equation for predicting the hydraulic conductivity of unsaturated soils. Soil Sci. Soc. Am. J. (44):892-898.

Van Genuchten, M.Th., F.J. Leij and S.R. Yates. 1991. The RETC code for quantifying the hydraulic functions of unsaturated soils. US Salinity Lab., Riverside, CA.

Van der Salm, C. 2001. Assessment of the regional variation of weathering rates of loess and clay soils in the Netherlands. Water, Air, and Soil Pollution (131):217-243.

Van der Salm, C., J. Dolfing, J.W. van Groenigen, M. Heinen, G. Koopmans, J. Oenema, M. Pleijter and A. van den Toorn. 2006. Diffuse belasting van oppervlaktewater met nutrienten uit de veehouderij; Monitoring van nutriëntenverliezen uit grasland op zware klei in Waardenburg. Alterra report 1266, Alterra, Wageningen, the Netherlands.

Van Beek, C.L., C. van der Salm, A.C.C. Plette and H. van de Weerd. 2008. Nutrient loss pathways from grazed grasslands and the effects of decreasing inputs: experimental results for three soil types. Nutr. Cycling Agroecosyst. (83):99-110.

Van Dam J.C., J. Huygen, J.G. Wesseling, R.A. Feddes, P. Kabat, P.E.V. van Walsum, P. Groenendijk and C.A. van Diepen. 1997. Theory of SWAP version 2.0. Technical Document 45. DLO Winand Staring Centre, Wageningen, The Netherlands, 167 pp.

Van Laar, H.H., J. Goudriaan and H. van Keulen. 1992. Simulation of crop growth for potential and water-limited production situations (as applied to spring wheat). CABO-DLO, simulation report 27.

Van Schaik, N.L.M.B., R.F.A. Hendriks and J.C. van Dam. 2010. Parameterization of macropore flow using dye-tracer infiltration patterns in the SWAP model. Vadose Zone Journal (9):95-106.

Van Stiphout, T.P.J., H.A.J. van Lanen, O.H. Boersma and J. Bouma. 1987. The effect of bypass flow and internal catchment of rain on the water regime in a clay loam grassland soil. J. Hydrol. (95):1-11.

Villholth, K.G., K.H. Jensen and J. Fredericia, 1998. Flow and transport processes in a macroporous subsurface-drained glacial till soil. I: Field investigations. J. Hydrol. 207 98-120.

Wösten, J.H.M., G.J. Veerman, W.J.M. de Groot and J. Stolte. 2001. Water retention and hydraulic conductivity functions of top- and subsoils in The Netherlands: The Staring Series. Alterra report 153, Alterra, Wageningen, the Netherlands.

Appendix 1 Parameter values for the Andelst scenario

This appendix provides an overview of the parameter values for the Andelst drainpipe scenario. Variable names in the PEARL input file are underlined.

Simulation period	
Begin time (TimEnd), end time (TimEnd) and number of warm-up years (InitYears)	01-Jan-1986 until 31-Dec-2005, first five years are warming-up years
Boundary conditions	
MeteoStation (observation station for weather data)	Daily observations, taken from weather station 'De Bilt' at 40 km from Andelst field-site.
OptEvp (option for potential evapotranspiration)	Input (reference evapotranspiration according to Makkink)
OptRainfallEvents (PEARL uses a file with rainfall duration to calculate the rainfall intensity)	Yes. Rainfall duration assigned to first hours of day.
OptIrr (irrigation option)	No irrigation applied
OptLbo (type of lower boundary condition)	Cauchy
LowerBoundaryFile (time series of hydraulic heads)	DINO bore hole B39H0311, observations done fortnightly. Corrected for altitude differences (13 cm).
RstAqt (vertical resistance of underlying aquitard)	5 d
Soil properties	
SoilProperties (texture and organic matter)	Table 1 of this report
Rho (dry bulk density)	Table 1 of this report
VanGenuchtenPar (soil physical characteristics)	Table 2 of this report
LenDisLiq (dispersion length)	0.05 m for the entire soil profile

Diffusion coefficient for gas and liquid phase	
OptCofDifRel (option for tortuosity)	according to Millington and Quirk (1960)
ExpDifLiqMilNom (parameter in nominator)	2
ExpDIfLiqMilDen (parameter in denominator)	0.667
ExpDifGasMilNom (parameter in nominator)	2
ExpDifGasMilDen (parameter in denominator)	0.667
Ponding depth	
ZPndMax (for runoff from the field)	0.01 m
ZPndMacMax (for runoff into macropores)	0.00 m
Macropore parameters	
ZAHor (depth of plough layer)	0.26 m
ZIca (bottom depth of internal catchment domain)	0.80 m
ZSta (bottom depth of permanent macropores)	1.60 m
VolStaTop (volume fraction of static macropores at top)	0.03 m^3 m^{-3}
FraIcaTop (fraction of internal catchment domain at top)	0.90
PowMac (power in distribution function of internal catchment domain)	1
DiaPolMin (minimum diameter of soil polygons)	0.031 m
DiaPolMax (maximum diameter of soil polygons)	0.555 m
FraThiLayMix (runoff extraction efficiency ratio)	0.125
FraSorByp (fraction of sorption sites in bypass domain)	0.02

Drainage parameters	
RstRapDraRef (resistance for rapid drainage)	14 d^{-1}
RstDra_1 (matrix drainage resistance)	140 d^{-1}
ZDra_1 (drain depth)	0.80 m
DistDra_1 (distance between the drains)	10 m
Parameters of the TOXSWA metamodel	
AreaField (lineic area of adjacent field)	100 m^2 m^{-1}
AreaUpstream (lineic area of upstream catchment)	200 m^2 m^{-1}
FraUpstreamTreated (fraction of upstream catchment treated)	1
ParAlphaTOXSWA (parameter α of metamodel)	2
VolDitch1 (lineic volume of adjacent ditch)	0.55 m^3 m^{-1}
Soil evaporation	
FacEvpSol ('crop factor' for evaporation from bare soil)	1.2
OptSolEvp (option for reduction of soil evaporation)	according to Boesten and Stroosnijder
CofRedEvp parameter β for reduction of evaporation)	0.79 $cm^{1/2}$
PrcMinEvp (minimum precipitation to start new drying cycle)	0.01 m d^{-1}
Crop parameters	
crop type	winter wheat
Crops (emergence and harvest date)	27 October – 20 August each year
CrpPar (crop parameters)	Table 3 of this report
HLim1 (no water extraction at higher pressure heads)	0 cm
HLim2 (pressure head above which reduction starts)	-1 cm
HLim3U (pressure head below which reduction starts at high evaporative demand)	-500 cm
HLim3L (pressure head below which reduction starts at low evaporative demand)	-900 cm

HLim4 (no water extraction at lower pressure heads)	-16000 cm
CofIntCrp (parameter of interception module)	0.25
Soil management	
DelTimEvt (repeat interval)	1 year
TillageDates (tillage date)	15 October
ZTil (tillage depth)	0.20 m

National Institute for Public Health and the Environment
P.O. Box 1 | 3720 BA Bilthoven
www.rivm.com